CARBON MOLECULAR SIEVES AS CATALYSTS, CATALYST SUPPORTS, AND IN ADVANCED MATERIALS APPLICATIONS

BY

GERALD C. GRUNEWALD

A DISSERTATION PRESENTED TO THE GRADUATE SCHOOL
OF THE UNIVERSITY OF FLORIDA IN PARTIAL FULFILLMENT
OF THE REQUIREMENTS FOR THE DEGREE OF
DOCTOR OF PHILOSOPHY

UNIVERSITY OF FLORIDA

1989

TO MY FAMILY FOR THEIR CONSTANT SUPPORT

ACKNOWLEDGEMENTS

There have been a large number of people who have helped to make my journey through graduate school very enjoyable. The list presented here is by no means complete. Foremost, I would like to express my gratitude to my research advisor, Russell Drago, whose support and guidance have been essential to my education. Besides showing me the excitement of chemical research, Doc has also contributed significantly to my knowledge of two-on-two basketball and has taught me the fine art of eating spaghetti without cutting it. I would equally like to thank Ruth Drago whose humor and hospitality helped to make Gainesville a home away from home. Maribel Lisk also deserves special thanks. Her friendship and assistance, along with her seemingly endless supply of stationery goods, have been most appreciated.

My coworkers during my years in the Drago group have been a valuable source of knowledge and advice as well as being great friends. Former group members Jeff Clark, Andy Griffis, Ken Balkus, Rich Riley, Pete Doan, Ed and Cindy Getty, and Shannon Davis helped a great deal in showing me "the ropes." Present group members Larry Chamusco, Ngai Wong, Bobby Taylor, Tom Cundari, Al Goldstein, Mike Naughton, and Steve Petrosius have been comrades, compatriots, and cohorts in both scientific and social endeavors. I would also like to thank my roommates of the renowned Thunderdome. Mark Hail, Mark Barnes, Don Ferris, and Steve Showalter have been great friends as well as often being good cooks and housecleaners. A special thanks is also due to the

Stranger band who provided many a night of great entertainment for the revelers of the Inorganic and Analytical Divisions.

One other former Drago group member has also had a significant influence on my career. I would like to thank my future wife, Cindy Bailey, for her love, support, and advice. Although there are a lot of things I will miss in Gainesville, the frustration of a long-distance relationship and the high phone bills will not be among them. Lastly, I would like to thank my family for their constant prayers and support. In particular, I want to thank my brother-in-law, George Fisher, who was a great help in preparing this manuscript.

TABLE OF CONTENTS

	page
ACKNOWLEDGEMENTS	iii
LIST OF TABLES	vi
LIST OF FIGURES	vii
ABSTRACT	x
CHAPTERS	
1 GENERAL INTRODUCTION	1
2 PREPARATION AND CHARACTERIZATION OF CMS MATERIALS	8
Introduction	8
Experimenatal	33
3 CARBON MOLECULAR SIEVES AS CATALYSTS	37
Introduction	37
Experimental	43
Results and Discussion	48
4 CARBON MOLECULAR SIEVES AS CATALYST SUPPORTS	66
Introduction	66
Experimental	76
Results and Discussion	88
5 CARBON MOLECULAR SIEVES IN ADVANCED MATERIALS APPLICATIONS	145
Introduction	145
Experimental	150
Results and Discussion	154
6 CONCLUSIONS	169
REFERENCES	172
BIOGRAPHICAL SKETCH	184

LIST OF TABLES

Table		page
2-1.	Elemental Analysis of PAN Pyrolysis in Various Carrier Gases	13
2-2.	Surface Area of PPAN Samples	19
2-3.	Physical Properties of AX21	21
2-4.	Elemental Analysis of AX21	22
3-1.	Ethyl Benzene Reactivity Over PPAN Catalysts at 250^{0} C	49
3-2.	Ethyl Benzene Reactivity Over PPAN Catalysts at 350^{0} C	50
3-3.	Ethyl Benzene Reactivity Over AX21 and Other Catalysts at 350^{0} C	54
3-4.	Butene Reactivity Over CMS Catalysts	57
3-5.	Ethanol Reactivity Over CMS Catalysts	59
3-6.	Reactivity of C_3 Oxygenated Substrates Over AX21 Catalysts	62
4-1.	Commonly Studied Fischer - Tropsch Systems	68
4-2.	Typical Methanol Oxidation Reaction Routes	73
4-3.	Effect of Carrier Gas Cycling on Acetaldehyde Reactivity Over Ru/PPAN	110
4-4.	Methanol Reactivity Over Molybdenum Doped Catalysts	115
4-5.	Deep Oxidation of CH_2CL_2 Over Doped AX21 Catalysts	143
5-1.	Results of LiCl/PPPO Ion Selective Electrode Experiments	165

LIST OF FIGURES

Figure		page
1-1.	Formation and reaction cycle of PPAN	4
1-2.	Formation of PPPO	7
2-1.	Pyrolysis profile of PPAN	11
2-2.	Formation of pyridone moieties in PPAN structure	14
2-3.	DRIFT spectra of PAN and PPAN	16
2-4.	Infrared comparison of PPAn samples prepared under various conditions	17
2-5.	Infrared spectrum of PPO before pyrolysis	24
2-6.	Infrared spectra of PPO during pyrolysis	27
2-7.	DSC of undoped PPO	29
2-8.	DSC of Ti(O) doped PPO	30
2-9.	DSC of LiCl doped PPO	31
2-10.	DSC of $CoCl_2$ doped PPO	32
3-1.	Schematic diagram of reactor setup	46
3-2.	Proposed mechanism for AX21 dehydrogenation activity	56
3-3.	Proposed mechanistic routes for conversion of n-propanol	63
4-1.	DRIFT spectra of PPAN and $Ru_3(CO)_{12}$/PPAN	80
4-2.	DRIFT spectrum of unsupported $Ru_3(CO)_{12}$	81
4-3.	DRIFT spectrum of $Ru_3(CO)_{12}$	82
4-4.	GC traces for reactant gas cycling experiments	91
4-5.	Mass spectrum of propane peak showing ^{13}C incorporation	93

4-6.	Product distribution of Ru/PPAN versus Ru/Al_2O_3 . . .	94
4-7.	Alkene production in Ru/PPAN system	96
4-8.	ASF plot of PPAN versus Al_2O_3	97
4-9.	SEM of Ru/Al_2O_3 before and after catalysis	99
4-10.	SEM of Ru/PPAN before and after catalysis	100
4-11.	Product distribution of Ru/AX21 versus Ru/Al_2O_3 . . .	102
4-12.	ASF plot of AX21 versus Al_2O_3	103
4-13.	Effect of CO addition to CO_2 methanation reaction . .	106
4-14.	Effect of acetaldehyde addition to CO/H_2 reaction . .	108
4-15.	Proposed mechanism for product enhancement from aldehyde addition.	112
4-16.	SEM of bulk MoO_3 before and after reaction	120
4-17.	SEM of MoO_3/SiO_2 before and after reaction	121
4-18.	SEM of MoO_3/AX21 before and after reaction	122
4-19.	XRD of MoO_3/SiO_2 before reaction	125
4-20.	XRD of MoO_3/AX21 before reaction	126
4-21.	XRD of MoO_3/SiO_2 after reaction	127
4-22.	XRD of MoO_3/AX21 after reaction	128
4-23.	XPS of the Mo 3d orbitals of bulk MoO_3	131
4-24.	XPS of the Mo 3d orbitals of MoO_3/AX21 pre-catalyst	132
4-25.	XPS of the Mo 3d orbitals of MoO_3/SiO_2 pre-catalyst	133
4-26.	XPS of the Si 2s orbital of MoO_3/SiO_2 pre-catalyst	135
4-27.	XPS of the Mo 3d orbitals of MoO_3/AX21 post-catalyst	136
4-28.	XPS of the Mo 3d orbitals of MoO_3/SiO_2 post-catalyst	137

4-29. XPS of the C 1s orbital of MoO_3/SiO_2 post-catalyst 138

5-1. Schematic of cell design in ion selective electrode experiments 153

5-2. Cyclic voltammogram of Ti/PPPO system in N_2 and O_2 156

5-3. Effect of pH on Ti/PPPO O_2 reduction system 157

5-4. Effect of cathodic and anodic extreme potential variation on Ti/PPPO O_2 reduction system. 159

5-5. Effect of scan rate variation on Ti/PPPO O_2 reduction system 162

Abstract of Dissertation Presented to the Graduate School of
the University of Florida in Partial Fulfillment of the
Requirements for the Degree of Doctor of Philosophy

CARBON MOLECULAR SIEVES AS CATALYSTS, CATALYST SUPPORTS, AND IN ADVANCED MATERIALS APPLICATIONS

By

Gerald C. Grunewald

December 1989

Chairman: Russell S. Drago
Major Department: Chemistry

The ability of activated carbons prepared from both natural and synthetic precursors to function as molecular adsorbents has been known for a very long time. Such materials operate efficiently as general adsorbents because their pore sizes are very large and thus they are unselective. In addition to their excellent adsorption capabilities, carbonaceous materials have also been reported to catalyze dehydrogenation reactions and a great deal of work has been done with carbon based systems in advanced materials applications. For the most part, however, typical charcoal and other activated carbon adsorbents differ widely from one sample preparation to the next, are commonly poorly characterized, and generally are not considered to be chemically reactive entities.

In this study, Carbon Molecular Sieves (CMS) materials prepared from the pyrolysis of polymeric precursors have been investigated as

catalysts, catalyst supports, and in advanced materials applications. These CMS systems are shown to be active catalysts for the oxidative dehydrogenation and dehydration of a variety of substrates. In several cases, the activity of these materials exceeds that of inorganic oxide based catalysts. Metal doped CMS systems have also been studied in several different types of reactions and the CMS supports are found to have inherent advantages over the widely employed inorganic oxides. Synergistic interactions between dopant metal species and CMS supports are observed and characterized. The CMS systems have been further investigated for use as novel electrodes, electrocatalysts, and structural composites.

CHAPTER 1
GENERAL INTRODUCTION

Inorganic oxides such as alumina and silica have been widely studied and employed in a host of industrial processes as heterogeneous catalysts and catalyst supports for the past fifty years.[1-3] The introduction of synthetic zeolites in the early 1960s sparked a further surge of research into materials science and catalysis.[4] In the ensuing years hundreds of patents, books, and papers have described the application of zeolites to a plethora of separation processes and shape selective catalysis systems. Currently a new class of materials has been prepared which has the potential to equal or surpass the alumino-silicate compounds in industrial operations. Carbon Molecular Sieves (CMSs), which are produced from the controlled pyrolysis of polymers or polymeric precursors, are being actively studied. Initial investigations have shown these materials to be very effective in gas separation studies,[5-7] pressure swing absorption experiments,[8] and in a variety of catalytic systems.[9-11] Despite these encouraging preliminary results, there have been surprisingly few publications on CMS systems and the majority of these reports are in the European and Japanese patent literature.[12-17] In discussing CMS's, it is important to note that the term has been used in the literature to describe a wide variety of materials. Studies of carbonaceous compounds with sieve-like properties were reported as early as the late 1930's.[18-21] Much of this

work focused on natural organic substances such as coals and charcoals which had sorption properties generally related to their porosity. Due to their amorphous nature, however, the pore sizes of these materials ranged a great deal between samples. More versatility and reproducibility in pore dimensions were obtained through the pyrolysis of synthetic polymeric precursors. Pyrolyzed polyvinylidenechloride was determined to have slit shaped pores which were efficient in separating molecules based on steric limitations.[22] Branched hydrocarbons such as isobutane were successfully separated from their straight chain isomers. Sieves based on pyrolyzed polyfurfuryl alcohol were shown to have similar separation capacities. These materials were even employed as catalytic supports in hydrogenation reactions. In separate studies, Trimm and Cooper[23,24] and Schmitt and Walker[25] demonstrated that platinum doped pyrolyzed polyfurfuryl alcohol would selectively hydrogenate linear over branched alkenes. The catalytic hydrogenation was due to the metal, but the sieve provided the selectivity. The most effective polymeric precursor to date has been polyacrylonitrile. Sieves composed of pyrolyzed polyacrylonitrile have been established to have shape selectivities greater than 100:1 for molecules which differ by as little as 0.2 Å in their critical diameter.[26] The most recent development in carbon molecular sieve manufacturing has been the thermal activation of petroleum coke and coal tar pitch residues to produce materials with very high surface areas.[27,28]

The research described in this dissertation concentrates on three different CMS systems for use as catalysts, catalyst supports, and in advanced materials applications. Pyrolyzed polyacrylonitrile (PPAN) has

been prepared, characterized, and studied as a catalyst in oxidative dehydrogenation reactions and as a support in heterogeneous catalytic systems for synthesis gas (CO and H2) conversion. AX21, a commercially available CMS, has been characterized and studied as a catalyst in both dehydration and dehydrogenation reaction schemes and as a synergistic support in a variety of catalytic transformations. Pyrolyzed poly (2,6-dimethylparaphenylene) oxide (PPPO) has been prepared, characterized, and studied in several advanced materials applications as a novel support for new electrocatalysts and as ion selective electrodes. The specific characteristics of these materials which make them ideal for the studies described are discussed below for each of the three CMS systems.

The interesting structural and physical changes that occur during the pyrolysis of polyacrylonitrile (PAN) have been studied periodically for the last thirty years. Burlant and Parsons reported that upon thermal treatment, PAN undergoes a chemical reaction leading to discoloration and the appearance of an EPR signal.[29] IR studies attribute these observations to a cyclization and dehydrogenation process as shown in Figure 1-1.[30-37] The formation of this doubly conjugated ladder structure is believed to give the material its semiconductor nature.[38-40] Due to the ability of the condensed pyridine ring moiety of PPAN to be hydrogenated (step 4 of Figure 1-1) and subsequently dehydrogenated via air oxidation (step 5 of Figure 1-1), PPAN has been studied for a number of catalytic processes. The dehydration and dehydrogenation of alcohols,[41] the isomerization and dehydrogenation of olefins[41,42] and the dehydrogenation of ethyl

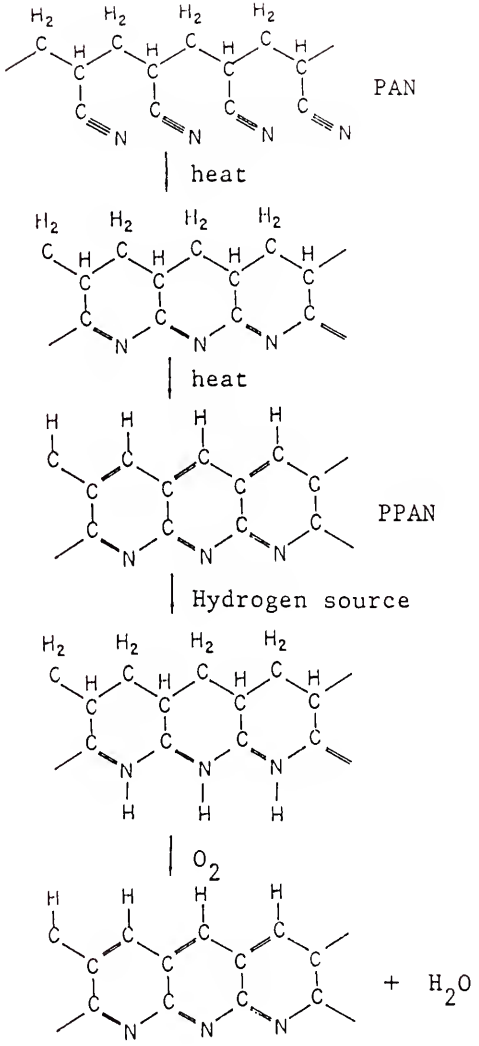

Figure 1-1. Formation and reaction cycle of PPAN.

benzene[43] have all been studied on various PPAN systems. Metal doped PPAN catalysts have also been employed for reaction schemes such as the decomposition of nitrous oxide,[44] the epoxidation of ethylene,[45] and the oxidation of cumene and ethyl benzene.[46]

AX21 is a truly remarkable CMS. It is prepared by a patented process involving the high temperature pyrolysis of polymeric petroleum coke in the presence of large amounts of KOH.[28] The surface area of this material, as measured by the standard BET method,[18] is in excess of 3000 m^2/g. This value underscores the extraordinary nature of the material. The theoretical maximum for surface area based on a monolayer of carbon including the area on both sides of the plane is 2620 m^2/g.[47] Exposure of both sides of every carbon atom is an impossibility for a solid with any physical integrity. Thus this compound is on the threshold of sensitivity for surface area measurement techniques and is among the most porous materials ever synthesized. In addition to the phenomenal surface area, AX21 also has exceptional adsorption capabilities. Studies have shown that this material has four to five times the adsorption capacity of other typical highly adsorbent carbonaceous compounds.[48-50] These properties make AX21 an attractive candidate for catalytic studies since high surface area combined with a strong affinity for a substrate are key parameters for successful catalytic systems.

Poly (2,6-dimethylparaphenylene) oxide (PPO) is a very versatile polymer which is used for a variety of purposes. The high decomposition temperature, due to the stability of the ether linkage, makes this material ideal for applications such as heat-exchange fluids and high-

temperature lubricants.[51,52] The pyrolysis of this polymer cleaves some of these ether linkages and causes a significant amount of cross-linking. This process leads to a product having functionalities such as those shown in Figure 1-2.[53] With respect to industrial lubricants and other similar applications, the formation of this highly crosslinked, completely insoluble, material is clearly not desirable. This compound is, however, potentially useful as a template in which a variety of dopants can be added and the chemistry of the dopant probed while it is contained in the pyrolyzed polymer matrix. This type of host-guest interaction has not been investigated previously for dopants such as metals or ionic salts; however, some polymer blend studies have shown that PPO can stabilize other polymers in thermal degradation studies. Polystyrene (PS) has been shown to be thermally stabilized in the presence of PPO due to a cage-like effect in which the PPO encapsulates the PS constituent.[54]

In studying these three particular CMS systems, the research centers on the novel chemical structure and reactivity of these materials which impart to them unique properties. The specific reactions and applications that are studied in this work are chosen in order to utilize these exceptional features. The focus of the research is on the treatment of CMS materials as chemical entities. Much of the work done to date has been in studying the physical nature, e.g. pore sizes and adsorption capacity, of CMS systems. The work presented here shows that the chemical reactivity of various CMS materials is quite versatile and is potentially applicable to a variety of industrial processes.

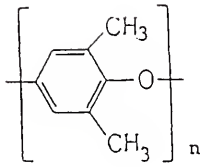

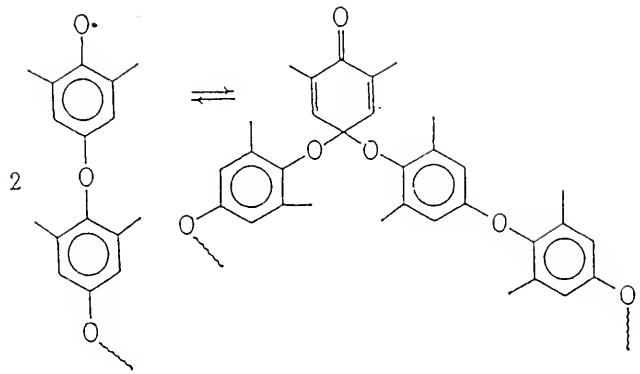

Figure 1-2. Formation of PPPO

CHAPTER 2
PREPARATION AND CHARACTERIZATION OF CMS MATERIALS

Introduction

Pyrolyzed Polyacrylonitrile (PPAN)

Although the condensed pyrdine ring structure of PPAN shown in Figure 1-1 has been invoked by virtually all researchers who have studied this material, most agree this is an over simplification of a much more complex structure.[32-37] Upon initial observation, the formation of the conjugated ladder structure appears straightforward. The nitrile group acts as a nucleophile to attack the adjacent chain. This is followed by dehydrogenation of the newly formed ring to yield the proposed structure. In practice, however, the synthetic path to PPAN has many side routes. PAN is an atactic polymer. The oligomer shown in Figure 1-1b is drawn as an isotactic fragment. When present in this configuration, the "zippering" of the backbone to form the cyclized product can readily occur. Unfortunately, PAN has not been synthesized with any large degree of stereo regularity on a bulk scale.[55,56] Some work has been done on the electrocatalytic deposition of thin PAN films on metal electrodes which is proposed to yield isotactic species, however, the polymer coating formed is only a few monolayers thick.[57,58] Clearly, any hope to use these materials as catalysts requires a

preparative method that can generate reasonably large quantities. Due to this lack of isotacticity, the bonding rearrangements that occur during the thermal process can proceed in different directions and give rise to a significant amount of crosslinking. In light of the complexity of this synthetic process, it is easy to understand why there are many variations among PPAN materials that have been reported.

In this research effort, PPAN materials are prepared for use in a variety of catalytic studies as both catalysts themselves and as catalyst supports. A number of different substrates as well as a variety of dopants are examined. Because of the nature of this work, which involves continuous comparisons to be made from experiment to experiment to optimize conditions, it is essential that the PPAN materials be the same from each preparation. Furthermore, since the proposed active species for dehydrogenation catalysis is the condensed pyridine ring structure, the preparation employed should maximize the content of this active species in the final product. The two most important parameters to control in order to accomplish these goals are the pyrolysis procedure and the nature of the carrier gas. Among the reported PPAN studies, a wide variation in heating cycles and carrier gas compositions have been employed. A lot of time has been spent in our laboratory in designing optimal conditions for reproducible PPAN preparation.

Thermo-Gravimetric Analysis (TGA) and Differential Scanning Calorimetry (DSC) were carried out by Jeff Clark at the University of Florida and the results are described in this Ph.D. dissertation.[59] This work was used to help design a suitable pyrolysis procedure. In

isothermal TGA studies, weight loss occurs sooner and to a greater extent as heating temperature is increased in successive experiments. Temperature programmed TGA work shows similar results. Faster heating rates cause increased weight loss. The DSC studies compliment the TGA experiments. The onset of weight loss corresponds to a large exotherm. In isothermal studies, the sharpness of the exotherm increases with temperature. Temperature program DSC work shows that the size and specific temperature of the exotherm are directly proportional to scan rate. The simultaneous weight loss and exotherm are proposed to be due to the cyclization of the nitrile groups. Further weight loss and a much smaller exotherm are due to the last dehydrogenation step. It is clear from these results that the heating process should be done in stages and that the progression from step to step should be done very slowly. If the heating rate is too fast, the exothermicity of the process will cause a runaway reaction leading to large weight loss, extensive crosslinking and the formation of a very complicated network.

The pyrolysis profile shown in Figure 2-1 is found to yield samples which are reproducible in their color homogeneity (black), EPR signal (very intense organic radical with g = 2.01), elemental analysis, and Infrared spectra. This heating cycle is different from that employed in most of the reported studies. Several of the literature preparations invoke simply heating isothermally at 200-250^{0} C for a few hours.[38,39,46,57] Another common preparation involves a two-step process where the sample is initially heated isothermally at 200^{0} C in an air atmosphere and then subsequently heated at 400^{0} C in a N_2 atmosphere.[31-37] It has been our experience that the first of these

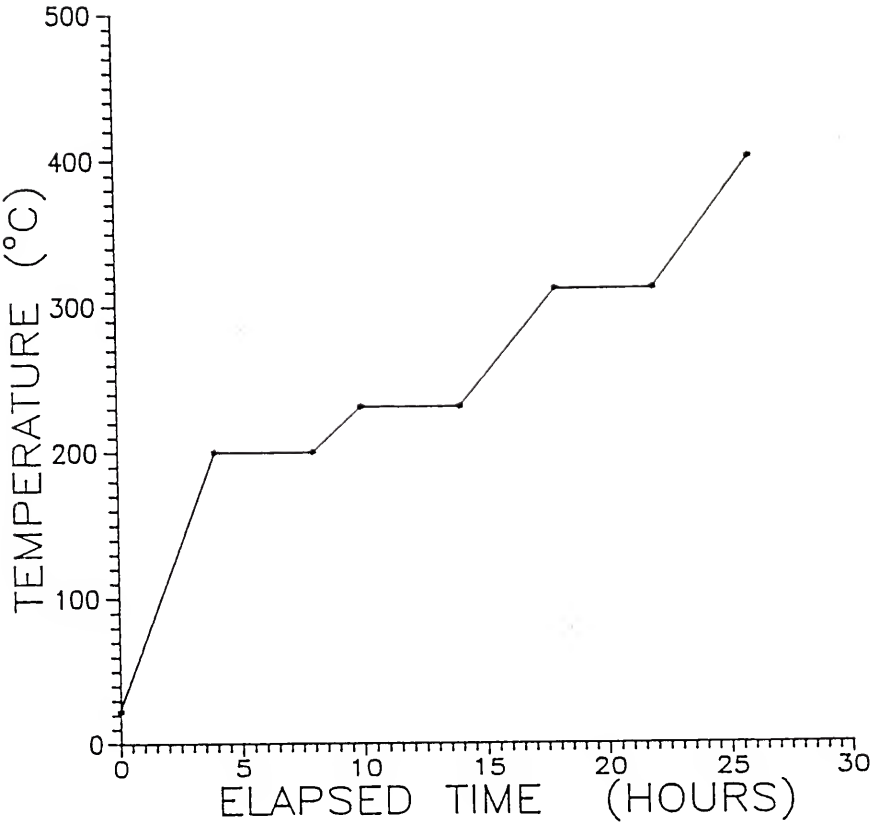

Figure 2-1. Pyrolysis profile of PPAN.

methods does not fully pyrolyze the sample. The color of the product is usually brownish and there is still a significant amount of nitrile functionality observed in the IR of the product. The second method does yield a homogeneous black product with no nitriles remaining; however, both elemental analysis and IR show that there is a lot of oxygen incorporation in the final material.

The presence of oxygen in the end product has proven to be a ubiquitous observation among PPAN samples prepared under a variety of conditions. Table 2-1 contains the elemental analysis results of PPAN samples pyrolyzed in several different carrier gas atmospheres. It is evident that the product is quite sensitive to oxygen incorporation even under what should be anaerobic conditions. There is a significant amount of disagreement in the literature over this observation. Grassie and McGuchan pyrolyze in a N_2 atmosphere and still observe the presence of oxygen.[32-34] They invoke a pyridone type structure such as that shown in Figure 2-2 to account for this. Coleman and Petcavich observe the presence of oxygen containing species even when the pyrolysis is carried out under reduced pressure.[35] Rafalko as well as Chung and co-workers, however, report elemental analyses consisting of over 99% C, H, and N.[36,37] In comparing these various literature results to the present work, again there are important experimental differences to be noted. All the literature studies cited use thin films of PAN weighing about 100 mg. In order to produce enough material for a series of catalytic experiments from the same batch, it is necessary to use 5-7g of PAN in the pyrolysis step. This large sample size makes it difficult to remove all intestitial air which is felt to be the source of the

Table 2-1 Elemental Analysis of PAN Pyrolyses in Various Carrier Gases

SAMPLE	PYROLYSIS ATMOSPHERE	%C	%H	%N	TOTAL
1	before pyrolysis	67.10	5.86	26.16	99.12
2	N_2	69.73	2.95	21.07	93.75
3	air	65.02	3.19	22.64	90.85
4	NH_3	69.99	3.15	22.38	95.47
5	CO	69.76	2.70	21.05	93.51

The non C, H, or N constituent is found to be O.

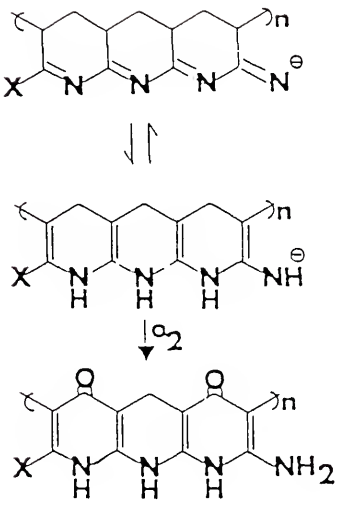

Figure 2-2. Formation of pyridone moieties in PPAN structure.

incorporated oxygen. Due to the exothermicity of the structural transformations, it is not advantageous to tightly pack pyrolysis tubes. When the samples are packed together, the heat generated from the first cyclization raises the temperature of the system too quickly and causes undesirable charring. Thus, the PAN powder is layered out in a horizontal pyrolysis tube.

The presence of the oxygen would suggest that there is a significant amount of the pyridone moiety in the product prepared in this work. Infrared studies, however, do not support this. Figure 2-3 shows the complete spectrum overlay of both PAN and PPAN. The key comparative features are the loss of the C≡N stretch at 2240 cm^{-1} and the growth of broad peaks from 1600 - 1200 cm^{-1}. These can be assigned to the various C=C, C=N, and C-C, C-N functionalities. Figure 2-4 is an expansion of the essential double bond region. This spectrum is displayed in the absorbance mode so that it can be directly compared to the spectrum reported by Coleman and Petcavich.[35] The absence of broad shoulders in the 1700 cm^{-1} region, which is indicative of C=O stretches resulting from pyridone moieties, suggests that there is not an appreciable amount of pyridone functionality in the samples prepared by our method. The oxygen present may be involved in chain terminating hydroxyl species, since there are broad absorptions above 3200 cm^{-1}.

After devising a method of preparing reproducible PPAN samples with a large amount of condensed pyridine ring functionalities, the next goal was to increase the surface area of the product. Results of studies employing PPAN materials as catalysts and catalyst supports are discussed in the following two chapters. One of the key parameters for

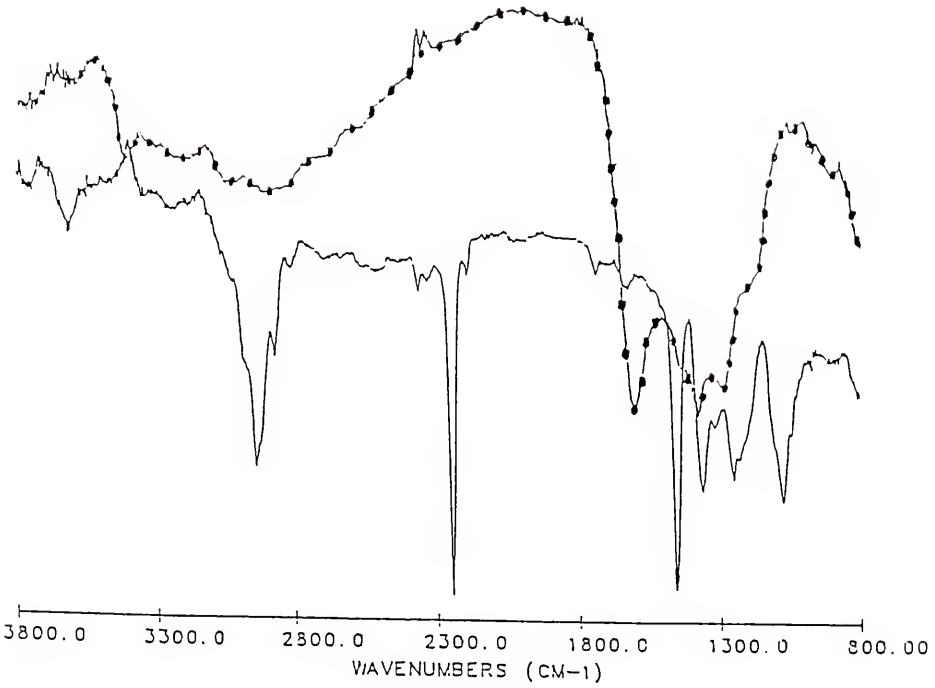

Figure 2-3. DRIFT spectra of PAN and PPAN.

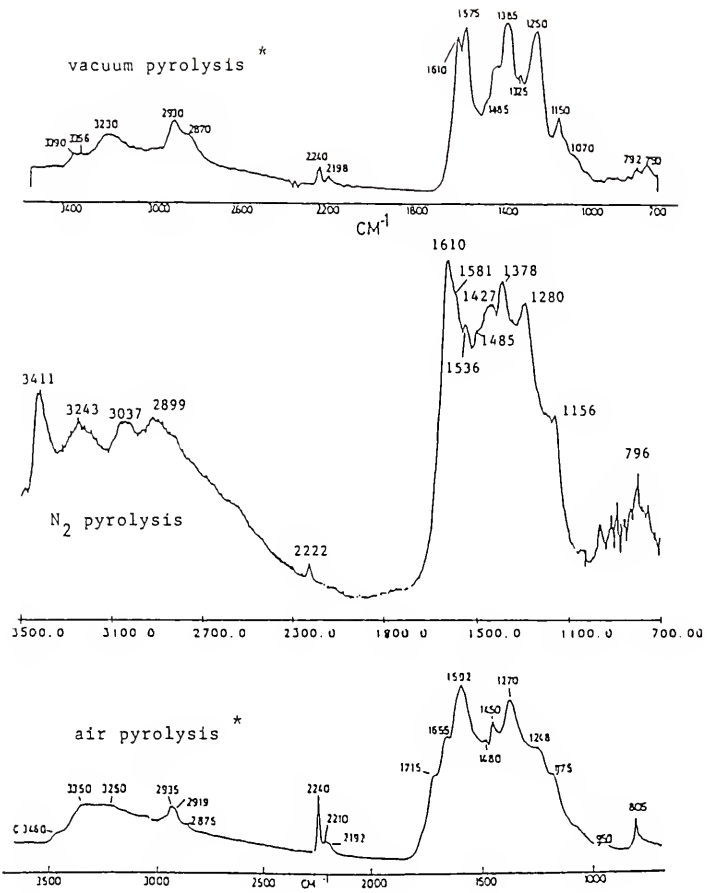

Figure 2-4. Infrared comparison of PPAN samples prepared under various conditions.

either of these applications is to have as high a surface area as possible. The pyrolysis of PAN according to the method described here, as well as the various literature methods, yields a product with a very low surface area. Reported surface areas range between 8-17 m^2/g. The PPAN samples prepared in this study are found to have surface areas in the 9-12 m^2/g range. In order to increase these values, a series of co-pyrolysis agents are investigated. Table 2-2 outlines the effects various dopants have on the surface area of the final PPAN product. It is evident that the most success is achieved with a 50-50 mixture of PAN and NH_4Cl. NH_4Cl decomposes to NH_3 and HCl during the pyrolysis procedure. As the gases volatilize out, they create channels which greatly increase the surface area. Since the decomposition of NH_4Cl occurs at 360^o C, it is an excellent dopant to employ. The final dehydrogenation step leading to the fused pyridine ring structure is proposed to occur between 300-320^o C. Thus the volatization of the dopant occurs after the desired structure is formed. The surface area of this material is 50 m^2/g which is about an order of magnitude higher than the undoped PPAN. IR and elemental analysis on the product of this doped sample verify that all of the dopant is removed by the end of the pyrolysis procedure. Catalytic studies (vide infra) show that this higher surface area increases the reactivity of the sample.

AX21

The AX21 carbon molecular sieve is purchased from the Anderson Development Company. The material is made by a direct chemical activation route in which petroleum coke is reacted with excess KOH at

Table 2-2 Surface Area of PPAN Samples

SAMPLE[a]	DOPANT	SURFACE AREA m^2/g
PPAN 1	none N_2 pyrolysis	8
PPAN 2	none air pyrolysis	10
PPAN 3[b]	50% NH_4Cl	50
PPAN 4[b]	50% NaCl	28
PPAN 5[b]	50% sucrose	17

a) These sample names will be used throughout the rest of this text when describing particular PPAN material.

b) These pyrolyses are all done in N_2. Dopant percentages are based on weight. The samples are stirred in 300 ml H_2O after pyrolysis to wash out any remaining dopant material.

500° C. This produces an intermediate product that is subsequently pyrolyzed at 900° C to yield active carbon which contains potassium salts. These salts are removed by successive water washings. More detail on the preparation of this material is reported elsewhere.[60] Since the AX21 material is commercially available, most of the characterization studies have been done by the producer. A list of the more relevant ones to catalytic studies is given in Table 2-3. As was mentioned in Chapter 1, the reported surface area of this material is known to have been overestimated. The theoretical maximum for a carbonaceous material is 2620 m^2/g.[47] This inflated value, however, exemplifies the unusual nature of this material.

Transmission Electron Microscopy (TEM) shows this material to be composed of interwoven carbonaceous lamellae that form a three dimensional network with molecular size channels throughout.[61] These channels produce pores which give the material its sieving properties. Unlike standard activated charcoals, the pores of the AX21 material are considerably smaller and have a very narrow size range. The pore size for AX21 is 5-7 Å, whereas that for typical bone charcoal can range from twenty to several hundred Å.[62] Another difference between the AX21 compound and other typical carbonaceous adsorbents is its incredible adsorption capacity. Studies have shown this material to be far more adsorbent than other widely used CMS compounds.[48-50]

Outside of the adsorption properties and pore structure, these materials have proven to be rather difficult to characterize--particularly from a chemist's point of view. Even elemental analysis, a seemingly facile technique, became more difficult than anticipated.

Table 2-3 Physical Properties of AX21

Surface Area, BET,	m^2/g	2800 - 3500
Total Pore Volume,	ml/g	1.4 - 2.0
Bulk Density,	g/ml	0.27 - 0.32
Screen Analysis:		
passes 100 mesh,	wt%	90 - 99
passes 200 mesh,	wt%	70 - 85
passes 325 mesh,	wt%	55 - 70

Table 2-4 lists the elemental composition of a very dry AX21 sample. To obtain this data, the sample had to be run at least three separate times for all the elements and a total of five times for the carbon quantification. The necessity of the subsequent runs was not that the sample was heterogeneous, but rather that it didn't always combust completely. Some of the carbon became refractory, i.e. non-combustible, and thus led to inaccurate results. The 2.5% elemental composition which is unaccounted for in Table 2-4 is felt to be due mostly to the carbon not fully combusting, as opposed to the presence of other impurities not screened for in the analysis. The experimental support for this contention comes from Electron Diffraction Spectroscopy (EDS) which was done in conjunction with Scanning Electron Microscopy (SEM) on several of the metal doped AX21 samples. The results of these studies will be discussed in more detail in Chapter 4, but it serves to mention here that no other elements, outside of the metal dopant and those listed in Table 2-4, were observed in any of the elemental analysis scans from EDS.

Other common characterization techniques such as IR and EPR do not reveal much information. Unlike PPAN, which can be studied quite well with the DRIFT technique, AX21 displays a completely featureless spectrum. Since elemental analysis shows in excess of 6% oxygen content, it is surprising that no hydroxyl, carbonyl, ether, or any other oxygenated chromophore is observed. IR analysis is even more unusual when doped AX21 samples are attempted. Figure 2-5 shows the spectrum overlay of MoO_3 alone and MoO_3/AX21 in transmittance mode. As is shown, the spectrum for the latter system appears as an inversion of

Table 2-4 Elemental Analysis of AX21

%Carbon	89.23[a]
%Oxygen	6.18
%Hydrogen	0.00
%Nitrogen	0.01
%Sulfur	0.24
%Ash	1.84[b]

Note: The cumulative error associated with all these separate analyses causes the theoretical maximum total to be only 99%.

a) Values varied from 88.6 - 91.2%.

b) Values varied from 1.29 - 2.39. Composition is virtually all potassium.

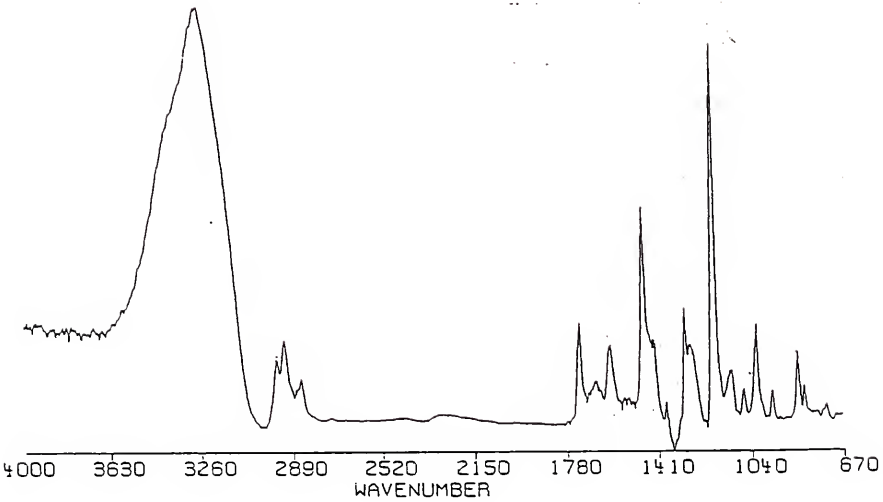

Figure 2-5. Infrared spectrum of PPO before pyrolysis.

the dopant. Apparently, the AX21 material absorbs all of the IR energy via some type of charging mechanism. In all the DRIFT experiments the sample is mixed with about a hundred fold excess of KBr. Thus, the total absorption is not due to the opaqueness of the sample. In fact the reflected beam throughput of the AX21 samples is higher than many of the PPAN samples. The total absorption of the IR energy is due to the AX21 material and is not an instrumental artifact.

Since the PPAN samples are highly paramagnetic and AX21 is prepared from pitch residues, it was expected that the latter material would also have an intense delocalized organic radical signal in its EPR spectrum. Initially it was difficult to obtain a spectrum at all because the samples absorb H_2O so readily. When excessively dry, however, the AX21 material is observed to have no paramagnetic content.

Much characterization work has been done on the metal doped AX21 system. The results of X-ray Diffraction (XRD), X-ray Photoelectron Spectrocopy (XPS), and Scanning Electron Microscopy (SEM) are discussed in Chapter 4. For the most part though, these techniques characterize the dopant and its interaction with the AX21 support more than the AX21 material itself. Several new methods are currently being applied to these materials which may prove to be quite informative. ^{129}Xe NMR, which can yield information regarding the chemical nature of the pore site environment, is just beginning to be investigated by several research groups.[63-67] Although there have not been any studies published on CMS systems yet, this may prove to be a promising technique in the future. Titrametric calorimety is another method which can yield fundamental chemical information on solid materials. Drago and co-

workers have studied a Pd/charcoal system and have been able to quantify the acidic nature of this material.[68] The extension of this technique to CMS materials such as AX21 could provide a wealth of information.

Pyrolyzed Poly (2,6 dimethylparaphenlyene) oxide (PPPO)

As is shown in Figure 1-2, the pyroloysis of poly (2,6-dimethylparaphenlyene) oxide (PPO) produces a highly crosslinked matrix. The major experimental evidence to support this proposed structure comes from Pyrolysis IR studies. Figure 2-6 shows the IR spectrum of PPO at three different temperatures during its pyrolysis. It is evident that there is no real change in the general features of the spectrum as the material is pyrolyzed. The only noticeable variation is a gradual decrease in the intensity of all the peaks. Concomitant with this overall decrease in intensity, is the observation of a color change from white to yellow to eventually black. This darkening of the sample is the cause of the decrease in intensity. Unlike PPAN, pyrolysis does not bring about any new functional moieties, but rather just rearrangements of the ether linkages to produce a highly interwoven, template structure.

The advanced materials applications discussed in Chapter 5 involve the entrapment of various metal and ionic species in the cavities of the PPPO matrix. To verify that the presence of the dopants does not change the nature of the PPPO structure, Pyrolysis IR studies were done on both Fe(0)/PPO and LiCl/PPO composites. In both cases, the spectra do not differ from that of the PPO itself. EPR spectroscopy done on the undoped material shows a very large delocalized organic radical with a

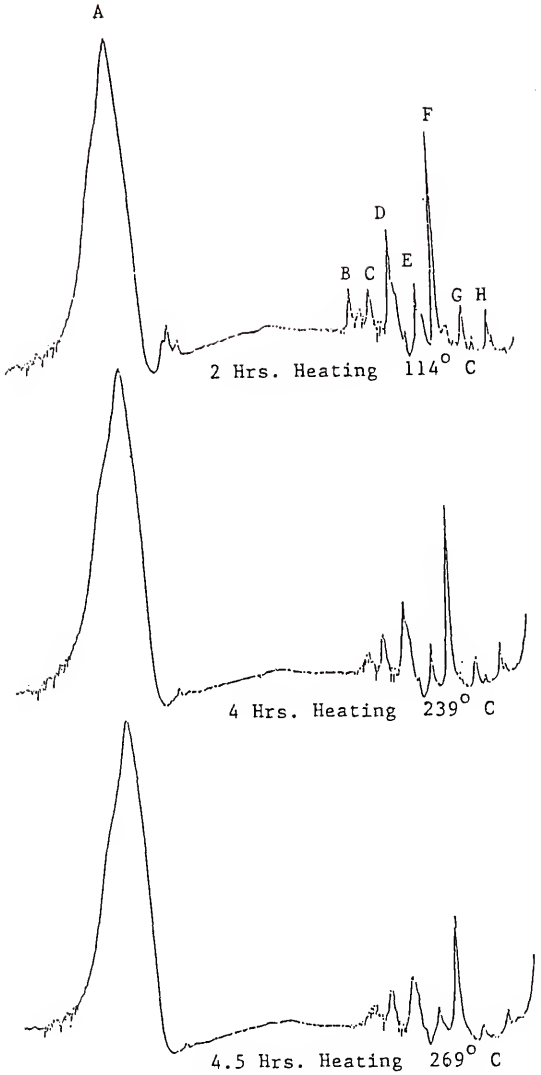

Peak	cm^{-1}
A	3258
B	1729
C	1605
D	1469
E	1306
F	1189
G	1020
H	857

Figure 2-6. Infrared spectra of PPO during pyrolysis.

g value of 2.01. This is essentially the same as that for the PPAN material.

Thermo-Gravimetric Analysis (TGA) and Differential Scanning Calorimetry (DSC) were conducted on the undoped and several of the doped composites. The TGA shows virtually no weight loss until 330^{o} C in any of the samples. As is discussed in the experimental section of this chapter, the pyrolyses in this study are done isothermally at 250^{o} C. This lack of any weight loss supports the proposal that the sample just crosslinks and does not produce any significant amount of volatiles. The DSC results are worthy of further discussion. Figure 2-7 shows the DSC for the PPO material itself. It is evident that there are essentially no endo- or exothermic processes occurring in the temperature range studied. A very small endotherm is detected at 210^{o} C, but this is on the threshold of the instrumental limitations. Figure 2-8 displays the DSC for a Ti(0)/PPO sample. Again the spectrum is virtually nondescript save an even smaller endotherm at 210^{o} C. Thus the polymer itself and zero valent metal doped composites undergo no discernable thermochemistry in the temperature range of interest. Samples containing doped metal salts, however, behave significantly different. Figure 2-9 shows the DSC for a LiCl/PPO composite. There is a reasonably large endotherm at 247^{o} C. The heat absorbed by the system corresponds to 10.33 J/g. Figure 2-10 displays the DSC for a $CoCl_2$/PPO composite. Like that of the LiCl doped system, there is an appreciable endotherm. The peak maximum occurs at 246^{o} C and has a value of 13.55 J/g. Each of these DSC studies were run several times and were found to be quite reproducible. Slower, faster, or isothermal heating

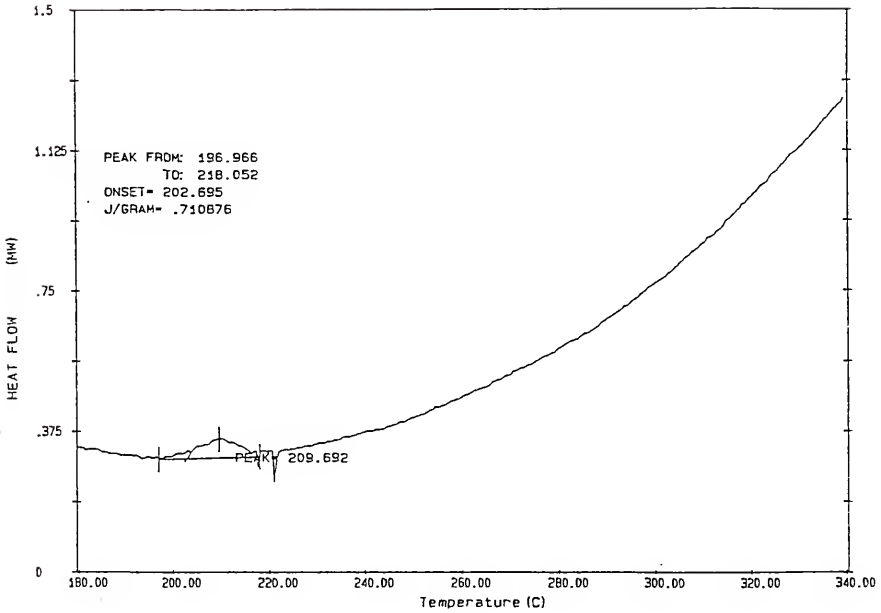

Figure 2-7. DSC of undoped PPO.

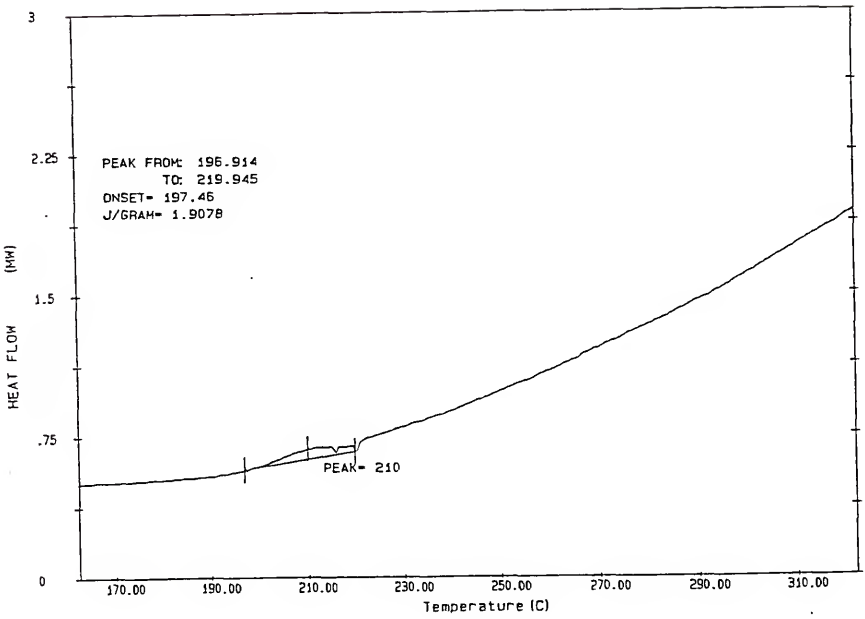

Figure 2-8. DSC of Ti(O) doped PPO.

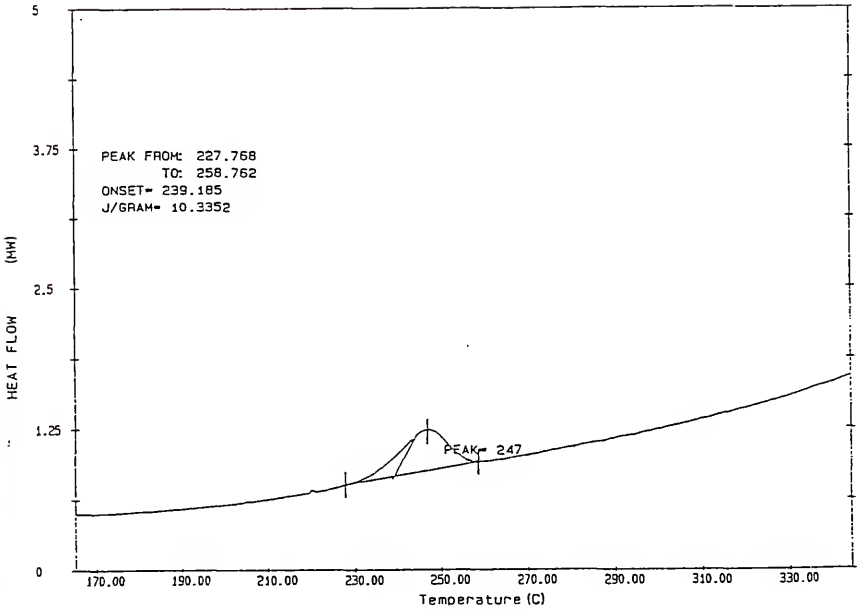

Figure 2-9. DSC of LiCl doped PPO.

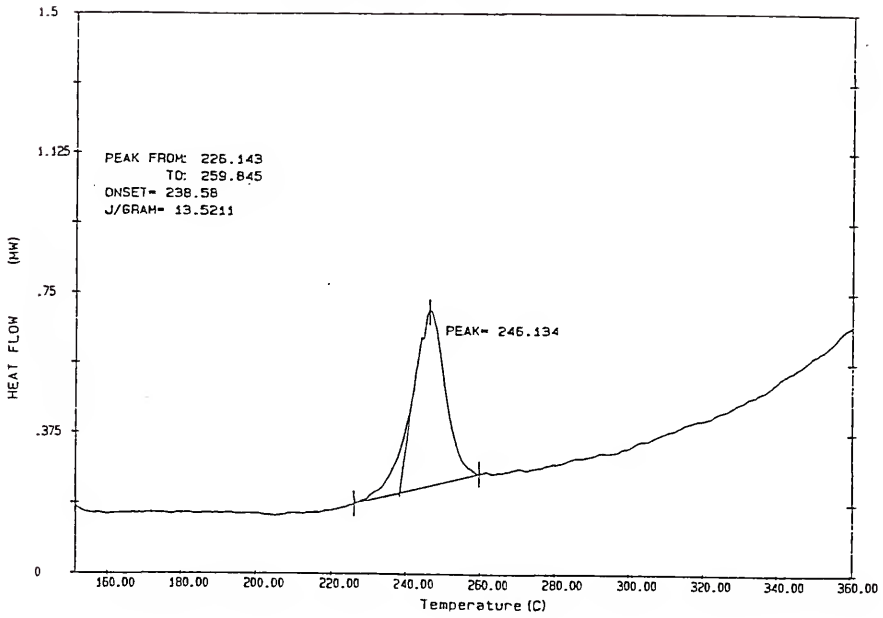

Figure 2-10. DSC of $CoCl_2$ doped PPO.

made little or no difference in the peak height or peak location in any of the samples. These results suggest that there is some process driven by entropy occurring with the salt doped samples that is not going on in the other systems. This is most likely associated with the dissolution of the ionic dopant in the polymer matrix. The majority of the endotherm would be a function of the lattice energy of the salt with some minor contributions possibly coming from structural rearrangements of the PPO matrix to accommodate ionic species. Since the endotherm is greater for a divalent ion than a monovalent ion, the is support for the proposal of lattice energy being an essential component of the process.

Experimental

PPAN

Polyacrylontrile samples were purchased from both Aldrich and Polysciences. Additional samples were prepared by the radical initiated polymerization of acrylontrile according to literature methods.[31] No significant differences were observed in the PPAN product prepared from the various PAN sources. The pyrolyses were carried out in a horizontal tube furnace. Typically 5g of the sample were layered out in a pyrex tube fitted with a male 24/40 ground glass joint at one end and tapered to a standard size hose connection spout at the other. Initially a sintered glass frit was employed at the tapered end, but these were very difficult to clean and often retained the liquid effluents of the pyrolysis degradation products. Subsequent runs simply employed a small glass wool plug at the tapered end. The PAN sample is slowly poured in

and layered out over a 3-4 inch space. This sample is usually not in contact with the glass wool plug. As mentioned previously, tightly packing the sample into the tube is not advantageous because the exothermicity of the process causes packed sample to char. Carrier flow (10 ml/min) is maintained through the pyrolysis tube by fitting a specially made cap on the end with the ground glass joint. This cap consists of a 24/40 female joint with 2 septa holes. The carrier gas line is attached to one end; the thermocouple is placed through the other. A Type J thermocouple is used with the end of the stick in contact with the sample bed. The temperature is maintained by an Omega CN 2000 programmable temperature controller which conducts the pyrolysis according to the temperature profile in Figure 2-1. A bleach bubbler is attached to the out gas end in order to deactivate the various Cyano moieties that are evolved during the pyrolysis procedure.

The various co-pyrolyzed samples discussed in Table 2-2 were prepared by grinding the appropriately weighted mixtures in a mortar and pestle and then placing them in the pyrolysis tube as usual. The samples co-pyroloyzed with NaCl were then stirred in 500 ml of H_2O overnight to wash out the salt.

Diffuse Reflectance Infrared Fourier Transform (DRIFT) spectroscopy was done on a Nicolet 5 DXB FTIR spectrometer fitted with a Barnes Analytical Diffuse Reflectance unit. Samples were mixed with at least a hundred fold excess of KBr in order to allow more signal throughput. The spectra were referenced against a pure KBr background. Electron Paramagnetic Resonance Spectroscopy was done on a Brukker EPR operated at room temperature. Elemental Analysis for C, H, and N were

performed by the University of Florida Department of Chemistry Microanalytical service. Analysis for oxygen content as well as routine checks on the C, H, and N data were done by Desert Analytics Microanalytical Laboratory of Tuscon, Arizona.

AX21

As mentioned earlier, this sample was purchased from Anderson Development Company of Adrian, Michigan. The samples were dried in vacuo at 100^{0} C for several hours prior to use. The complete elemental analysis was done by Desert Analytics.

PPPO

The sample was purchased from Polysciences Company. The pyrolysis was performed isothermally at 250^{0} C in either the same apparatus as the PAN samples or in a standard muffle furnace. Since many of the applications for the material required the use of pellets of the composites, samples were pressed in a 1 cm die at 10,000 psi on a Carver Laboratory Press prior to pyrolysis. Composites made with metallic species such as Fe(0) or Ti(0) were simply mixed by grinding in a mortar and pestle. Ionically doped composites such as LiCl/PPO were prepared by co-dissolving the appropriate mixtures of the materials (8% by weight doping was commonly used) in an azeotrope solvent composed of 7% C_2H_5OH in $CHCl_3$. This azeotrope works quite well because the ethanol dissolves the inorganic salt and the chloroform dissolves the polymer. When the solution becomes homogeneous (usually after about 15 minutes of stirring) the azeotrope solvent is rotovapped off. This method allows

coprecipitation of the dopant and support species and thus affords excellent dispersion.

The pyrolosis FTIR work was graciously performed by Professor Thomas Brill at the University of Delaware. The TGA and DSC studies were graciously conducted by Professor Michael Babich at the Florida Institute of Technology.

CHAPTER 3
CARBON MOLECULAR SIEVES AS CATALYSTS

Introduction

This chapter focuses on three different types of substrates and their reactivity with the CMS catalysts PPAN and AX21. An alkyl aromatic compound, ethyl benzene, has been studied in the dehydrogenation reaction to produce styrene. A linear olefin, butene, has been investigated in dehydrogenation studies to form butadiene. Lastly, a series of C_3 oxygenated compounds -- n- and iso-propanol, propionaldehyde, and acetone -- have been studied in dehydration and dehydrogenation reaction schemes. The first two of these catalytic transformations are large scale industrial processes. In 1987, the industrial production of styrene was 8,014 million pounds and that of butadiene was 2,931 million pounds. Estimates for the production in 1989 are even higher; 8,900 and 3,175 million pounds respectively.[69] The catalysts typically employed for all of these processes are composed of inorganic oxides.

The dehydrogenation of ethyl benzene to styrene can be accomplished by two different catalytic routes. The straightforward dehydrogenation, shown in equation 3-1below, is used for virtually all industrial production.[70,71]

$$(C_6H_5)CH_2CH_3 \text{ ----> } (C_6H_5)CH{=}CH_2 + H_2 \quad \Delta H^{o}_{800K} = 124kJ \qquad (3\text{-}1)$$

As is shown, this reaction is endothermic and is limited by equilibrium. In order to achieve acceptable conversions, high temperatures are required (in excess of 600^{o} C). Additionally, super-heated steam must be used as an additive. This provides extra heat needed for the reaction; reduces the ethyl benzene and hydrogen partial pressures to maximize yield; and keeps the catalyst clean and active. The catalyst employed is a promoted iron oxide system.[72,73] In a typical reaction scheme employing this catalyst, conversion is about 50% with over 90% selectivity to styrene.

In spite of the thermodynamic limitations, there are several advantages to the straightforward dehydrogenation from an industrial standpoint. Catalysts lifetimes are very long. Typical industrial catalysts can last 2-3 years in continuous operation. Catalyst producers consider a lifetime of least one year as a virtual requirement for any potential catalyst systems.[74] Another advantage to the direct dehydrogenation is that H_2 is obtained as a byproduct. In many industrial schemes this is used as a fuel to provide some of the heat required for the reaction.

Despite the long-standing success of the straightforward dehydrogenation reaction scheme, there has recently been a great deal of interest in the oxidative dehydrogenation process.[75-83] In the presence of O_2 (usually as air), the dehydrogenation is quite exothermic as a result of the formation of H_2O as a byproduct. This reaction is shown below in equation 3-2.

$$(C_6H_5)CH_2CH_3 + 1/2\ O_2 \text{ ---> } (C_6H_5)CH{=}CH_2 + H_2O \quad \Delta H^{o}_{800K} = -119\ kJ \quad (3\text{-}2)$$

Due to the favorable thermodynamics of this reaction scheme, the process should be able to operate at lower temperatures and complete conversion is theoretically possible.

As with the direct dehydrogenation, the systems most often studied for the oxidative process are based on promoted inorganic oxide catalysts. One of the major drawbacks of the early systems studied for this pathway is that selectivities are low. Since the primary use of styrene is as a monomer for polystyrene production, it is essential that the selectivity be very high in order that any small amount of side products can be completely removed. The bismuth - molybdenum catalyst, which is an industry standard for mild oxidations, has a selectivity of only about 50% in this reaction.[78] Recent studies employing other inorganic oxide systems, however, have shown much improvement with regards to selectivity. Murakami and co-workers have studied a SnO_2 - P_2O_5 catalyst and found it to have moderate activity--greater than 30% conversion with greater than 80% selectivity--at 550^{o} C.[78-80] Their work has particularly focused on the role promoters play in modifying the acid-base properties of the catalysts. Emig and Hofmann have reported a ZrO_2 - P_2O_5 system which is slightly more active in the same temperature range -- conversions up to 55% with over 80% selectivity.[83] Vrieland has similarly worked with phosphate promoted catalysts and has recently reported a cerium pyrophosphate system which exhibits 76% conversion with 90% selectivity at 605 ^{o}C.[74,81]

In addition to focusing on the acid-base properties of the system, the latter two studies also investigated the role of carbonaceous overlayers on the surface of the catalyst. It was determined that each of the various systems studied had an induction period during which a thin uniform layer of carbon built up on the surface. A subsequent study suggested that the nature of the layer is a circular pattern of condensed rings.[81] In another recent study, Cadus and co-workers similarly found carbon overlayers present on a sodium doped alumina catalyst.[82] They provide a mechanism to show how the carbonaceous species, not the inorganic oxide, bring about the catalytic transformation.

Since the actual catalytic surface is primarily carbon and carbonaceous substances such as charcoals have been known for a long time to have some dehydrogenation ability,[84,85] it is possible that the bulk of the catalytic reactivity in such systems is a function of the carbon. The major role of the inorganic oxide constituents may merely be to modify the acid-base properties of the carbon. This is the premise for employing CMS catalysts in the oxidative dehydrogenation of ethyl benzene to styrene.

As mentioned previously, the dehydrogenation of butene to butadiene is a widely studied industrial process. The typical catalyst is a mixture of Bi_2O_3 - MoO_3 which is usually referred to as bismuth molybdate. This system requires a reaction temperature of at least 500^{o} C to yield a conversion of 40% with 95% selectivity.[86] The process is virtually always done via an oxidative route as shown by the reaction below:

$$CH_2=CH-CH_2-CH_3 + 1/2\ O_2 \text{ -----> } CH_2=CH-CH=CH_2 + H_2O \quad (3\text{-}3)$$

Recently a number of other inorganic oxide based systems have been shown to be even more active under similar reaction conditions. Lambert and Germain report that a tin cadmium phosphate catalyst exhibits 88% conversion with 71% selectivity at 470° C.[87] Herniman and co-workers have employed a tin antimony mixed oxide catalyst and have observed comparable activity.[88]

The mechanism that is commonly invoked for these mixed oxide catalysts focuses on lattice oxide ions as the active sites where adsorption and dehydrogenation of the alkene occur.[89] The role of the gaseous oxygen reactant is to reoxidize the catalyst. This is accomplished by dissociation on the surface to form oxide ions and then diffusion through the bulk to the active site.[90] It is fairly well established from kinetic studies that the reaction is zero order in oxygen at oxygen to butene ratios above 0.5.[91]

In light of the proposed mechanism for inorganic oxide catalysts which utilizes the oxide species to a significant extent, one would initially conclude that CMS based catalysts should not have much reactivity in butene dehydrogenation schemes. Alternatively, if CMS systems are active, other mechanistic interactions would seem more plausible. CMS systems have, however, been shown to be active for butene conversion and an oxide migration type mechanism has been proposed. Ademodi and co-workers report that a PPAN based system oxidatively dehydrogenates butene to butadiene to about 35% conversion at 350° C with essentially 100% selectivity.[92] The mechanism is not

fully delineated, but it is proposed to involve adsorption, dissociation, and migration of oxygen species through the sieve material. Since AX21 is far more porous than PPAN and since it contains an appreciable amount of oxide functionalities, this should also be an interesting system to study for the conversion of butene to butadiene.

The final class of substrates to be investigated in this chapter, the various alcohol and related oxygenated compounds, are not nearly as attractive from an industrial standpoint as ethyl benzene or butene. There are far better ways of producing large scale quantities of propylene, for example, than dehydrating n- or isopropanol. In fact, this is opposite of the usual direction such catalytic transformations are pursued--oxygenated products are typically more desirable. The study of such reaction sequences is nonetheless beneficial. By examining a variety of substrates, a better understanding of the reactivity of CMS catalysts can be obtained. Furthermore, the series of C_3 compounds offers the gamut of organic functionalities: straight-chain alcohol, branched-chain alcohol, aldehyde, and ketone. An analysis of the reactivity of these catalysts towards the respective compounds, as well as the nature of the product distributions, should provide a handle on the mechanistic interactions that are occurring.

The study of the alcohol substrates also offers a further opportunity to compare the reactivity of CMS catalysts to inorganic oxide systems. Much work has been done with various Al_2O_3 based catalysts in alcohol dehydrogenation and dehydration reaction schemes.[93,94] The activity is a function of the Lewis acidity of the catalyst with the products being formed via carbocation intermediates.

Although carbonaceous materials are not usually considered to have much Lewis acidity, several studies have shown carbon based catalysts to be active for alcohol substrates with reaction pathways similar to the inorganic oxide systems. A thorough examination of the reactivity of these substrates over both types of catalysts should provide a better understanding of their similarities and differences in catalytic transformations.

Experimental

Reagents

Ethyl benzene was purchased from Fisher Scientific Company and was purified by vacuum distillation prior to use. Several later experiments were performed with ethyl benzene samples that were not vacuum distilled and the results were the same as in the purified systems. 1-Butene was purchased from Matheson Gas Products as C.P. grade with 99.0% minimum purity. Samples were checked by gas chromatography (GC) to verify that there were no detectable impurities present. Ethanol, 200 proof, was purchased from Florida Distillers Incorporated and was dried over 4 Å molecular sieves prior to use. n-Propanol, iso-propanol, and propionaldehyde were all purchased from Eastman Kodak Company as reagent grade and were dried over 4 Å molecular sieves prior to use. Each sample was checked by GC to verify purity. Reagent grade acetone was purchased from Fisher Scientific and was dried in the same manner as the other substrates prior to use. Other chemicals employed as GC standards for product verification--benzene,

toluene, butadiene, diethyl ether, acetaldehyde--were reagent grade and used as received.

Preparation of Catalysts

The PPAN samples were prepared as described in the previous chapter. AX21 samples were dried in vacuo at 100 ^{o} C for at least 8 hours prior to use. Unused portions were stored in a desiccator for future experiments.. The activated charcoal (AC) material was purchased from Mallinckrodt Incorporated and was dried in vacuo in the same fashion as AX21. The AC material has a nominal surface area of 800 m^2/g. Al_2O_3 was chromatographic grade and was purchased from Davisson. It was calcined at 350^{o} C prior to use. The nominal surface area of the Al_2O_3 sample is 360 m^2/g. The cerium pyrophosphate catalyst was synthesized from $Ce(SO_4)_2$ (Alfa) and H_3PO_4 (Fisher Scientific) according to the method of Vrieland.[74] The industrial mixed oxide catalyst--93% Fe_2O_3, 5% Cr_2O_3, 2% KO_2 on MgO--was prepared according to the method of Ghublikian.[95] All the oxide samples were purchased from Fisher Scientific and used without further purification.

Reactor

The reactor is a fixed-bed flow reactor modelled after that designed and described by Clark.[59] For the butene system, the butene and air reactants are mixed through a two-stage glass bubbler and then the blended gas stream is fed into the reactor. In all the other systems, the substrate is delivered as a liquid via a syringe pump. The pump is also modelled after a design by Clark,[59] but additionally is

fitted with an adjustable gear box which enables variable flow rates to be administered. Temperature is monitored by a thermocouple (type J connected to an Omega Engineering CN 300 temperature controller) which is encased in a glass tube that is in contact with the catalyst bed. Unless otherwise stated, 0.5g of catalyst is used in each experiment. Catalyst bed height is approximately 30 mm for all CMS systems. A schematic diagram of the reactor setup is shown in Figure 3-1.

In the liquid feed systems, a six inch layer of glass beads (Fisher Scientific) is placed on top of the catalyst to facilitate complete vaporization of the substrate and to allow thorough mixing with the carrier gas before contact with the catalyst. Liquid products are condensed in a trap that is maintained at 0^{o} C. Blank experiments in which the system was set up with the reactor tube filled with glass beads were run for all substrates. No activity was observed in any of these blank systems.

Analysis

Routine product analysis is done via gas chromatography. Pre-catalyst and post-catalyst gas samples, as well as post-catalyst liquid samples, are periodically examined for each experiment. Typical injection sizes are 0.5 ml for gas samples and 0.15 ul for liquid samples. For the ethyl benzene experiments, a Varian 3400 GC fitted with a 3m Dega S column and a Flame Ionization Detector is employed. The column temperature is ramped from 75 - 150^{o} C at 10^{o}/min. Data analysis is performed with a Varian 4290 recorder/integrator. For butene and the various oxygenated substrates, a Varian 940 GC fitted

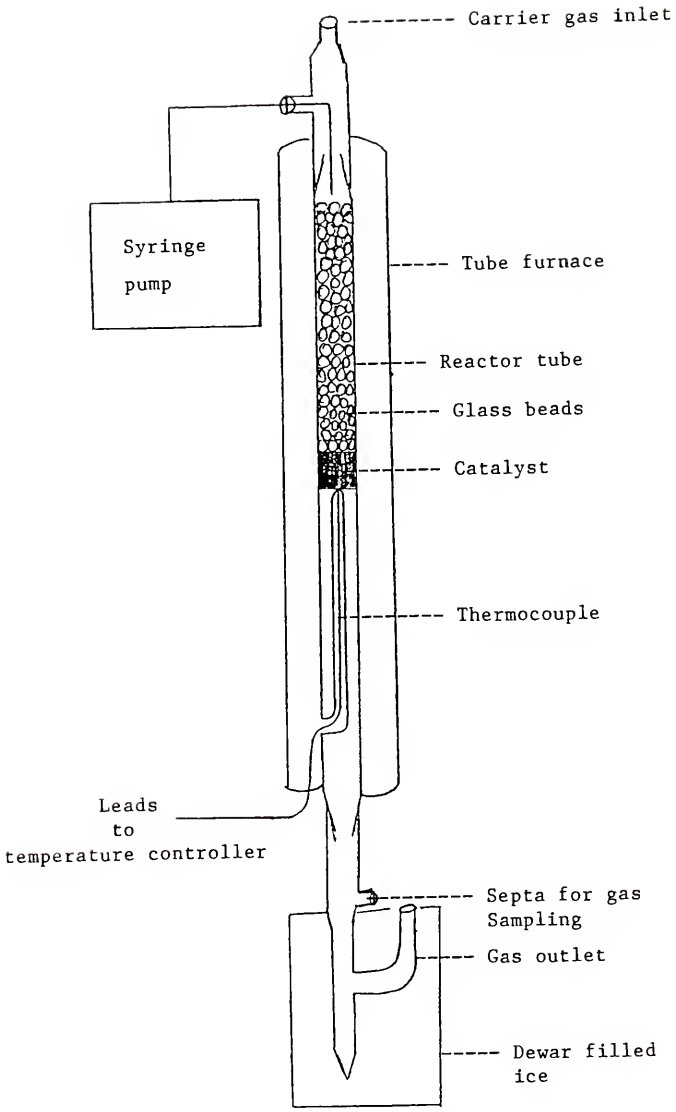

Figure 3-1. Schematic diagram of reactor setup.

with a 6 ft. Hayesep Q column and a Flame Ionization Detector was operated isothermally at 130^{o} C. Data analysis is performed on a Hewlett Packard 3390A recorder/integrator. Further product identification and verification is done by GCMS using a Varian 3400 GC interfaced with a Finnegan MAT ITDS 700 Mass Spectrometer. The column employed for this technique is a 15m DB1 column operated isothermally at 40^{o} C. Quantification for all GC data is done by standard calibration methods. Reported conversion percentages are based on the difference between the moles of substrate entering the reactor and the amount present in the post reactor stream.

Results and Discussion

Ethyl Benzene Substrate

As mentioned in the background section, one of the major advantages of the oxidative dehydrogenation process is that it can operate efficiently at lower temperatures than the direct dehydrogenation scheme. Nevertheless, most of the recently reported oxydehydrogenation catalysts have been studied in the 450^{o}-600^{o} C temperature range.[74-83] Since these systems must first form the active carbonaceous overlayer--a step most likely requiring a significant amount of heat--it is quite possible that the CMS catalysts can function at significantly lower temperatures. Another motivation for operating at reaction temperatures below 450^{o} C is that this is the final pyrolysis temperature of the PPAN samples used in this study. As discussed in the previous chapter, PPAN can be further pyrolyzed up to

1500° C to go all the way to the formation of carbon fibers. Our results have shown, however, that the condensed pyridine ring structure--which is the proposed catalytic species (vide infra)--is maximized at temperatures up to 450° C. Reaction temperatures above 450° C will lead to further structural rearrangements and the formation of volatile surface species which could lower catalyst activity and complicate product analysis.

The first series of catalytic experiments were performed at 250° C. Table 3-1 shows the results for various PPAN systems in the ethyl benzene oxydehydrogenation reaction. The reported product analyses are calculated from post-catalyst gas samples according to the method described in the experimental section of this chapter. It is evident that the PPAN catalysts have slight to moderate activity with high selectivity to the styrene product. Also shown in Table 3-1 are the results for an Al_2O_3 sample in this reaction scheme. This experiment is done in order to compare the reactivity of a typical high surface area (360 m^2/g) inorganic oxide under the particular reaction conditions employed. As is shown in the table, the oxide sample is not very active.

The observation of this type of reactivity at such a low temperature is quite encouraging. Since the above study is performed at less than half the temperature commonly employed for this reaction, a series of studies are done at higher temperatures to see if the activity can be further increased. The results for the PPAN materials in the oxydehydrogenation of ethyl benzene at 350° C are shown in Table 3-2. It is observed that all systems are far more active at this temperature

Table 3-1 Ethyl Benzene Reactivity Over PPAN Catalysts at 250° C

SAMPLE	CARRIER GAS	%CONVERSION[a]	%SELECTIVITY[b]
PPAN1	air	5.3	85.0
PPAN1	N_2	0.1	48.9
PPAN2	air	6.1	81.3
PPAN2	N_2	0.1	50.1
PPAN3	air	10.2	86.7
PPAN3	N_2	0.8	43.2
Al_2O_3	air	0.8	60.0

CONDITIONS: Substrate delivery--0.2 ml/hr. Carrier flow--5 ml/min. Reaction time--20 hrs for air runs, 4 hrs for N_2 runs.

a) non-styrene products are CO_2, benzene, toluene, and benzaldehyde.

b) percentage of all products that are styrene.

Table 3-2 Ethyl Benzene Reactivity Over PPAN Catalysts at 350^{o} C

SAMPLE	%CONVERSION	%SELECTIVITY
PPAN1	11.6	90.5
PPAN2	14.6	76.0
PPAN3	22.3	95.6
PPAN3 (N_2 carrier)	2.5	80.0
Al_2O_3	1.6	62.5

CONDITIONS: Same as those in Table 3-1.

than at 250^{o} C. Since 350^{o} C is still far below the reaction temperature of other reported catalyst systems, all further catalytic studies for this reaction are done at this temperature.

Several observations can be made form the data in Table 3-2. It is clear that surface area is a key factor to the level of activity. PPAN3 which was co-pyrolyzed with NH_4Cl and thus has a significantly higher surface area than the undoped PPAN1 sample, is twice as active for the conversion of ethyl benzene to styrene. This is not at all surprising since a higher surface area allows more substrate/catalyst interaction. Such a direct effect between surface area and activity has been shown for a wide variety of heterogeneous catalyst systems.

It is also evident from the data in Tables 3-1 and 3-2 that this catalytic process is occurring via an oxidative route. When the system is operated in the absence of O_2 (present in the air carrier flow) the activity is only slight and it subsides within a couple of hours. The system can be cycled back and forth, however, between active stage (air carrier) and inactive stages (N_2 carrier). Upon return to an air flow, reactivity is returned virtually immediately. This series of experiments was followed through five complete cycles and no loss in activity or selectivity was observed. The mechanism typically invoked for dehydrogenation processes over PPAN catalysts involves hydrogen abstraction from the substrate producing a hydrogenated PPAN moiety. The catalytic cycle is completed by reaction with O_2 to yield H_2O and the original catalyst structure. This reaction scheme was previously shown in Figure 1-1. The inability of the PPAN to be dehydrogenated is

the reason suggested for the eventual loss of activity in the N_2 carrier experiments.

Despite the fact that this mechanism has been widely proposed to account for the catalytic activity of PPAN samples,[31,34,41-43] it should be recalled that PPAN1 and PPAN3 also contain 8.5% by weight oxygen and oxygenated carbonaceous residues have been proposed as active catalysts for this reaction. PPAN2 which is partially prepared in air according to the method of Degannes and Ruthven,[43] has an appreciably higher oxygen content -- 13%. Furthermore the DRIFT results discussed in the previous chapter show that some of this oxygen content is present in carbonyl functionalities not unlike the polynapthoquinone moieties proposed by Cadus[82] and Emig and Hoffman.[83] In light of this, one might expect PPAN2 samples to have a higher reactivity than the other PPAN samples. This, however, is not the case. PPAN2 is only slightly more active than PPAN1, less active than PPAN3, and has a lower selectivity than either of the N_2-carrier preparations. It is concluded from this then, that the majority of dehydrogenation activity in the PPAN samples reported here takes place by the typical mechanism depicted in Figure 1-1. Any participation by oxygenated moieties is considered to be minimal.

The direct relationship between higher surface area and higher activity was the motivation for investigating the commercially available CMS system prepared from coal pitch residues. AX21 possesses one of the highest surface areas ever measured -- >2500 m2/g. Additionally, the novel structure and the oxygen content of this material make it a very close analogue to the carbonaceous overlayer species present on the

inorganic oxide catalysts discussed previously. The results of these commercially available CMS materials, as well as the data for samples of the industrial Fe_2O_3/Cr_2O_3 catalyst and Vrieland's cerium pyrophosphate system are shown in Table 3-3.

It is evident that under the experimental conditions of this study, the two literature-preparation samples are not very active. This is not unexpected since neither of these systems is reported to have much activity at 350^{o} C. AX21, on the other hand, is remarkably active. Conversion of 80% with greater than 90% selectivity is observed in a single pass. Like the PPAN systems, this is an oxidative process which can be cycled. When run in N_2 carrier flow, the activity drops immediately. When air is returned, the formation of styrene is readily observed. This system is also active over a long period of time. An extended run was followed for 120 hours in continuous operation and no appreciable loss in conversion or selectivity is seen. The sample can even be removed from the system for several days and activity is re-established when the reactor is set up again. Pre-catalyst and post-catalyst weight is further monitored in order to determine if the sample itself is being oxidized under the reaction conditions. No appreciable catalyst weight loss is observed in any of the AX21 runs described here for the oxydehydrogenation of ethyl benzene.

Clearly, a significant amount of this increased reactivity is due to the extraordinary surface area of the AX21 material. This alone, however, can not explain the overwhelming activity. The activated charcoal (AC) system has a surface area of 800 m2/g, and yet its activity is only slightly greater than PPAN3, the "high surface area"

Table 3-3 Ethyl Benzene Reactivity Over AX21 and Other Catalysts at 350^{0} C

SAMPLE	%CONVERSION	%SELECTIVITY
AX21	80.0	90.1
A.C.[a]	26.0	84.2
CeP_2O_7[b]	6.7	92.5
Fe/Cr/K/Mg[c]	0.9	45.1
AX21 (N_2 flow)	5.2	40.4

CONDITIONS: Same as those in Table 3-1.

a) Activated Charcoal

b) Prepared according to reference 74.

c) Prepared according to reference 95.

PPAN material (50 m2/g). The microscopic structure of AX21, which is composed of carbonaceous lamellae, gives this material an exceptional adsorption capability. Toxicological studies have shown that these materials adsorb considerably more substrate than other highly adsorbent carbonaceous materials.[48-50] This affinity for substrate, together with a surface chemical structure which is especially suited for this type of catalytic transformation (due to the oxygen content) surely contributes to the outstanding reactivity of AX21 in this reaction. The specific mechanism for the AX21 catalyst is most likely analogous to that proposed by both the Cadus[82] and Emig[83] groups. Shown in Figure 3-2, this reaction scheme invokes a concerted hydrogen abstraction from the substrate by the oxygen functionalities of the carbonaceous overlayer formed from coke deposition on an inorganic oxide surface.

Butene Substrate

Although there is not near as much evidence on the role of carbonaceous materials in the dehydrogenation of butene as there is for ethyl benzene, there have been several reports of CMS type materials being used in this reaction scheme. Table 3-4 shows the results for the dehydrogenation of butene to butadiene over a variety of catalyst materials. It is evident that only the AX21 sample has any appreciable activity under the reaction conditions employed. The Al_2O_3 sample is essentially unreactive and as before, this is not unusual at these low reaction temperatures (250^{o} C). It is surprising though, that the PPAN systems are not more active in this reaction scheme since Ademodi and

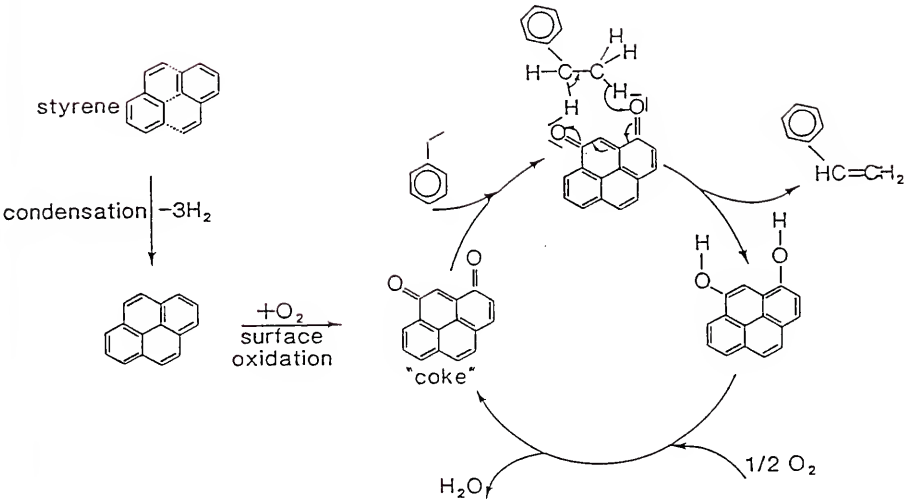

Figure 3-2. Proposed mechanism for AX21 dehydrogenation activity.

Table 3-4 Butene Reactivity Over CMS Catalysts

SAMPLE	%CONVERSION	%SELECTIVITY*
PPAN1	1.0	84.0
PPAN3	1.2	83.3
AX21	11.0	91.8
Al_2O_3	<1.0	---

CONDITIONS: Reaction temperature--250° C. Substrate feed--2 ml/min. Carrier feed--3 ml/min.

* Percentage of products which is butadiene. Other products are C_1 - C_3 hydrocarbons.

co-workers reported a PPAN system that has 20% conversion at 250° C[92] The Ademodi catalyst is prepared in a slightly different manner and the authors do not present any characterization studies. Another difficulty is that some of the reactor data, such as catalyst bed height, is not given. As discussed in Chapter 2, there are some problems with comparing PPAN samples from one author to the next.

The results for AX21 show that this material has moderate activity with excellent selectivity to butadiene. The conversion of 11% appears low compared to the reactivity of this catalyst towards ethyl benzene, however, other studies have shown carbonaceous materials to have less reactivity in this system than in ethyl benzene systems. Emig and Hoffman report considerably lower reactivity for their carbonized zirconium phosphate system in butadiene conversion as opposed to ethyl benzene.[83]

Oxygenated Substrates

In order to extend the study of the catalytic reactivity of CMS materials, a series of oxygenated substrates are investigated. Initial work is done with ethanol. The dehydrogenation of ethanol to acetaldehyde is well characterized on inorganic oxide catalysts.[96,97] The results for the reactivity of this substrate over CMS catalysts at 230° C is shown in Table 3-5. Again the results for an alumina run are also included to directly compare the reactivity of CMS materials to commonly employed inorganic oxides. At 230° C, the Al_2O_3 sample is found to have very little activity. The PPAN catalyst (PPAN3, the high surface area sample) is considerably more active. Overall conversion is

Table 3-5 Ethanol Reactivity Over CMS Catalysts

SAMPLE	CARRIER	%ACETALDEHYDE*	%ETHYL ACETATE*	%DIETHYL ETHER*	%OVERALL CONVERSION
Al_2O_3	air	<1	--	--	--
PPAN3	air	55	30	5	20
AX21	air	57	36	6	70
AX21	N_2	38	0	38	8

CONDITIONS: Reaction temperature--230° C. Substrate flow--0.2 ml/hr.Carrier flow--5 ml/min. Reaction time--20 hrs for air runs, 4 hrs for N_2 run.

* Percentage of stated product among all products.

20% with the major products being acetaldehyde and ethyl acetate. The former product is the result of the direct dehydrogenation of ethanol. The latter product must occur via a secondary condensation reaction in which an acetaldehyde fragment reacts with an unconverted ethanol molecule. As with the other substrates studied in this chapter, the key mechanistic step involved here is hydrogen abstraction. The extensive work in this area by Iwasawa proposes that the alcohol adsorbs dissociatively to form a bound alkoxide.[96] This is followed by hydrogen abstraction to produce the dehydrogenated product. PPAN has been shown previously to be efficient at hydrogen abstraction with alcohol substrates.[31,41,97] The nature of the product profile, acetaldehyde being the major product, shows that the catalyst preferentially abstracts a hydrogen from the methylene carbon.

As might be expected from the ethyl benzene and butene systems, AX21 is far more active than the PPAN system. Overall conversion is 70% with a product profile very similar to the PPAN catalyst. The major products are again acetaldehyde and ethyl acetate. The similarity in the selectivities between PPAN and AX21 towards ethanol conversion suggest that the two materials operate through similar mechanisms. The significantly greater activity of AX21 over PPAN, however, exemplifies how much stronger a hydrogen abstraction catalyst is the former CMS moiety.

The ethanol results are enlightening in that some reactivity information is obtained, but since there is really only one possible hydrogen abstraction site (it would be highly unlikely for any abstraction to occur at the methyl hydrogens) not much mechanistic

information can be learned. For this reason a series of C_3 substrates are examined. The straight-chain alcohol, n-propanol, the branched-chain alcohol, isopropanol, the aldehyde, propionaldehyde, and the ketone, acetone, are each studied for their reactivity with the AX21 catalyst.

The results for the C3 substrates are shown in Table 3-6. The reaction temperature (230^0 C), catalyst weight (0.5g), carrier flow (5ml/min), and substrate flow (0.2 ml/min) were all the same as for the ethanol experiment. It is evident that the alcohols were quite susceptible to both dehydration and dehydrogenation. The aldehyde substrate was equally reactive, however, the products are significantly different--they are all C_2 species. Acetone is virtually unreactive as a substrate. Analogous to the ethanol system, the reactivity for the C_3 substrates is dependent on the nature of the carrier flow. When N_2 is used in place of air, product formation ceases.

For n- and iso-propanol, the major product is propylene. Proposed mechanistic pathways to this and the other products observed for the former substrate are shown in Figure 3-3. The latter substrate reacts via similar routes. As is shown, the initial coordination of the propanol occurs via the donor oxygen to a Lewis acid site on the catalyst surface. This mode of coordination is often invoked in alcohol oxidation processes.[96,98] The formation of propylene is the result of hydrogen abstraction from the secondary carbon (labeled C_2 in Figure 3-3) by a surface oxygen species. This step is drawn in Figure 3-3 as a hydride abstraction which produces a carbocation. The formation of the alkene is shown to occur in a subsequent step. It is

Table 3-6 Reactivity of C_3 Oxygenated Substrates Over AX21 Catalyst

SUBSTRATE	PRODUCTS	%[a]	OVERALL CONVERSION[b]
n-propanol	propene	63	40
	propanal	13	
iso-propanol	propene	70	46
	acetone	20	
propanal	acetaldehyde	69	48
	ethanol	10	
	ethylene	8	
acetone	-------		< 1

CONDITIONS: Reaction temperature--230° C. Carrier flow--5 ml/min. Substrate flow--0.2 ml/hr.

a) Percentage of stated product among all products.

b) Other products include small amounts of ethers and esters.

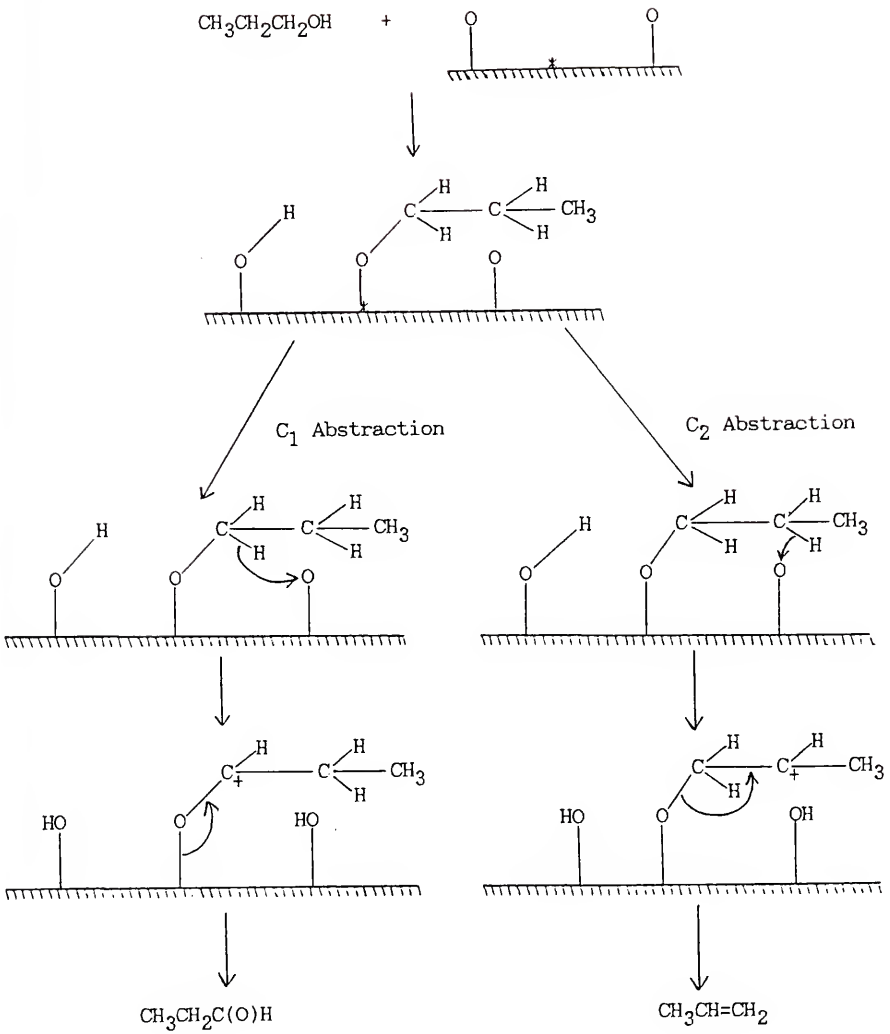

Figure 3-3. Proposed mechanistic routes for conversion of n-propanol.

quite possible that a concerted process which incorporates both of these stages is occurring. This is analogous to the proposed mechanistic pathway in the ethyl benzene system. The formation of propionaldehyde must occur through abstraction from the functionalized carbon (labeled C_1 in Figure 3-3). The fact that a secondary carbocation is more stable than a primary one most likely accounts for the predominance of the alkene product. The observation of a small amount of di-n-propylether shows that coupling reactions can also occur. It should additionally be noted that there is a small amount (<2%) of acetaldehyde and ethylene produced in the n-propanol system. These products are formed via secondary reactions of the propionaldehyde species (vide infra). This shows that the catalyst is able to readsorb and cause further reaction of the primary products.

As is shown in Table 3-6, the propionaldehyde substrate yields all C_2 products. This seemingly unusual result can best be explained by a hydrogen atom abstraction mechanism. Abstraction of the aldehydic hydrogen atom gives rise to and RCO$^{\cdot}$ species. This then decarbonylates to produce the C_2 fragment, R$^{\cdot}$, which on further reaction accounts for the various products observed. Again this is most likely a concerted process since attempts to detect a radical intermediate have proved unsuccessful.

These results demonstrate that the AX21 material can function in either hydride or hydrogen atom abstraction reactions depending on the nature of the substrate. Hydrogen atom abstraction occurs rather easily on an aldehydic species such as propionaldehyde; whereas, hydride abstraction is more facile on alcohol substrates. In the case of

acetone, neither hydride or hydrogen atom abstraction should occur readily and as expected, this substrate is found to be unreactive.

CHAPTER 4
CARBON MOLECULAR SIEVES AS CATALYST SUPPORTS

Introduction

This chapter focuses on the study of CMS materials as supports for three different types of heterogeneous catalytic systems. In the first, PPAN and AX21 have been doped with ruthenium species and have been investigated in the Fischer-Tropsch reaction. A great deal of work has been done on this system employing inorganic oxide supports. Virtually all of these catalysts yield broad product distributions. The goal of this study is to devise a system which will be active towards the conversion of synthesis gas (CO and H_2) with high selectivity to small molecular weight products. The second catalyst system studied employs MoO_3 doped AX21 for the oxidation of methanol. As discussed in the previous chapter, AX21 itself is active towards alcohol substrates. Methanol, however, is one of the most difficult alcohols to catalytically transform. The objective of this study is to combine a catalytically active metal species with a similarly active support to produce a system which can display a synergism between its constituents. Lastly, molybdenum and tungsten doped AX21 systems have been investigated in the deep oxidation of chlorinated hydrocarbons. There is a growing interest in developing catalytic systems which can fully oxidize various organic pollutants, e.g. CH_2Cl_2, to compounds that are

easily disposed like CO_2 and HCl. The goal of this study is to combine the exceptional adsorption capabilities of the support with the oxidative catalytic ability of the metal dopant. In each of these applications, the specific structure and properties of the CMS materials offer unique advantages towards accomplishing the prescribed goals.

Fischer and Tropsch first reported the catalytic conversion of synthesis gas to higher hydrocarbon products in 1926.[99] During the more than 60 years since that time, there has been a great deal of work conducted in the field. Traditionally this reaction has been performed under rather severe conditions--pressures of 100-200 atmospheres and temperatures in excess of 400^{o} C. Throughout the study of this process, though, there has been a wide range of conditions employed. Table 4-1 lists some of the different systems that have been investigated. Included in Table 4-1 are the conditions for the SASOL plant in South Africa which is the only presently operating industrial facility that uses the Fischer-Tropsch reaction for the production of hydrocarbons.

It is evident that many of the transition metals show some activity for CO hydrogenation. In considering a industrially viable system, however, overall activity is not the most significant parameter. Selectivity to a certain desirable range of products is of paramount importance. Virtually all Fischer-Tropsch systems eventually give rise to a Schulz-Flory product distribution.[100,101] This model, which was originally derived to explain polymerization sequences, can be described by the equations below:

$$W_n = n\,(1-\alpha)^2\,\alpha^{n-1} \qquad (4\text{-}1)$$

$$\log W_n/n = n \log\alpha + \log\left[(1-\alpha)^2/\alpha\right] \qquad (4\text{-}2)$$

Table 4-1 Commonly Studied Fischer - Tropsch Systems

Typical Metal Dopants

Ru, Rh, Os, Fe, Co

Common Supports

SiO_2, Al_2O_3, MgO, TiO_2

Typical Reaction Conditions

Pressure: 100 - 200 atm

Temperature: 300 - 400^{o} C

Reported Ranges

Pressure: 1 - 2000 atm

Temperature: 150 - 450^{o} C

SASOL Plant

Catalyst: promoted Fe_2O_3

Pressure: 25 atm

Temperature: 220 - 340^{o} C

The variables in these equations are defined as follows: n is the carbon number of a particular polymer unit or, in the case of Fischer-Tropsch systems, it is the number of carbons in a particular product; W_n is the weight fraction of that product among all the products; and α is the probability of chain growth. This parameter is a function of the degree of polymerization and rates of propagation and termination.

Equation 4-2 shows that a linear function should be obtained from a plot of log W_n/n vs n. Such a plot is called an Anderson-Schulz-Flory (ASF) graph.[102-104] The slope of the line is related to α which in Fischer-Tropsch terminology describes the chain growth of the reaction process. As the α value increases, so does the chain length of the hydrocarbons formed. This produces a broader product distribution. Hydrocarbons up to a chain length of C_{30} are not unusual in many active Fischer-Tropsch systems. Since Equation 4-2 is derived from a polymer model, there are certain deviations from linearity when it is applied to the Fischer-Tropsch process. C_1 values always fall above the line and typically are not considered part of the data set. The model is designed for the linking of methylene fragments such as would occur in a growing polymer chain. Since CH_4 is formed by direct hydrogenation of a surface carbide fragment, its production is not related to the polymer model. Many experimental systems also have C_2 and C_3 values which deviate somewhat from linearity. Above C_4 though, most systems fit ASF plots very well.

In the aftermath of the oil crisis in the mid 1970's, there was an explosion of interest in alternatives to petroleum based routes for hydrocarbon production. Much effort was focused on Fischer-Tropsch

systems for the formation of gasoline range products.[71,105,106] Many systems, most of which employed Group VIII metals supported on high surface area inorganic oxides, were reported to be highly active. Despite the research enthusiasm, however, the production of gasoline range products via CO hydrogenation never became significantly cost competitive with petroleum pathways. It now seems apparent that, at least for the foreseeable future, the only realistic market for the Fischer-Tropsch process is in the selective production of small molecular weight hydrocarbons and oxygenated products which can be used for the production of specialty chemicals. It would be particularly desirable to make alkenes such as ethylene and propylene by this route.

The problem with designing a system to selectively produce the products mentioned above has already been pointed out. Most CO hydrogenation systems exhibit a broad product distribution with limited selectivity towards the low molecular weight compounds. As mentioned previously, there is a great deal of similarity in the reactivity of the many metal species studied. The mechanism most often invoked for low selectivity is related much more to the oxide support than it is to the metal dopant.[107-110] Initially, inorganic oxides such as silica and alumina provide excellent dispersion of the metal species. Since there is no great chemical attraction between the oxide or hydroxyl nature of the support and the metal dopant, however, the metals tend to migrate on the surface of the support during the course of the reaction. This migration produces a significant growth in metal crystallite size. Such a phenomenon causes only a slight decrease in activity, but it has a detrimental effect on the selectivity. The sintering of metal species

leads to very broad product distributions.[108-110] To devise a Fischer-Tropsch system for the selective production of light hydrocarbon products then, it seems prudent to focus on the choice of a proper support as opposed to the design of new metal species. Prospective supports should have the ability to strongly interact with small metal clusters and through this interaction, prevent the formation of large metal crystallites.

This criteria was the motivating factor for employing PPAN and AX21 as supports in heterogeneous Fischer-Tropsch systems. The condensed pyridine ring functionality of PPAN should provide a much stronger interaction in an acid-base sense than the oxide and hydroxyl species of inorganic oxides. AX21 should likewise be able to inhibit cluster formation, but for a completely different reason. The pores and cavities associated with the structure of this material should provide isolation of small metal clusters in much the same way as alumino-silicate zeolite materials have been employed.[111-114] Both of these support systems have the additional advantage of being catalysts themselves. As was suggested earlier, olefin products are more desired than paraffins. The dehydrogenation ability of these CMS materials, such as that discussed in the previous chapter enables the possibility of synergistic interactions between the metal dopant and the carbonaceous support.

In addition to the design of Fischer-Tropsch systems with improved selectivity, mechanistic studies of the basic Fischer-Tropsch reaction and systems active for CO_2 reduction have also been investigated with CMS supports. In the former work, acetaldehyde is used in a co-feed

with syn gas. By following the fate of this additive, some very interesting information is obtained regarding the fundamental reaction steps of the Fischer-Tropsch process. Lastly, these systems are shown to have appreciable activity towards CO_2 reduction. Studies conducted with CO/CO_2 co-feeds further demonstrate how product selectivity can be influenced.

The oxidation of methanol is one of the most widely studied industrial catalytic processes. It is well documented that there are two main reaction pathways for this substrate.[115] The predominance of one over the other depends mostly on reaction temperature. In the so-called low-temperature scheme, the major products are methyl formate (MF) dimethoxymethane (DMM) and dimethyl ether (DME). In the high-temperature systems, formaldehyde can be produced with high selectivity. This latter process is performed on a major industrial scale. Formaldehyde is projected to be the fifth largest produced organic chemical in 1989.[69] The relevant reactions and conditions of these two processes are shown in Table 4-2.

Although the primary focus in methanol oxidation is on the high temperature production of formaldehyde, there is a growing interest in low temperature systems which can selectively produce methyl formate. This product is formed through a dimerization of formaldehyde units in the so-called Tischenko reaction.[116-118] Methyl formate has been shown in a number or recent studies to be a versatile intermediate for the synthesis of such high volume products as acetic acid,[119-121] dimethyl formamide,[122] and ethylene gylcol.[123]

Table 4-2 Typical Methanol Oxidation Reaction Routes

1. Low Temperature Process

$$2\ CH_3OH + O_2 \text{ ------> } CH_3OC(O)H + 2\ H_2O$$

$$3\ CH_3OH + \tfrac{1}{2}O_2 \text{ ------> } CH_3OCH_2OCH_3 + 2\ H_2O$$

CONDITIONS: Reaction temperature--200-240o C
Reported catalysts--MoO_3, $Cu_2Cr_2O_4$
23% conversion
86% selectivity (MF)

2. High Temperature Processes

$$CH_3OH + \tfrac{1}{2}O_2 \text{ ------> } CH_2O + H_2O$$

CONDITIONS: Reaction temperature--600-800^{o} C
Reported catalysts--$FeMoO_4$ or Ag
80-90% conversion

In light of the reactivity of AX21 toward alcohol substrates which was discussed in the previous chapter, this catalyst is employed for methanol oxidation studies. Since a great deal of work had already been conducted in the low temperature regime, initial studies are done at 230^{o} C. The goal is to design a system which will exhibit higher reactivity with appreciable selectivity to the desired product--under these conditions, methyl formate. Higher reaction temperatures are also studied in the attempt to produce formaldehyde. Both the undoped AX21 and a variety of Mo/AX21 systems are found to be active for the conversion of methanol. The doped systems are found to be especially interesting due to an apparent synergism between the metal and the support. This phenomenon is unique in that it is not observed for inorganic oxide supported systems. A series of surface science techniques have been conducted on the Mo doped AX21 catalysts as well as similarly prepared SiO_2 supported systems. Scanning Electron Microscopy (SEM), X-ray Diffraction (XRD), and X-ray Photoelectron Spectroscopy (XPS) have revealed some insight into the nature of the doped metal species and how it changes during the course of the reaction.

The last section of this chapter focuses on the deep oxidation of chlorinated hydrocarbons. The industrial production of these materials for use as solvents, pesticides and a host of other applications has been rising continuously over the past ten years. Due to the widespread use of these materials, there is a growing environmental pollution problem associated with their improper and inefficient disposal.[124] These compounds prove to be particularly difficult to dispose of because they do not burn efficiently in typical waste incineration plants. This

problem is further complicated by the fact that the by-products formed from incomplete incineration are often more hazardous than the original starting material. In light of this, there is a great deal of interest in catalytic systems which can fully degrade chlorinated hydrocarbons to much more easily handled materials such as CO_2 and HCl. The systems most often studied for such reactivity involve transitional metal oxides doped with a variety of constituents.[125] Recently an electrolytic oxidation system was reported to be efficient for a variety of chlorinated hydrocarbon species including aromatic systems.[126]

Several molybdenum and tungsten doped AX21 systems are studied for their reactivity towards CH_2Cl_2. This substrate is chosen for two reasons. First, its conversion should be relatively easy to follow. Secondly, it is a relevant system to study, since CH_2Cl_2 is by far the largest industrial chlorinated hydrocarbon pollutant.[124] The use of the AX21 support should offer several advantages over unsupported systems or those employing inorganic oxide supports. Much of the work discussed so far has shown that AX21 offers a significantly higher and more stable degree of dispersion than inorganic supports. This increased surface area of the active metal species should improve the reactivity of this system in much the same way as it does for other catalytic reaction schemes. Additionally, the extraordinary adsorption capability of the AX21 support can greatly enhance the reactivity of the system. This should especially be true in "real-world" operations where the organic pollutant is only present in small concentrations. A lot of work is being done in employing carbonaceous materials for ground water purification.[47] The work described in this section thus combines the

two current methods for toxic waste clean up. The CMS support is employed to more efficiently adsorb the specific pollutant from the waste stream and the metal dopants are present for the deep catalytic oxidation of these materials.

Experimental

Reagents

Synthesis Gas Conversion

The reactant gases were delivered directly from their respective cylinders and were not further purified. The carbon monoxide (Matheson Gas Products) used was Coleman Purity grade with a minimum purity of 99.5%. The carbon dioxide (Matheson) sample was Coleman Instrumental grade having a minimum purity of 99.99%. The hydrogen (Liquid Air Corp.) supply was prepurified grade with a minimum of 99.9%. The ruthenium metal dopings were prepared from both $RuCl_3$ (Alfa) and $Ru_3(CO)_{12}$ (Strem Chemical Company). The acetaldehyde (Fisher Scientific) reactant was dried over 4Å molecular sieves prior to use and was stored in the chemical refrigerator. Identification of products via gas chromatography was aided by the use of Scotty Analyzed Gases (Scott Specialty Gases Company). Three different samples were employed: Can Mix 1 containing C_1 - C_6 linear paraffins; Can Mix 3 containing C_2 - C_6 normal olefins plus acetylene; and Can Mix 32 containing C_1 - C_4 linear paraffins plus isobutane. Isotopic labelling studies were conducted using a 25% ^{13}C labelled CO sample (Isotec Incorporated, Dayton Ohio).

The methanol reactant (Eastman Kodak Company) was spectro grade and was dried over 4Å molecular sieves prior to use. The absence of impurities was verified by gas chromatography. The air supply (Liquid Air) was U.S.P. breathing quality. The various metal dopants employed were reagent grade and were used without further purification. MoO_3 and Na_2MoO_4 were purchased from Aldrich Chemical Company. The ammonium molybdate sample was purchased from Mallinkcrodt under the name of Acid Molybdic. This commonly used reagent is nominally $(NH_4)_2MoO_4$ but is essentially 85% MoO_3
with added NH_4OH. The standards for product identification--Methyl formate (Fisher), dimenthoxymethane (Chem Service Company, West Chester, Pennsylvania), and dimethyl ether (Matheson)--were reagent grade and used without further purification.

Deep oxidation of chlorinated hydrocarbons

Methylene chloride (Mallinkcrodt) was reagent grade and was used without further purification. The absence of impurities was verified by gas chromatography The various metal dopants were reagent grade. The molydenum species and the air supply were the same as those in the methanol oxidation studies. All the tungsten samples -- WO_3, Na_2WO_4, $(NH_4)_2WO_4$ were purchased from Aldrich. The molecular formula for the last species is not completely accurate. The supplier provided elemental analysis data which reported the W content to be 66.9% by weight. The simplified formula given above corresponds to 64.79% tungsten. The value give by the supplier was used when calculating molar quantities for catalyst preparation.

Preparation of Catalysts

The preparation of the PPAN and AX21 support materials was described in Chapter 2. The AX21 sample was dried for eight hours in vacuo at 100^{o} C prior to use. This is done in order to obtain an accurate weight of the sample. The ruthenium doped catalysts for synthesis gas conversion were prepared by combining 0.05g of $Ru_3(CO)_{12}$ or $RuCl_3$ with 2.45g of PPAN or AX21. For either dopant, this loading corresponds to approximately 1% by weight Ru metal--0.98% in the case of $RuCl_3$ and 0.96% for $Ru_3(CO)_{12}$. For the $Ru_3(CO)_{12}$ doped samples, the mixed powders were refluxed in 60ml of hexane (a mixture of isomers) for a minimum of six hours. The term reflux is not totally accurate since only the $Ru_3(CO)_{12}$ dissolves. This heating and mixing process, however, serves to better disperse the metal cluster onto the support. For the $RuCl_3$ doped samples, a similar reflux step is employed using H_2O as the solvent. After the heating and mixing process is completed, the respective solvents are removed by rotary evaporation. The catalysts are then dried in vacuo at 60^{o} C (100^{o} C for the H_2O systems) for eight hours. A $Ru_3(CO)_{12}$ doped Al_2O_3 sample used in comparative catalytic studies was prepared analogous to that of the PPAN and AX21 supported systems.

In addition to the solvent deposition route described above, doped PPAN samples were also prepared by mixing the Ru species and PAN together before pyrolysis and firing the combined mixture. This technique did not prove to be very successful though, since none of the catalysts prepared in this manner exhibited any reactivity. It is

believed that this method is unproductive because the metal dopant gets buried in the interior of the support matrix and is thus not readily accessible to reactant gases.

The presence of the $Ru_3(CO)_{12}$ cluster on the PPAN and Al_2O_3 supports can be verified via DRIFT Spectroscopy. Figure 4-1 shows the IR spectra of PPAN before and after being doped with $Ru_3(CO)_{12}$. The metal carbonyl stretching frequencies can be observed in the 2000-2200 cm^{-1} region. Figures 4-2 and 4-3 display the metal carbonyl stretching frequency region for unsupported $Ru_3(CO)_{12}$ and $Ru_3(CO)_{12}$/PPAN. It is evident that the peaks for the supported system are shifted to lower wavenumbers indicating a bonding interaction with the support. There has been a great deal of work in relating the position of the peaks to the type of the metal/support interaction and to the nature of the metal species.[127-130] The Ru/Al_2O_3 system, for example, has been well characterized by IR assignments. The IR spectra for the Ru/PPAN system, however, are not suitable for this type of detailed analysis. The peaks are very broad and due to the high level of noise inherently associated with PPAN IR spectra, inferences drawn from exact peak locations can not be conclusive.

The various molydenum and tungsten doped samples were prepared by the same solvent deposition method. In all cases, deionized H_2O was used. For the MoO_3/AX21 sample, 0.5 g of the metal oxide was mixed with 2.5g of dry support. This loading corresponds to 3.47×10^{-3} moles of Mo and 11% by weight metal content. This level of loading was chosen because most literature work on support MoO_3 systems is in the 8-12% range.[131-133] In order to maintain a degree of consistency between the

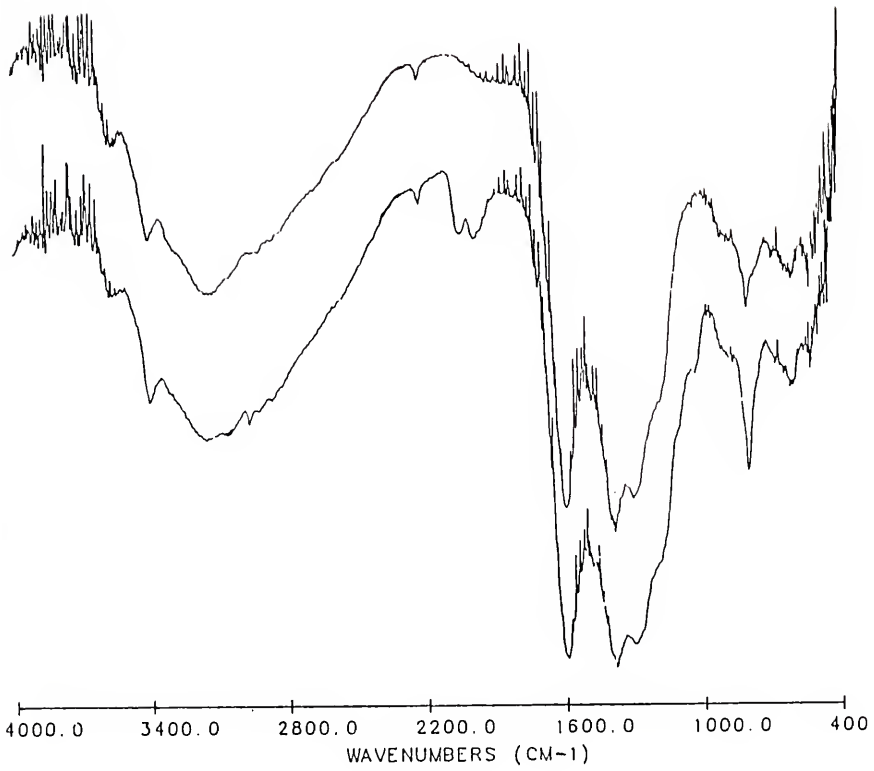

Figure 4-1. DRIFT spectra of PPAN and $Ru_3(CO)_{12}$/PPAN.

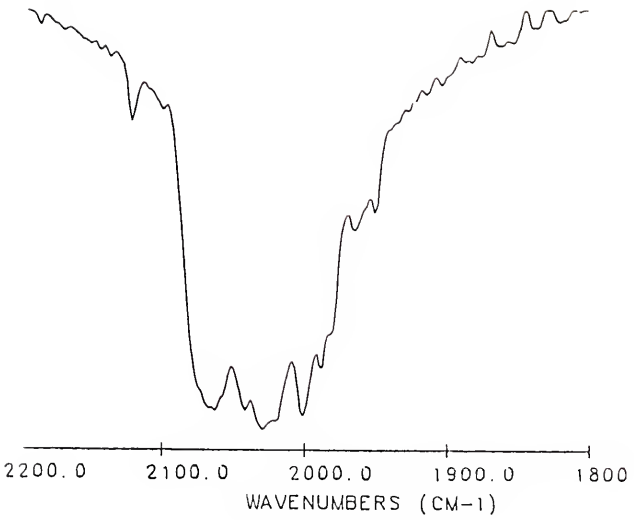

X=	1933.8	Y=	84.541
X=	1949.6	Y=	72.091
X=	1964.4	Y=	69.826
X=	1980.9	Y=	55.733
X=	1987.7	Y=	50.699
X=	2001.0	Y=	44.523
X=	2019.6	Y=	43.876
X=	2028.9	Y=	42.688
X=	2041.1	Y=	45.250
X=	2062.5	Y=	45.146
X=	2066.2	Y=	45.591
X=	2119.6	Y=	84.696

Figure 4-2. DRIFT spectrum of unsupported $Ru_3(CO)_{12}$.

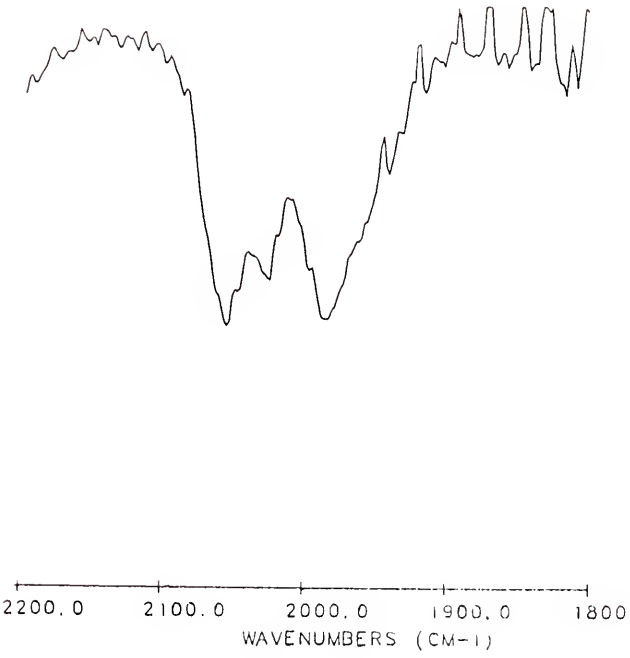

X=	1960.2	Y=	13 192
X=	1985.1	Y=	12 927
X=	1994.8	Y=	13 093
X=	2016.3	Y=	13 207
X=	2022.5	Y=	13 041
X=	2044.5	Y=	13 020
X=	2052.4	Y=	12 901

Figure 4-3. DRIFT spectrum of $Ru_3(CO)_{12}$/PPAN.

various metal dopant precursors, this molar value was used for all the other Mo and W species. For the Na_2MoO_4 sample, for example, 3.47×10^{-3} moles of Mo corresponds to 0.71g, so this amount is combined with 2.45g of AX21.

Reactors

The reactor for all of the studies conducted in this chapter is a fixed bed flow reactor of the same type as that employed in the experiments of the previous chapter. Unless otherwise stated, 0.5g of catalyst is used in all experiments. For the synthesis gas conversion experiments, gas delivery was metered via a three stage silicon oil bubbler fitted with rotoflow valves. The design of this device has been described elsewhere.[134,135] The top two stages were always used for H_2 and CO flow respectively. The bottom could be used for N_2 purging, CO_2 reactant flow, or for HCl reactant flow. When the latter species was employed, concentrated sulfuric acid was used in place of the silicon oil. The total flow rate of gas reactants was normally maintained at 4ml/min. In most syn gas experiments the ratio of H_2/CO was 3:1. Several studies were done with higher CO levels up to a $H/_2CO$ ratio of 1:3.

For the acetaldehyde co-feed experiments, an additional bubbler was fitted directly to the top of the reactor tube just outside the oven. Connection to the reactor tube was afforded via a ground glass joint. The bubbler was filled with 3ml of acetaldehyde. In order to slow the rate of substrate delivery, the bubbler is placed in a Dewar and the temperature is maintained at 0^{o} C. The quantity of the aldehyde

going into the reactor can be monitored chromatographically through a pre-gas septum.

Reaction temperature for all syn gas systems is 220^{o} C. This temperature is monitored by a thermocouple encased in a glass tube in contact with the catalyst bed. The design of the oven and the other specifications of temperature control are the same as those in the experiments described in the previous chapter.

In the methanol oxidation studies, the substrate is delivered via the syringe pump described previously. The flow rate is maintained at 0.2ml/hr. Carrier gas flow, either N_2 or air, is monitored by a Cole Parmer variable flow controller. The flow rate is set at 5ml/min. In a typical experimental cycle, the initial heating stage is done in N_2 flow with the syringe pump turned off. After reaction temperature is reached, 230^{o} C unless otherwise stated, post gas samples are taken to verify that no thermal decomposition products are present. At this point carrier flow is switched to air. Post gas samples analyzed by gas chromatography show that it takes about two hours for the N_2 flow to be completely purged. After the air carrier flow is determined to have the proper N_2/O_2 ratio, the syringe pump is turned on. The post reactor effluent is collected in a trap which is maintained at 0^{o} C.

The air injections prior to substrate delivery also serve to detect any CO or CO_2 being produced by oxidation of the CMS material itself. No CO is observed in any of the systems. Trace levels of CO_2 are observed at 230^{o} C. Usually, the CO_2 peak is not even large enough to be integrated and thus is too small to be accurately quantified. At high temperature, however, this formation of CO_2 from the oxidation of

the CMS material is greatly increased. These observations are discussed in depth later in this chapter.

The experimental design for the deep oxidation studies is very similar to the other systems previously discussed. The substrate is delivered via the pre-reactor bubbler attached directly to the top of the reactor tube. The bubbler is filled with 5 ml of CH_2Cl_2. As in the acetaldehyde experiment, the delivery is slowed by cooling the bubbler in an ice bath. The carrier flow rate is also reduced so that only a small amount of CH_2Cl_2 is being delivered. The flow rate employed is less than 1 ml/min. The post reactor effluent is condensed in a trap which contains 10 ml of deionized H_2O. The purpose of this quenching in H_2O is to dissolve the HCl that is generated from the deep oxidation. The amount of acid formed can be quantified by titration with NaOH. Periodic gas sampling of the post effluent also establishes the activity of the system since CO_2 formation can be observed.

For all three of the heterogeneous catalytic systems discussed in this chapter, bed height and catalyst weight are measured before and after each experiment. Very little loss in either bed height or weight is observed in systems run at temperature below 250^{o} C. Above these temperatures, however, appreciable degradation of the CMS material occurs. This will be discussed further later in this chapter.

Analysis

Routine product analysis for all the systems discussed is done by Gas Chromatography. Both Flame Ionization Detection, suitable for hydrocarbon analysis, and Thermal Conductivity Detection, efficient for

N_2, O_2, CO, CO_2 and HCl analysis, are employed. The former was conducted on a Varian 940 GC fitted with a Hayesep Q column. The latter technique was conducted on a Hewlett Packard 5700A GC employing a Hayesep DB column. Quantification of data was done by a Hewlett Packard 3390A integrator/recorder. Samples are taken in both the gas phase at the exit of the reactor oven and from the liquid phase after the effluent has been condensed in the cold trap. Further product identification was offered through the use of GCIR and GCMS techniques. The latter method was already described in the preceding chapter. The former was accomplished with a Hewlett Packard 5890A GC using a DB 130 column in conjunction with a Nicolet 5 DXB FTIR.

Some of the products formed in the systems discussed here are not amenable to GC detection and quantification. In light of this, a couple of titration methods have been employed. To quantify formaldehyde produced in the high temperature methanol oxidation studies, the sulfite titration method of Walker is practiced.[136] The reaction involved for the titration is shown below:

$$CH_2O + Na_2SO_3 + H_2O \text{ -----> } NaOH + CH_2(NaSO_3)OH. \quad (4\text{-}3)$$

The method is done by adding a few drops of phenolphthalein indicator (0.5g phenolphethalein in 50ml ethanol) to a 1.0m solution of Na_2SO_3 (12.6g Na_2SO_3 in 100ml D.I. H_2O). The solution turns magenta because SO_3^{2-} (aq) is a base. The color is returned to clear with the addition of several drops of a standard 1.0 N HCl titrant solution. The next step is to add a weighed amount of the reaction solution to be

titrated. The flask is shaken to allow complete mixing. The solution turns magenta again to indicate that base is present. The quantity of NaOH(aq) generated is determined by titration with the HCl solution. The % formaldehyde present in the sample can be readily calculated from the equation below:

$$\% \text{ formaldehyde} = \frac{\text{ml Acid titer x Normality of acid x } 3.003}{1 \text{ x Weight of sample}} \qquad (4\text{-}4)$$

The constant, 3.003, comes from the fact that one ml of 1.0N acid is equivalent of 0.03003g of CH_2O.

As mentioned above, the quantification of HCl produced in the deep oxidation studies is also determined titrametrically. A standard 1.0 M NaOH solution is used with a phenolphthalein indicator. The number of moles of HCl produced is equivalent to twice the number of moles of CH_2Cl_2 oxidized according to the balance equation shown below:

$$CH_2Cl_2 + O_2 \text{ ---> } 2HCL + CO_2 \qquad (4\text{-}5)$$

Characterization of the catalytic materials is conducted by a variety of spectroscopic techniques. DRIFT Spectroscopy is performed as was previously described in Chapter 2. Scanning Electron Microscopy is performed with a Jeol JSM 35C electron microscope using an acceleration voltage of 25 kV. Samples are initially examined at 300X in order to insure the regions to be studies at higher magnification are representative of the whole. Micrographs are taken at 6000X and 40,000X. The author would like to acknowledge Richard Krockett of the

University of Florida's Major Analytical Instrumentation Center for his assistance with the SEM studies. X-ray Diffraction Spectroscopy (XRD) was run on a General Electric 3000 instrument using Cu α radiation. The author acknowledges the research group of Dr. T.E. Mallouk at the University of Texas at Austin for conducting the XRD studies. X-ray Photoelectron Spectroscopy (XPS) was run on a Kratos 9000 instrument. Samples were mounted on aluminum tape and were evacuated for eight hours prior to scanning. The author acknowledges Dr. Vaneica Young and Mr. Michael Clay of the University of Florida for their assistance in performing these XPS studies. For each of the surface techniques mentioned above, SEM, XRD, and XPS, the exact same samples were used.

Results and Discussion

Synthesis Gas Conversion

As mentioned in the introduction to this chapter, most of the transition metals exhibit some activity towards CO hydrogenation. Ruthenium was chosen as the metal constituent in this study since it has been shown to be very active for both CO[101,127,129,137-146] and CO_2 reductions.[147-150] Initially, work was conducted with $RuCl_3$ as the metal precursor. For most synthesis gas conversion systems, especially those operating at ambient pressures, the active metal species is zero valent. Thus, this Ru species needs to be reduced. Such a practice is quite common--metal halides have been widely studied as initial catalyst sources. The reduction step is typically done in H_2 flow at elevated temperatures. For this study, however, $RuCl_3$ did not prove to be a

successful precursor. The temperatures required to fully reduce the metal species (500-600^{0} C) exceeded the pyrolysis temperature of PPAN and caused further structural changes in the support.

In light of the difficulties associated with RuCl3, $Ru_3(CO)_{12}$ was selected as the metal dopant to be used in all the CO and CO_2 hydrogenation studies. There are several additional advantages to the choice of this species. The fact that the carbonyl functionality can be easily observed in the IR makes it very easy to verify that the cluster has initially been supported. Since both PPAN and AX21 are black, a simple visual inspection, such as can be done with Al_2O_3 or SiO_2 supports, (which are bright yellow when $Ru_3(CO)_{12}$ is supported on them), can not be used to insure the success of the solvent deposition. Another advantage to the use of $Ru_3(CO)_{12}$ has been shown by recent studies which suggest that the carbonyl precursor is superior to metal halide species because the breakdown of the cluster leads to smaller metal crystallite sizes.[151] The only disadvantage to the use of $Ru_3(CO)_{12}$ is that one must be sure that the observed hydrocarbon products are not solely from the hydrogenation of the carbonyl groups of the cluster. To preclude any confusion, the supported Ru catalysts are subjected to a H_2 pre-treatment at reaction conditions for several hours. During this time methane is observed as a product from the reduction of the cluster. When this reaction subsides, the CO/H_2 reactant stream is added and the Fischer-Tropsch activity (vide infra) is immediately observed. It has been shown in subsequent studies that the long term activity and overall product distribution are the same whether or not the H_2 pre-treatment step is done.

Both Ru/PPAN and Ru/AX21 are active catalysts for the conversion of synthesis gas to hydrocarbons. The systems have comparable activity and each have high selectivity for the light hydrocarbons. In both cases, the formation of products occurs with virtually no induction period following contact with the CO/H_2 reactant stream. Since these supports are significantly different, however, there are some distinctions in their reactivity. In light of this, the Ru/PPAN and Ru/AX21 systems will be discussed separately.

The formation of hydrocarbon products in the Ru/PPAN system is quite rapid. As mentioned in the experimental section, the systems are often pre-treated in H_2 only flow. Products can be observed as soon as five minutes after CO flow is begun, however, it takes 30-45 minutes for the reactant stream to equilibrate. After this time period, the activity and product distribution remains virtually constant throughout the experimental run. Typical systems are followed for 20 hours on stream. Long term runs up to six weeks in continuous operation have been done and no appreciable loss in activity or selectivity has been observed.

The systems can also be cycled in various reactant streams. If the CO flow is turned off and the system run only in an H_2 stream, the product distribution changes to form almost exclusively CH_4 and the activity ceases within two hours. Upon reintroduction of CO to the reactant stream, the product distribution returns to its previous form within a couple of hours. The results of a typical cycling experiment are shown in Figure 4-4. The top GC trace shows the contents of the post-reactor stream in an H_2 only flow. The only products are very

RT	AREA	AREA%	
0.45	43528	89.97	methane
0.86	4854	10.03	ethane

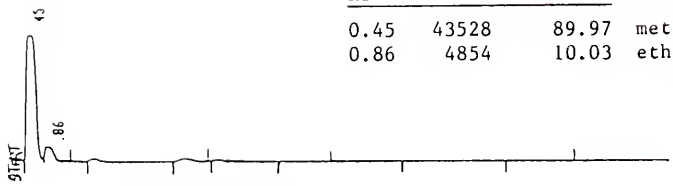

H_2 Only Flow

RT	AREA	AREA%	
0.44	645070	42.00	methane
0.84	157570	10.26	ethane
1.74	331420	21.59	propane
2.53	8017	0.52	acetaldehyde
4.24	144060	9.38	iso-butane
4.74	130670	8.51	butane
10.96	44852	2.92	iso-pentane
12.32	74069	4.82	pentane

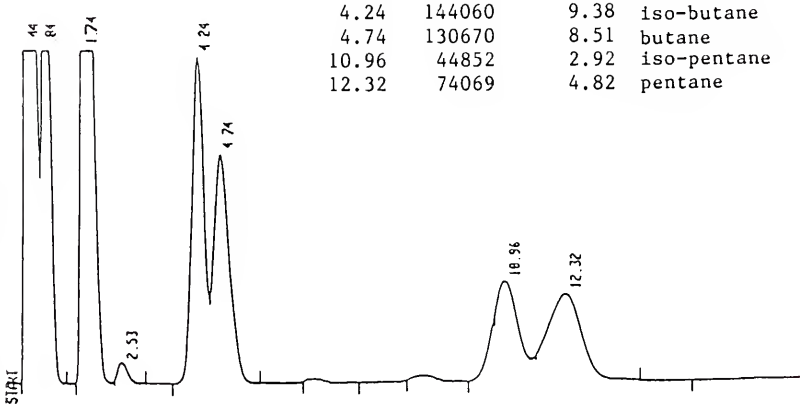

H_2 + CO Flow

Figure 4-4. GC traces for reactant gas cycling experiments.

slight amounts of methane and ethane. The bottom trace is from the post-reactor stream of the same system 0.75 hrs. after CO flow was reintroduced. The system is quite active for C_1 - C_5 hydrocarbons. This cycling process can also be done with a N_2 only flow. Under such a condition, the system remains dormant until the syn-gas flow is reinstated at which time hydrocarbon formation is again observed. Thermal cycling has also been investigated. Active systems can be removed from the reactor and allowed to cool to room temperatures. These systems regain their activity when the reactor set-up is reassembled.

Some labeling studies were done by employing ^{13}CO (25% enriched) in the reactant gas. GCMS analysis shows the incorporation of the label into the hydrocarbon products. Figure 4-5 displays the MS of the propane product formed from the reaction of ^{13}C enriched CO with H_2 over a Ru/PPAN catalyst. The observation of the 45 and 46 mass peaks shows that some of the label is present in the product.

As mentioned in the introduction, the motivation for employing PPAN as a support in the Fischer-Tropsch system is focused on the design of a catalyst which has improved selectivity for the small molecular weight hydrocarbons. The sustained activity demonstrated above is encouraging, but the true test of merit comes from a comparison between the PPAN support and an inorganic oxide support material. Figure 4-6 shows the results of similarly prepared Ru/PPAN and Ru/Al_2O_2 catalysts for syn gas conversion. It is evident that both systems are active, however, the Al_2O_3 supported catalyst has a much broader product

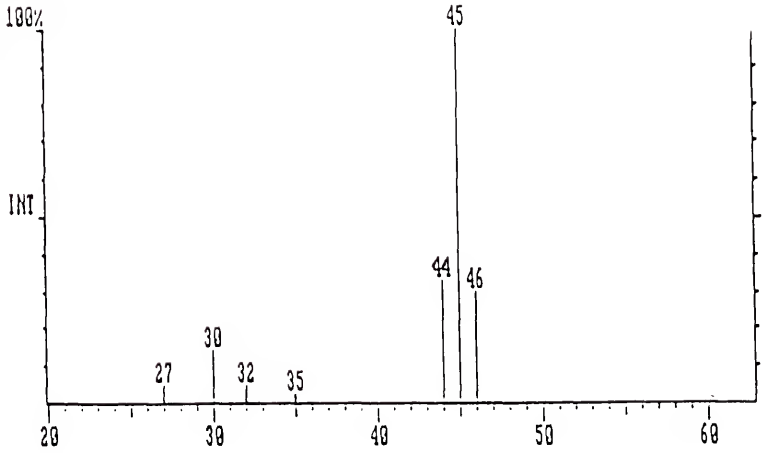

Figure 4-5. Mass spectrum of propane peak showing ^{13}C incorporation.

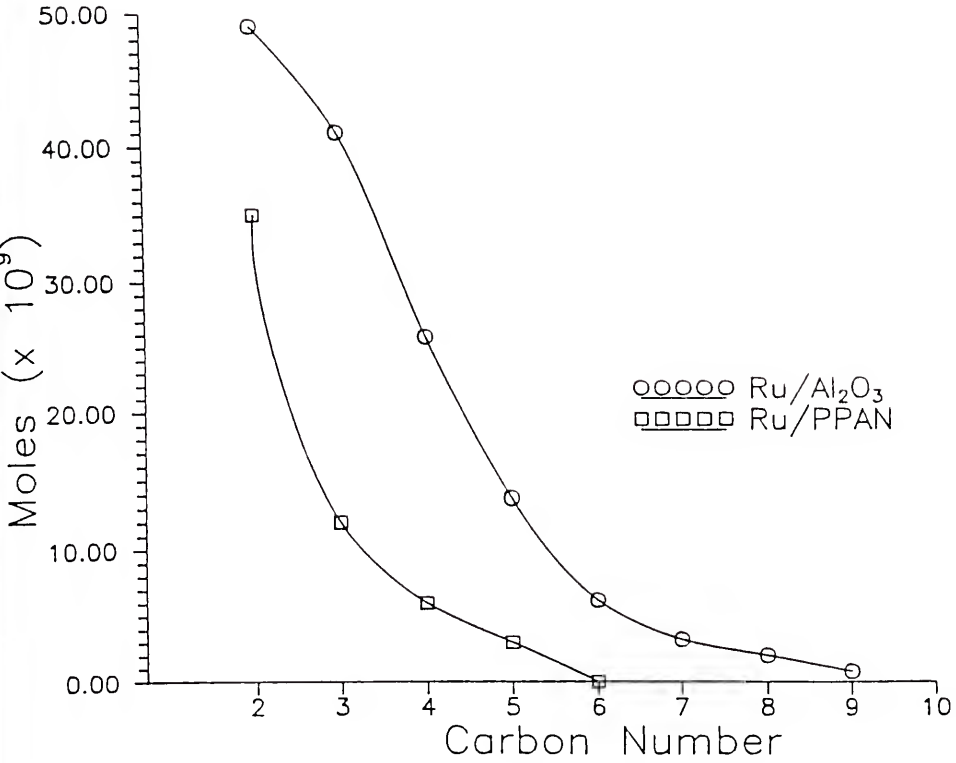

Figure 4-6. Product distribution of Ru/PPAN versus Ru/Al_2O_3.

distribution. Hydrocarbon products up to C_9 are observed for the Al_2O_3 system, whereas nothing above C_5 is seen for the PPAN based catalyst.

The molar quantities described in Figure 4-6 correspond to the sum of the respective alkene and alkane species produced. No oxygenated products, other than a trace amount of acetaldehyde, which may be an intermediate (vide infra), are observed in any of these systems. The reactant flow employed for these experiments was comprised of a 3:1 H_2/CO mixture. In such systems, where the H_2 is in a large excess, the majority of the products in both systems are paraffins. If the flow composition is switched to 1:3 H_2/CO, however, a considerably higher ratio of olefins can be made without effecting the product distribution. Figure 4-7 shows the amount of both alkanes and alkenes produced from a Ru/PPAN system operating with a 1:3 H_2/CO reactant stream. As is shown, the olefinic content predominates in several of the hydrocarbon products. Both the C_3 and C_4 products possess over 70% alkene content.

In terms of overall product formation, the Al_2O_3 system is about three times more active than its PPAN counterpart. As mentioned in the introduction, however, selectivity is just as important (if not more so) as activity in considering this reaction. It is clear that the PPAN catalyst has a much better selectivity for the smaller products. Figure 4-8 compares the ASF plots (from equation 4-2) for the two systems. The slope of the lines are significantly different with the Ru/Al_2O_3 having a chain propagation factor, α, of 0.44 while the Ru/PPAN has an α value of 0.33. The relatively good fit of the experimental data to the linear equation is evidence that both systems display the

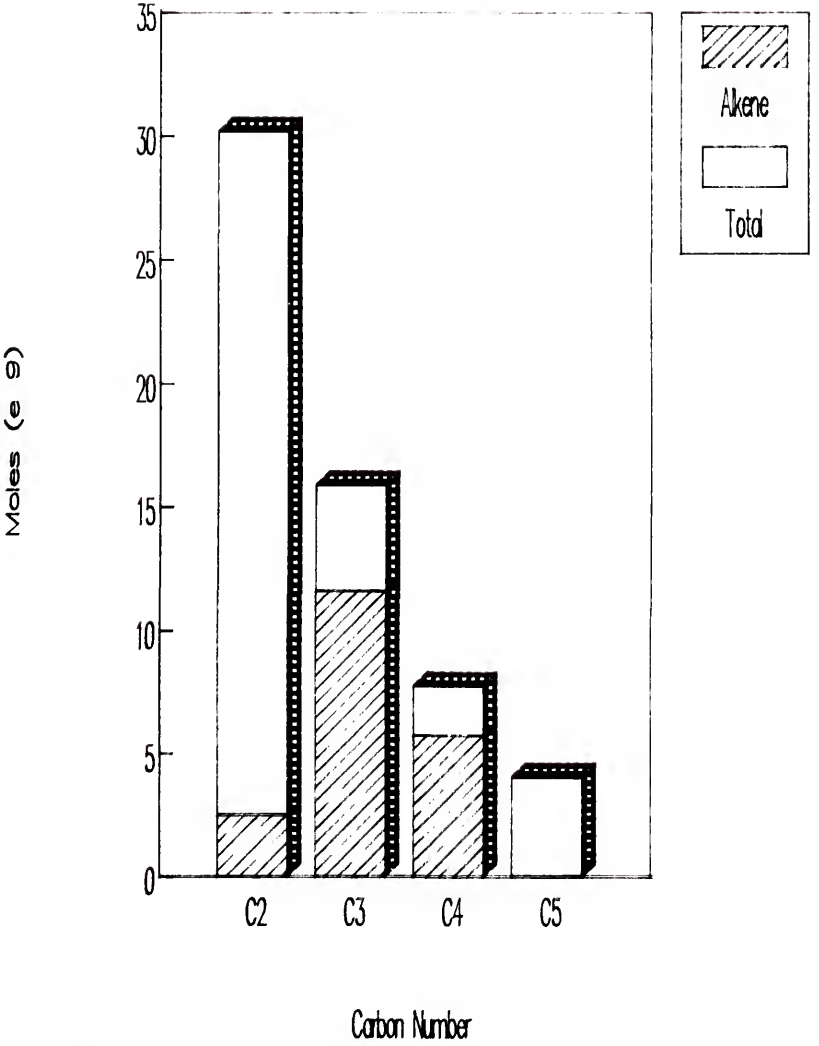

Figure 4-7. Alkene production in Ru/PPAN system.

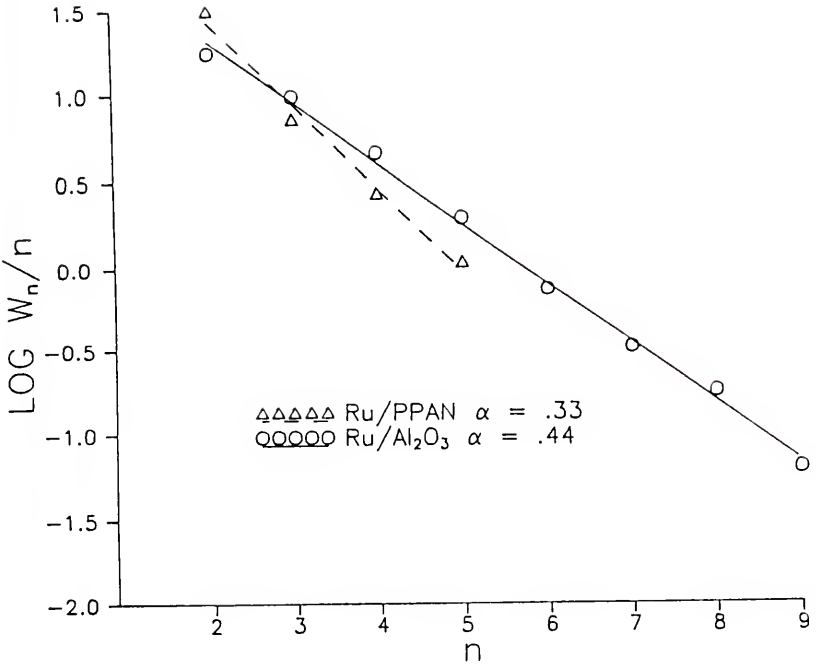

Figure 4-8. ASF plot of PPAN versus Al_2O_3.

Schulz-Flory distribution with the PPAN based system having a particular propensity towards small molecular weight hydrocarbons.

This long term selectivity for the light products is empirical evidence that the PPAN support inhibits the formation of large metal aggregates. In the attempt to obtain more direct support for this proposal, Scanning Electron Microscopy (SEM) was conducted on the Ru/Al_2O_3 and Ru/PPAN samples before and after catalysis. Figure 4-9 shows the SEM, at 25,000 X of a typical Ru/Al_2O_3 catalyst before and after a catalytic experiment. Although there are not many distinguishing features, comparison of the two micrographs shows that there appears to be a clustering or agglomerization present in the post-catalyst system that is not noticed in the pre-catalyst. This clustering is most likely due to sintering of the Ru particles on the Al_2O_3 support. Such a phenomenon is well documented in electron microscopy studies of metal dopants on inorganic oxide supports.[108,152-154] Figure 4-10 displays the SEM's (also at 25,000x) of a typical Ru/PPAN catalyst before and after an experimental run. The overall appearance of the pictures looks very much like other CMS materials that have been examined via SEM.[47] A comparison between the two micrographs shows that they are very similar and there does not appear to be much of a change. These SEM studies suggest than that the PPAN support aides in inhibiting the formation of large metal clusters and thus enables the system to produce small molecular weight products for long periods of time. The term "suggest" is important in the discussion because the SEM's are far from conclusive. Nonetheless, the experimental data and the microscopic analysis does support the

Figure 4-9. SEM of Ru/Al_2O_3 before and after catalysis.

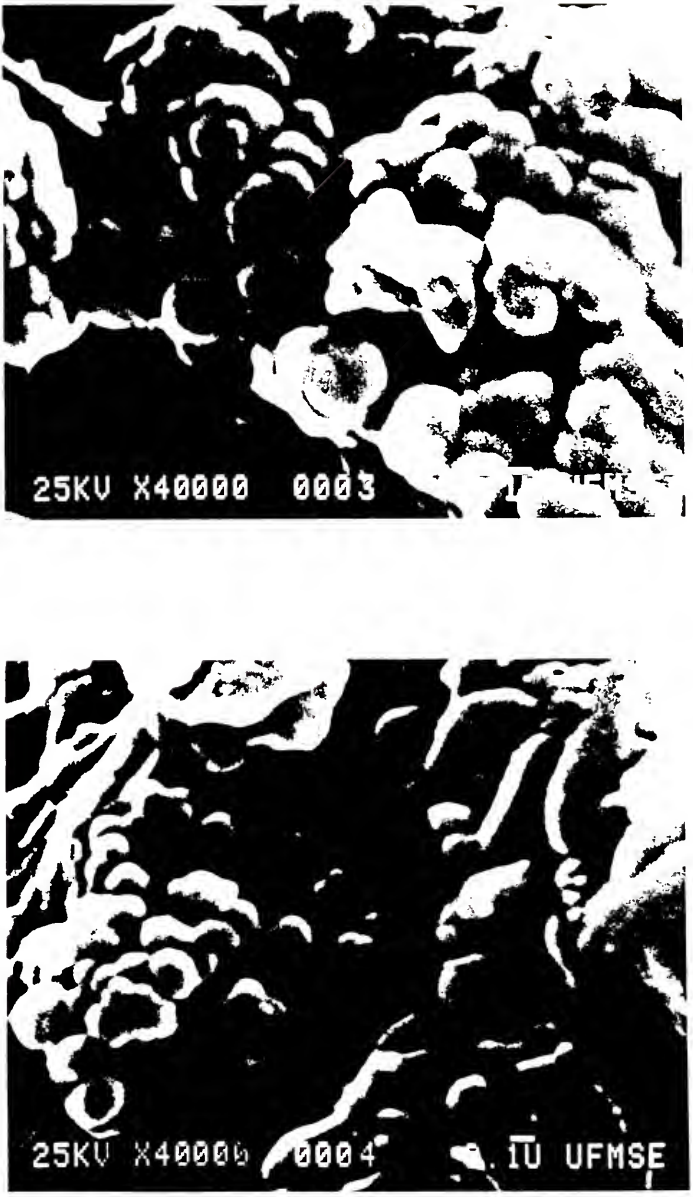

Figure 4-10. SEM of Ru/PPAN before and after catalysis.

contention that PPAN is a novel support which can impart advantageous properties to a heterogeneous catalytic system.

Ru/AX21 is also studied in the Fischer-Tropsch reaction. Figure 4-11 shows the product distribution of this system. For comparison sake, the same Ru/Al_2O_3 data as in Figure 4-6 is included. Like the PPAN system, the AX21 based catalyst also has improved selectivity for the small molecular weight products. The product distribution is even more novel because of the particular selectivity towards C_3 and C_4 products. The ASF plot for this system is shown in Figure 4-12. As is seen, the data does not fit a linear relationship very well. Thus the Ru/AX21 system has a non Schulz-Flory product distribution with a high selectivity for small molecular weight hydrocarbons. The reason for this novel reactivity is most likely related to the very porous nature of AX21 which gives it zeolite-like sieving properties. Not only do the pores and channels of these type of materials prevent the agglomeration of metal species, they also limit the size of the hydrocarbon fragment that can be made. The enhanced selectivity for C_3 and C_4 products and the complete lack of products higher than C_5 is strong evidence that the pore size of the AX21 support is not large enough for chain lengths any greater than C_4. Since the cavity effect is operating to influence the nature of the products being made, the Schulz-Flory model, which assumes methylene units can freely link, does not apply.

Another observation from Figure 4-11 is that the overall activity of the Ru/AX21 system is comparable to that of the Ru/Al_2O_3 catalyst and more active than the PPAN catalyst. The reasons for this are probably

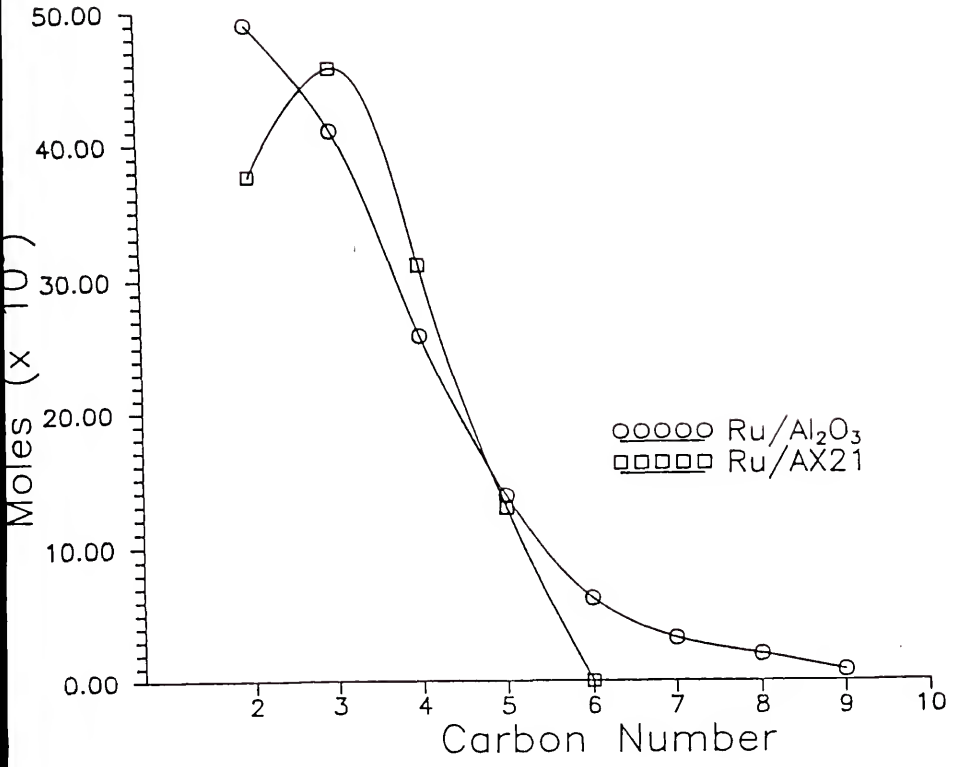

Figure 4-11. Product distribution of Ru/AX21 versus Ru/Al_2O_3.

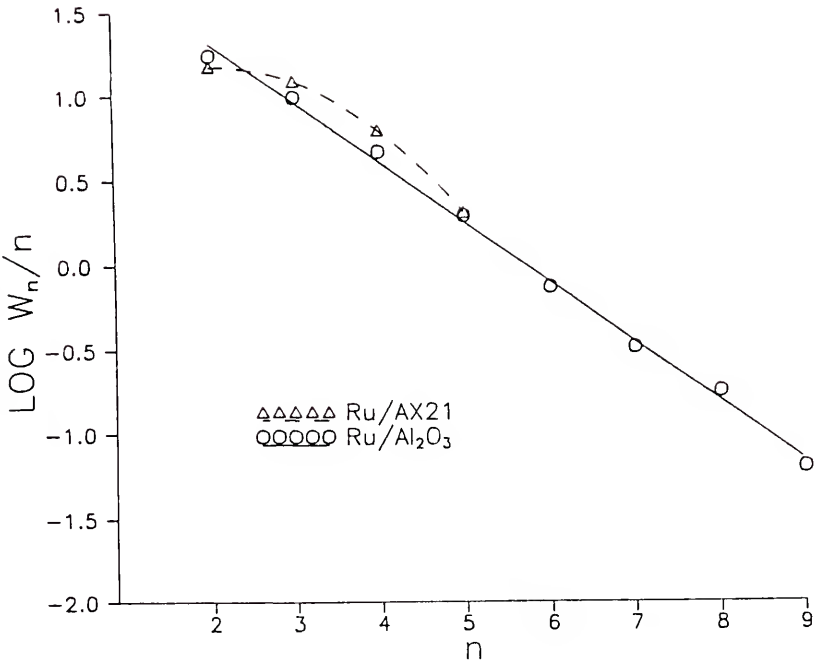

Figure 4-12. ASF plot of AX21 versus Al_2O_3.

related to the same factors as those pointed out in the previous chapter--higher surface area and greater adsorption capability. For both AX21 and CMS systems though, novel reactivity in the Fischer-Tropsch process has been demonstrated.

CO_2 Reduction Studies

Ru/PPAN catalysts have also been studies in CO_2 reaction schemes. The system is found to have high reactivity in the conversion of CO_2 to CH_4 via the methanation reaction shown below.

$$CO_2 + 4H_2 \text{ ----> } CH_4 + 2H_2O \qquad (4\text{-}6)$$

Using the stoichiometric ratio of reactants, the Ru/PPAN system exhibits 8% conversion (moles of CH_4 per moles CO_2 x 100%) at a reaction temperature of 220^{o} C. From the parameters of the experiment, 0.5g catalyst and 2 ml/min CO_2 flow, this corresponds to 2.3×10^{-3} turnovers per second. Turnovers are defined as moles of product per moles of catalyst--which in this case is based on moles of Ru present. This conversion rate is quite high. It is comparable to a recently reported Os/MgO system for CO hydrogenation.[155] This is particularly significant in light of the fact that CO based systems are typically considered to be more reactive than CO_2 systems.

Methane is the only product unless the reaction is carried out in a large excess of CO_2 (CO_2/H_2 ratio > 20 : 1). Under these conditions, small amounts of ethane and propane are also observed. Since the reduction of CO_2 is believed to go through a carbide

intermediate,[147-150] it was hoped that the surface C or C-H_n ($n < 3$) fragments could be intercepted by another species to give rise to products more desirable than methane. The first experiment was to add in a small amount of CO into the CO_2/H_2 feed of a running methanation system. Since CO can insert into metal-carbon fragments while CO_2 can not, it was thought that this procedure could lead to selective production of higher hydrocarbon products. Figure 4-13 shows the effect on product distribution a 1:10 co-feed of CO/CO_2 has on a system previously running soley in CO_2. As is seen, more than 20% of the methane that was being produced before the addition of the CO co-feed is subsequently converted to mainly C_2 and C_3 hydrocarbons. The amount of CH_4 being produced at this point was only slightly greater than that produced from CO reduction.

The second experiment to intercept the surface carbide fragment involved using HCl gas in the reactant stream in the hope of forming alkyl chlorides. Analogous to the previous experiment, HCl was added to a running methanation system. Samples taken within 10 minutes of the addition showed a reduction in the CH_4 production and the growth of a small amount of CH_3Cl. The formation of CH_3Cl reached a maximum within an hour at which time the overall activity of the system was greatly decreased. After two hours of HCl flow, activity virtually ceased. Some methanation activity was restored when the HCl flow was stopped, but after three cycles of $CO_2/H_2/HCl$ co-feed flow, the catalyst was not active. It is felt that the HCl reacts with the metal to form inactive Ru-chloro species.

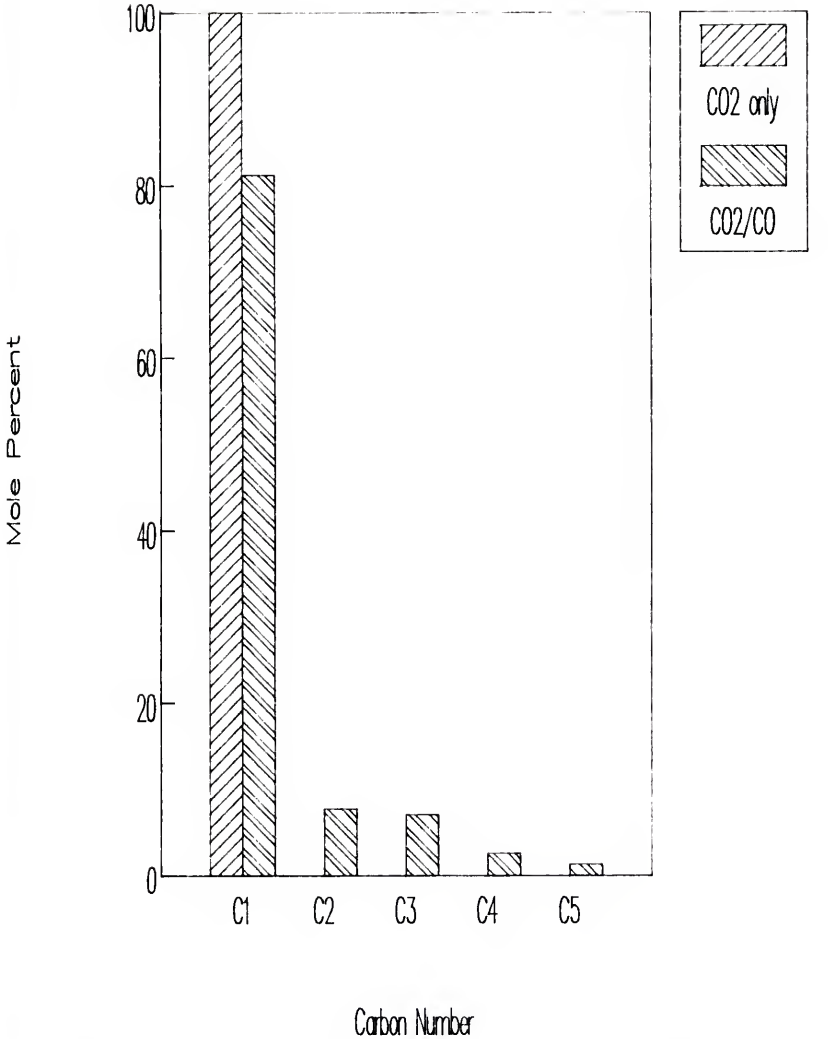

Figure 4-13. Effect of CO addition to CO_2 methanation reaction.

These experiments reveal that the reactivity of the catalyst system can be modified quite readily through proper choice of reaction conditions. Clearly, there is a great deal of interest in heterogeneous catalytic systems for the conversion of CO_2 to industrially useful products. The novel reactivity shown in this study may lead to the design of such systems.

Mechanistic Studies with Acetaldehyde Co-feed

As was mentioned above the only oxygenated product detected in the hydrogenation of CO was a trace amount of acetaldehyde. In order to investigate if this was a side product or an intermediate in the formation of higher hydrocarbon products, acetaldehyde was added to the reactant feed. The effect of this addition was dramatic. Figure 4-14 shows the product distribution of a typical system before and after $CH_3C(O)H$ treatment. It is evident that while the shape of the product distribution profile is similar, the activity for all products is greatly amplified. To further investigate the reactivity of aldehydes, analogous experiments are done with propanal. The results are virtually identical. Overall activity increases nearly fivefold while product distribution stayed the same (small amounts of C_6 and trace quantities of C_7 were detected with the propanal co-feed).

The enhancement of Fischer-Tropsch products via the addition of co-feeds to syngas has been shown in a number of studies. The use of ethylene as an initiator to the formation of higher products is well documented.[156-159] Mechanistic studies using diazomethane (CH_2N_2) and HCN have shown these species can lead to Fischer-Tropsch type

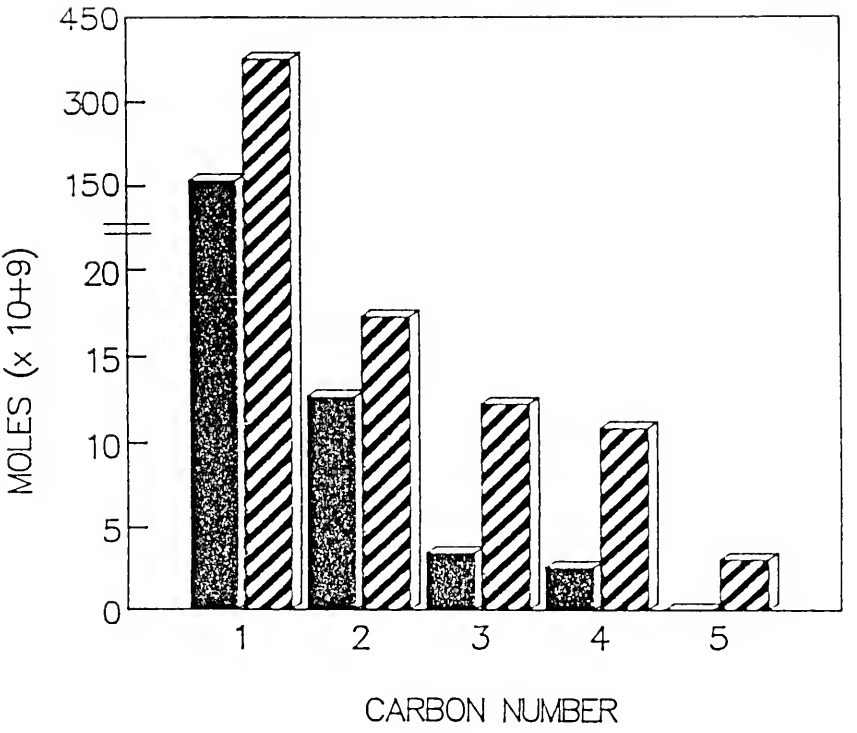

Figure 4-14. Effect of acetaldehyde addition to CO/H_2 reaction.

products.[160,161] The interesting aspect of the present work is that a knowledge of the role of adsorbed aldehyde species may lead to an understanding of the fundamental steps of the reaction. Through the years, a great deal of work has been done to elucidate the basic propagation steps. Fischer and Tropsch originally proposed in 1926 that chain growth proceeded via the "polymerization of methylene groups" on the surface of the metal.[98] This mechanism has recently received a lot of support in studies which suggest that CO dissociation is the first step followed by stepwise hydrogenation of the surface carbon fragments.[162-167] In light of this work, CO dissociation is now the generally accepted model for heterogeneous Fischer-Tropsch reactivity. There is an alternative mechanism though, which maintains that CO insertion into metal-alkyl fragments is the major chain growth process.[99,168,169] The well-documented phenomenon of carbonyl insertion into metal-alkyl ligands in homogeneous organometallic systems lends support for this mechanism. Since an adsorbed aldehyde species contains both a C-C fragment and a C-O fragment, monitoring its fate in the formation of products can help to determine if the latter mechanism contributes to the formation of products.

Table 4-3 describes the experiments that were done to elucidate the effect of carrier gas cycling on aldehyde activity. It is shown that with a N_2 carrier feed, both acetaldehyde and propanal are almost completely adsorbed by the system. When the gas flow is switched to H_2 it is observed that the majority of the aldehydes remain adsorbed although there is a small amount of hydrocarbon production. The absence of any oxygenates is in contrast to a recent study using a Cu/SiO_2

Table 4-3 Effect of Carrier Gas Cycling on Acetaldehyde Reactivity Over Ru/PPAN

GAS FLOW	ACETALDEHYDE RELATIVE % $CH_2C(O)H$ IN PRODUCTS AFTER 1 HOUR	OTHER PRODUCTS
pre gas	100[a]	---
N2	2.1	none
H_2	0	small[b] C_1-C_3
H_2 + CO_2	0	large[b] C_1
H_2 + CO	50.7	large C_1-C_5

a) 100% for the pre-gas is the total initial amount of aldehyde measured before the reactant stream enters the reactor.

b) Small and large product formation are relative to the system without aldehyde addition.

system which observed hydrogenation to alcohols under these conditions.[170] It is not until CO is added to this feed that a significant amount of aldehyde is noticed in the product stream. Concomitant with the reappearance of the aldehyde is the great enhancement of hydrocarbon products (compared to a system in the absence of aldehyde addition). Attempts were made to follow the adsorption/desorption processes with Diffuse Reflectance IR, but the results were inconclusive. As previously mentioned, PPAN materials are inherently difficult to resolve in the IR due to their intense black color. This, coupled with the fact that there are several broad absorptions present in the region where the adsorbate peaks would be located, precluded any type of direct spectroscopic investigation.

Figure 4-15 outlines our proposed mechanism to explain both the dependence of the adsorption/desorption of aldehydes on the carrier gas employed and the dramatic enhancement of hydrocarbon products observed when aldehydes are added. After the adsorption of the aldehyde, the C-O bond dissociates in a manner analogous to carbon monoxide dissociation and the C-C bond also dissociates. A recent study of adsorbed acetaldehyde on single crystal Ru invoked a similar dissociation sequence.[171] Once the system is at this point, it can go two different ways to yield products. In step 1, CO can insert to produce an acetyl fragment which can eventually desorb as an aldehyde. Recent studies have invoked such a step as a chain growth process.[172,173] In step 2, the surface adsorbed carbon species can be hydrogenated and the linking of methylene fragments can occur to give rise to the hydrocarbon products. Step 1 thus accounts for the reformation and subsequent

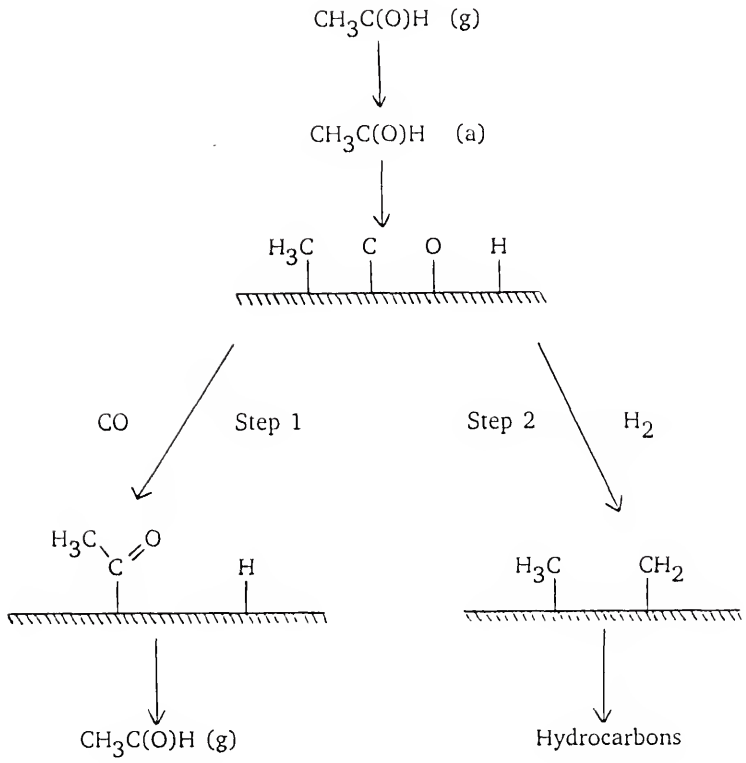

Figure 4-15. Proposed mechanism for product enhancement from aldehyde additon.

desorption of aldehydes when CO is added and Step 2 accounts for the increased product formation since two active surface hydrocarbon moieties are present.

The unique aspect of the mechanism suggested by our results is that it comprises the key features of the two major mechanisms that have been proposed for the Fischer-Tropsch reaction. Both CO dissociation into C and O surface species and CO insertion into surface hydrocarbon fragments are involved. About 50% of the aldehyde is reformed when CO is added via Step 1 and the rest of the bound aldehyde is converted to hydrocarbon products via Step 2. This result suggests that there is equal probability between the linking of methylene fragments and the insertion of CO into metal-hydrocarbon fragments. The observation of propanal in the products from acetaldehyde addition indicates that both of these processes can occur simultaneously. The futility of a labelling experiment is also demonstrated in Figure 4-15 where CO scrambling mechanisms abound.

One other observation that can be made from the data presented in Table 4-3 is that the methanation of CO_2 occurs independent of the adsorption of aldehyde. When a system which has adsorbed aldehyde present is subjected to a $H_2 + CO_2$ flow, the methanation occurs in the same manner that it does in the absence of aldehyde. CO_2 does not bring about the regeneration of the aldehyde nor are any products other than those from CO_2 reduction seen. This is consistent with the fact that CO_2 does not undergo insertion reactions in Fischer-Tropsch systems.

Methanol Oxidation

As mentioned in the introduction to this chapter there is a growing interest in the low temperature oxidation of methanol to methyl formate. The demonstrated reactivity of the AX21 system towards light alcohols discussed in the previous chapter suggests that this system may be active towards a methanol substrate. Initial experiments for the oxidation of methanol were done under the same conditions as the previous studies. The undoped AX21 system was active and selective for the formation of dimethoxymethane (DMM)--10.0% conversion with virtually 100% selectivity. This product, which is often observed in mixed oxide catalyzed systems that operate at low conversions,[174] is the full acetal of formaldehyde. This reaction was shown in table 4-2. Since DMM is readily hydrated back to formaldehyde and two equivalents of methanol, an attempt was made to increase the conversion of methanol to aldehydes by using co-feeds of methanol and H_2O. The addition of a significant of H_2O (> 10%) in the feed, however, is found to greatly decrease the overall conversion. The hydrophilic nature of the AX21 material enables H_2O to compete more efficiently for adsorption sites than methanol and thus inhibits its reactivity.

The fact that any activity is observed with a non-metallated catalyst is very interesting. To further enhance reactivity, the CMS catalyst was doped with various molybdenum species. This metal is chosen because many studies have shown molybdenum oxide moieties to be active catalysts for methanol oxidation.[175-177] The results for these experiments are shown in Table 4-4. It is evident that the MoO_3/CMS

Table 4-4 Methanol Reactivity Over Molybdenum Doped Catalysts

SAMPLE	MAJOR PRODUCT	%CONVERSION	%SELECTIVITY
SiO_2	---	---	---
AX21	Dimethoxymethane	10.0	98.0
MoO_3[a]	Methyl Formate	22.8	98.0
MoO_3/SiO_2	Methyl Formate	12.2	98.4
MoO_3/AX21	Methyl Formate	70.0	96.4
$(NH_4)_2MoO_7$/AX21	Methyl Formate	70.0	96.0
Na_2MoO_4/AX21	Dimethoxymethane	3.0	82.0
MoO_3/AX21 (N_2)[b]	Dimethoxymethane	2.2	90.9
MoO_3/AX21 (350)[c]	Formaldehyde	90	< 60
AX21[d]	Dimethoxymethane	10.0	43.0
MoO_3	Methyl Formate	13.5	57.0

CONDITIONS: Reaction temperature--230° C. Air feed--5 ml/min. Substrate feed--0.2 ml/hr. Reaction time--10 hrs.

a) 0.5g of bulk MoO_3 used for this experiment.

b) Product formation ceases after 3 hrs.

c) Reaction temperature is 350° C for this experiment. Conversion and selectivity numbers are not as exact because not all products are calibrated.

d) 0.05g of AX21 are placed on top of 0.10g MoO_3 in the reactor tube.

catalyst is far more active than either a similarly prepared MoO_3/SiO_2 catalyst or a bulk MoO_3 sample. It is further observed that among molybdena doped CMS systems, the Lewis acid form, MoO_3, is necessary for any significant activity.Ammonium dimolybdate, nominally $(NH_4)_2MoO_4$, is a common source of molybdic oxide for it evolves NH_3 and H_2O upon heating. Thus, at reaction conditions, it is essentially the same as the MoO_3 doped system. The doping level was altered accordingly so that the weight percentage of MoO_3 is the same for both systems. As expected, the catalysts have identical reactivity. Na_2MoO_4, on the other hand, is a chemically different molybdenum species that does not have the Lewis acidity of MoO_3 and thus the activity enhancement is not observed. The major product formed from methanol oxidation with the MoO_3 systems is methyl formate. This species is produced by a dimerization of formaldehyde units as shown in table 4-2. The activity of the MoO_3/CMS system is significantly greater than those recently reported.[116,178-180]

In order to probe the possible synergistic effect between MoO_3 and AX21, both of which catalyzed methanol oxidation on their own, an experiment is done where both species are present, but not intimately mixed. With 0.5g of AX21 layered on top of 0.10g of MoO_3 in the reactor tube (this is labeled as AX21/MoO_3 in Table 4-4) the experiment is run as usual. The observed activity is essentially that of the sum of the two species if they were present alone. It is interesting to note that the same result is obtained in a similar experiment with the MoO_3 on top and CMS on bottom; however, this latter system is not as active. The conversion rate is only about 8%.

The synergistic effect observed from the above results between the AX21 support and the MoO_3 is very interesting. The MoO_3/AX21 catalyst (and the similar $(NH_4)_2MoO_7$/AX21 system) is far more active than the sum of the activities of each of the constituents. Furthermore, the layering experiments show that not only do the constituents have to both be present, but also that they have to be intimately mixed. These layering experiments further demonstrate that the adsorption properties of the AX21 are a key parameter. Although both systems show the same type of reactivity, the system with AX21 on top is much more active. This suggests that the ability of the AX21 to adsorb the substrate, and hold it until it is transformed, is the major reason for the great enhancement of reactivity for the doped AX21 systems. The MoO_3/AX21 catalyst, which has the constituents intimately mixed, is best able to synergistically utilize the advantages of the respective components.

At the reaction temperature employed for the studies in Table 4-4 (230^oC), methyl formate is the expected product. Since MoO_3 is also a catalyst for formaldehyde formation (at higher reaction temperatures), experiments were done at 275^o C, 300^o C, 330^o C, and 360^o C with the MoO_3/CMS catalyst. As temperature increases, methanol conversion increases, however, selectivity decreases sharply. At temperatures above 300^o C, the major product is formaldehyde. By 360^o C, virtually 100% of the methanol is converted, but the selectivity to formaldehyde is less than 60%. Among the numerous other products observed are several hydrocarbons (ethane and propane being present in the greatest quantity) which are apparently formed in part from degradation of the AX21 material itself. This proposal is supported by the fact that we

observe a 50% weight loss of the catalyst after a 20 hour experimental run at this high reaction temperature.

The breakdown of the carbonaceous material should not be too surprising considering the conditions of this reaction. High temperature, oxidizing atmosphere, and the presence of MoO_3, a strong oxidizing agent, make degradation processes probable. Several points should nonetheless be noted. The appreciable catalyst weight loss is not observed with the same MoO_3/AX21 system for methanol oxidation at 230^0 C. The pre and post reaction weights are virtually identical after 48 hour runs. Furthermore, AX21 systems without MoO_3 doping can tolerate high reaction temperatures. In the ethyl benzene system discussed in the previous chapter, no significant loss in weight (or activity) is observed after 120 hours of continuous operation at a reaction temperature of 350^0 C. The observation of hydrocarbon products which arise in part from the breakdown of the AX21 support under high reaction temperature conditions is very interesting. Although this is obviously counter-productive, it is somewhat novel that the support material would react with adsorbed methanol fragments to make new products. When the system is run at these high temperatures with just a H_2O feed, there are no hydrocarbons formed. The degradation product is simply CO_2. Thus the CMS fragments actually form new bonds with the substrate moieties.

In order to further investigate the synergistic interaction of the low temperature systems a series of characterization studies studies have been done. SEM, XRD, and XPS techniques have been conducted on bulk MoO_3 before and after catalysis, MoO_3/SiO_2 before and after

catalysis as well as MoO_3/AX21 before and after catalysis. To ensure consistency these methods were performed on the exact same samples. SEM enables a visual observation of changes that occur with the various samples during the course of the reaction. XRD also affords an analysis of changes that occur as a result of a catalytic run--particularly with regards to metal crystallite size. XPS provides a detailed examination of the oxidation states of the various components both before and after catalysis.

Figure 4-16 shows the SEM's (at 6000 X) of the bulk MoO_3 system. The top micrograph is of the pre-catalyst. The MoO_3 crystallites are observed to have a cigar shape. The bottom micrograph is the same system after catalysis. It is quite evident that a large degree of sintering has occurred. The metal crystallite size has grown significantly and the shapes have amalgamated to large blocks. These observations are not at all surprising since unsupported metal oxide species sinter quite readily. Figures 4-17 and 4-18 display the micrographs of MoO_3/SiO_2 and MoO_3/AX21 respectively before and after catalytic experiments. In both of these figures, the pre-catalysis system is shown in the top microcraph and that of the post-catalysis run is in the bottom picture. The MoO_3/SiO_2 system is observed to have undergone sintering in much the same way as the unsupported MoO_3 system. The metal crystallite shapes appear as large blocks. It is also interesting to note the smoothness of the SiO_2 background in the bottom micrograph. This is due to the large amount of carbonaceous residues that were deposited on the catalyst as a result of the reaction. The MoO_3/SiO_2 pre-catalyst is an olive green color. The post-catalyst is

Figure 4-16. SEM of bulk MoO_3 before and after reaction.

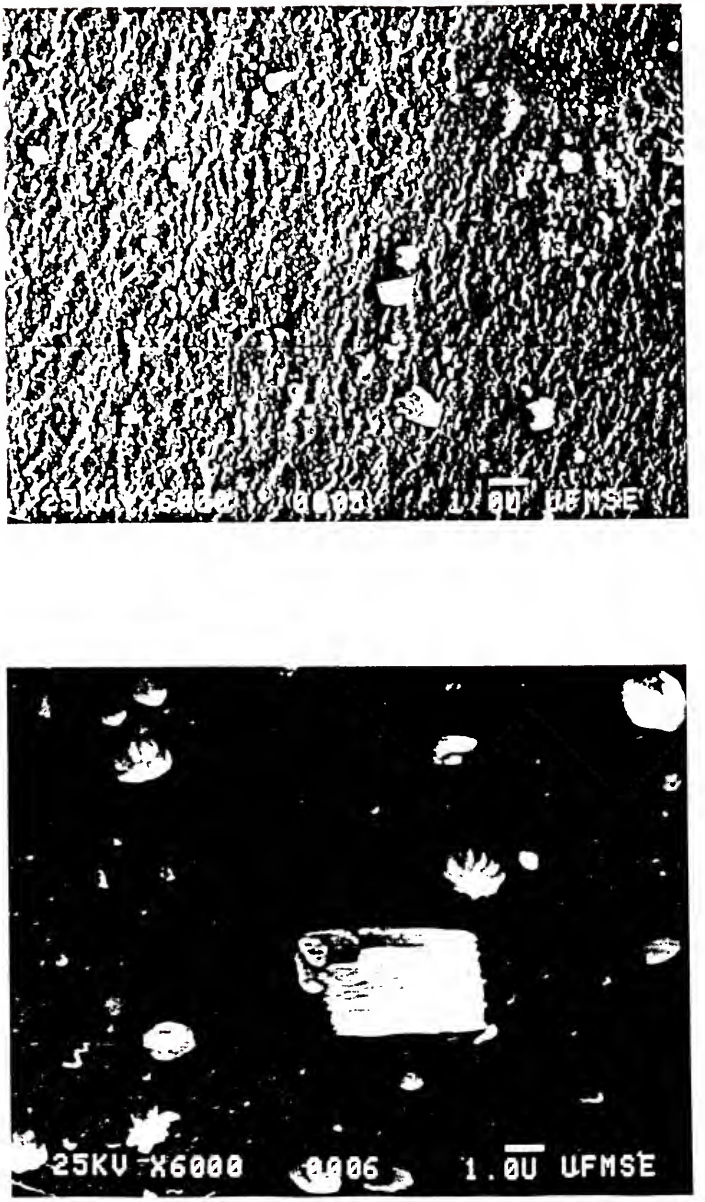

Figure 4-17. SEM of MoO_3/SiO_2 before and after reaction.

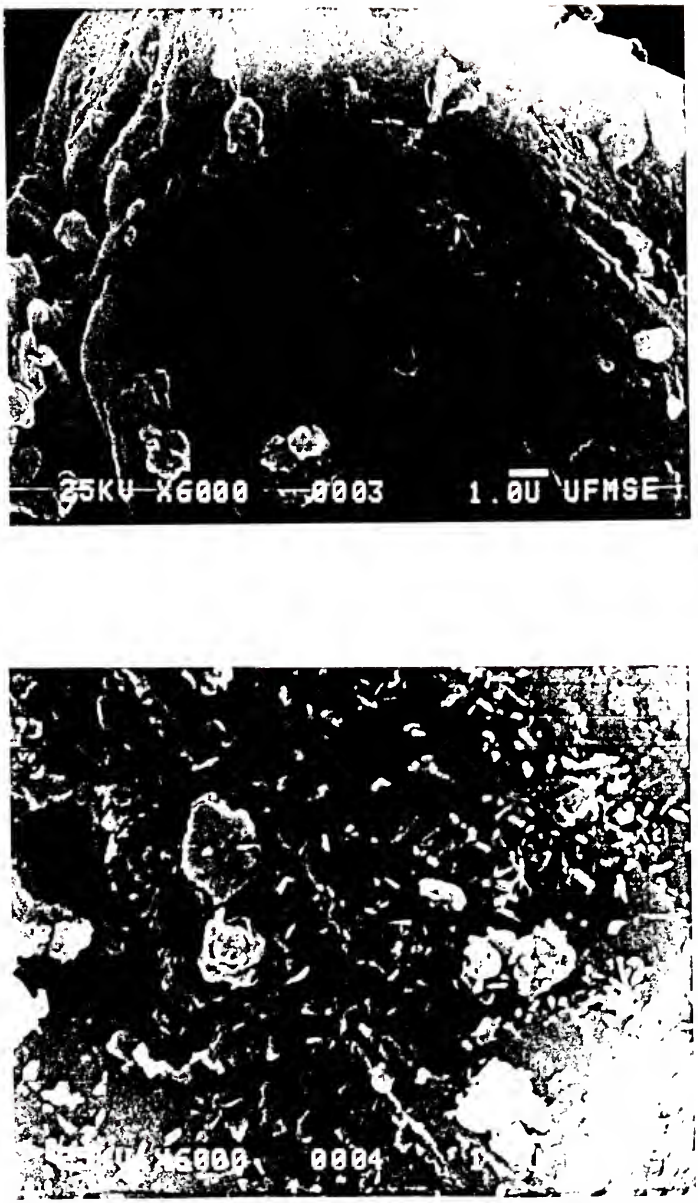

Figure 4-18. SEM of MoO_3/AX21 before and after reaction

completely black. The bottom micrograph in Figure 4-18 is of the MoO_3/AX21 post-catalyst. No large metal crystallite blocks are observed. It is clear that there has not been a great deal of sintering. The SEM results thus show that the AX21 support serves to inhibit any significant degree of grain growth.

As mentioned previously in the discussion of the SEM analysis of the Fischer-Tropsch systems, this technique is only qualitative and often not conclusive. In order to obtain more of a quantitative viewpoint on the particle size distribution and general crystalline nature of the metal species in these catalysts, XRD studies were carried out. In addition to gaining information regarding the type of crystalline phases that may be present, this technique can also determine the particle size of the metal dopants. This value is obtained via the Scherrer formula given below:[181]

$$t = \frac{0.9\ \lambda}{B \cos \theta} \qquad (4\text{-}7)$$

In this equation t is the crystallite size of the species being examined; θ is the Bragg angle of the particular peak selected; λ is the wavelength of radiation; and B is the net line width change caused by particle size. This is measured at the half maximum of the peak.

In light of the SEM results, it was expected that there would be a large increase in the MoO_3 particle size for the SiO_2 based system when comparing the pre and post catalyst. Similar thinking would suggest that there would not be any increase in the crystallite size on the AX21 supported system. Line broadening studies show, however, that there is

no significant difference in any of the samples--MoO_3/SiO_2 before and after catalysis and MoO_3/AX21 before and after catalysis--examined in this work. All four of the samples were found to have a crystallite size of 400 ± 50 Å. This rather substantial deviation is due to the fact that these particles are relatively large for a line broadening measurement technique. This method is usually applied to systems having particle sizes less than 200 Å. It is quite possible that there are significant differences between the samples studied, however, these differences are in the range of the deviation of the method.

The XRD patterns of the above samples also deviate from what one would expect. Figures 4-19 and 4-20 show the XRD pattern of the MoO_3/SiO_2 and MoO_3/AX21 systems respectively prior to a catalytic experiment. Despite the fact that the composition of the Mo species should be significantly different in these two environments, the XRD patterns are very similar. As mentioned previously, the MoO_3/SiO_2 compound has a green color after it has been dried in vacuum. This observation led to the hypothesis that this species was a molybdenosilicate compound. The MoO_3/AX21 system, on the other hand, was expected to have similar properties to bulk MoO_3. The XRD results show that there is no appreciable difference between the samples with regards to the nature of the Mo species. No discreet cystalline phases could be determined from these patterns. They could not be identified as MoO_3 or any other molybdenum oxide.

The XRD patterns for the MoO_3/SiO_2 and MoO_3/AX21 systems after catalysis are shown in Figures 4-21 and 4-22. Again it is observed that they are virtually identical to each other, however, they are

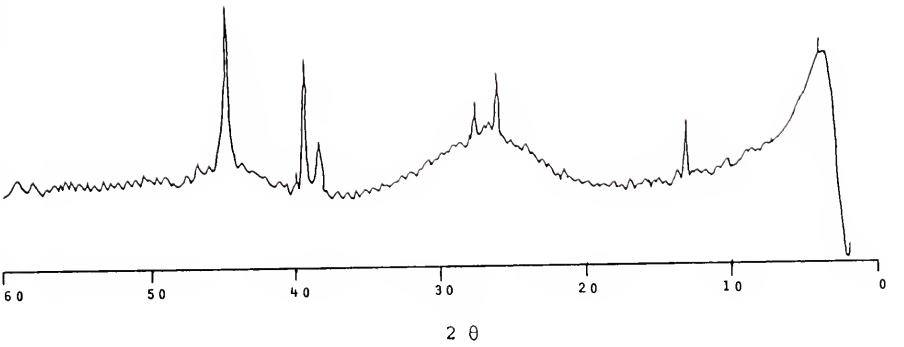

Figure 4-19. XRD of MoO_3/SiO_2 before reaction.

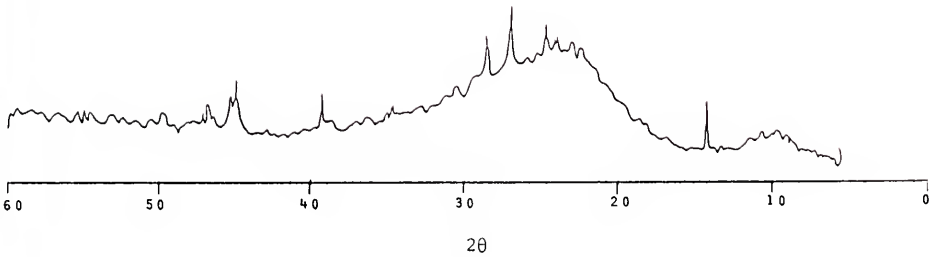

Figure 4-20. XRD of MoO_3/AX21 before reaction.

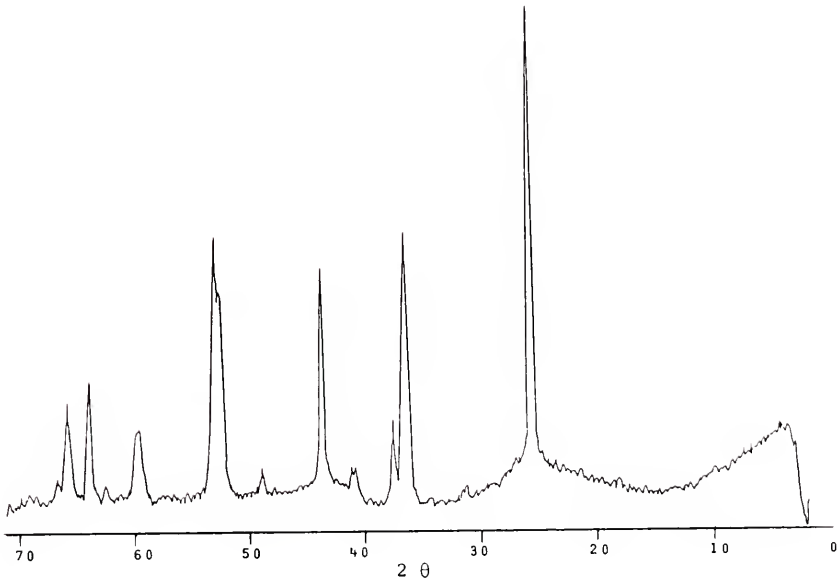

Figure 4-21. XRD of MoO_3/SiO_2 after reaction.

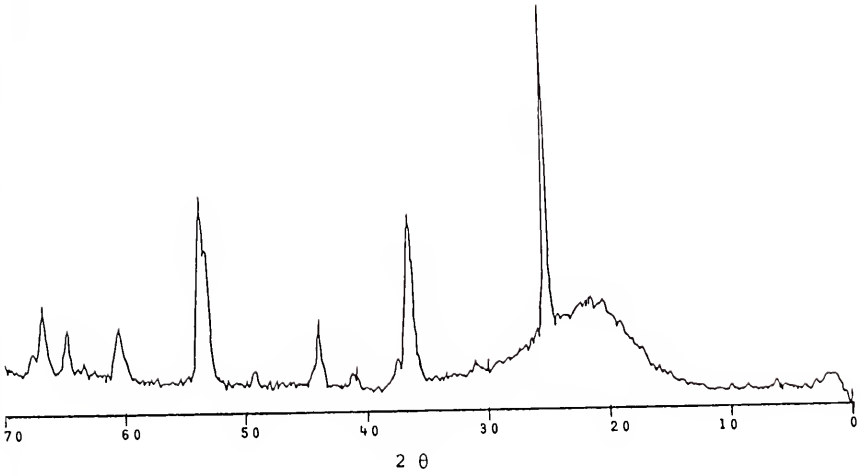

Figure 4-22. XRD of MoO_3/AX21 after reaction.

significantly different from the pre-catalysis spectra of Figures 4-19 and 4-20. These results suggest that these materials operate in similar fashions with respect to the role of the metal component in their catalytic activity. The considerable differences between the catalytic reactivity of these two systems must be related to factors other than specifc metal/support interactions. The enormous surface area that the AX21 material provides the system as a whole along with its exceptional adsorption capabilities are most likely the reasons for the significantly greater catalytic ability of this system.

One other inference can be made from the diffraction patterns of Figures 4-21 and 4-22. Like the others that have been drawn above, this observation is not what one would readily expect. The predominant crystalline phase of the molybdenum species present in these patterns matches very closely the literature values of MoO_2.[182] Since these reactions are run in an air atmosphere, it is quite suprising that the major molybdenum phase would be a reduced species. This is especially true in light of the fact that these catalysts, particularly the MoO_3/AX21, were still active for methanol oxidation. A possible explanation for this result may be related to the mechanism typically invoked for MoO_3 based oxidations. As mentioned in the introduction to chapter three, one of the oxygens from the oxide dopant is used in the catalytic process. The catalytic cycle is completed when oxides produced from the dissociation of oxygen molecules from the feed migrate through the lattice and reoxidize the metal species. Since XRD is a bulk technique, it is possible that a large amount of the metal species is in a reduced form with the fully oxidized components being mostly

concentrated at the surface. The fact that all of the catalysis is occurring on the surface would explain why the system is still active.

In order to investigate the nature of the molybedenum species at the surface, a series of XPS studies are conducted. Five separate samples were analyzed: bulk MoO_3 before reaction, MoO_3/SiO_2 before and after reaction and MoO_3/AX21 before and after reaction. The Mo 3d, O 1s, C 1s, and Si 2s orbitals were studied. Figure 4-23 shows the deconvoluted spectrum and the respective binding energies in the Mo 3d region of the bulk MoO_3 sample. Since this sample did not conduct very well a significant amount of charging occurred. The result of this is that the peaks appear at higher binding energy values than those usually reported for such a system.[183,184] Nevertheless this spectrum can be used for comparative purposes. The shape of the peaks, their relative areas, and the peak to peak separation is indicative of a typicalMo(VI) oxide system.

Figure 4-24 shows the spectrum of the Mo 3d region of the MoO_3/AX21 pre-catalyst. It is evident that the peak profile is identical to the MoO_3 system shown in the previous figure. Since the carbonaceous support is an excellent conductor of electricity, there is no charging present in this system. For this reason the exact values of the binding energies match quite well to other MoO_3 supported systems.[185-190] This experiment shows then that the molybedum species present on the surface of the MoO_3/AX21 system prior to catalysis is very similar to bulk MoO_3.

The Mo 3d region for the MoO_3/SiO_2 complex before catalysis is shown in Figure 4-25. The charging phenomenon is again present in this

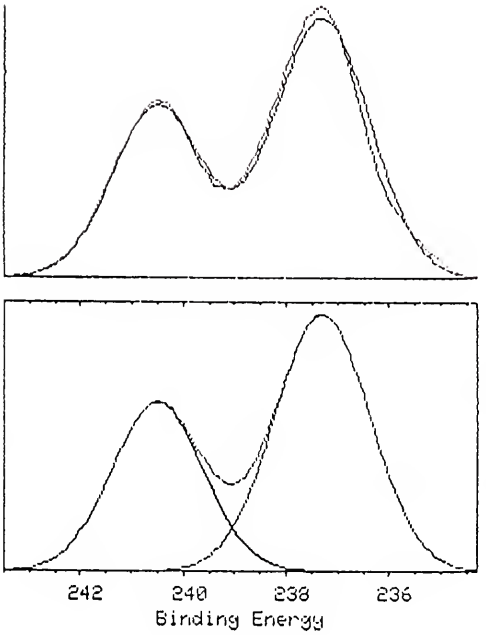

Line	Elmt.	Energy	Int.	FWHM	Area
GAUSS	M03D	237.3	95.6	2.3	61.4
GAUSS	M03D	240.5	63.1	2.1	38.7

Figure 4-23. XPS of the Mo 3d orbitals of bulk MoO_3.

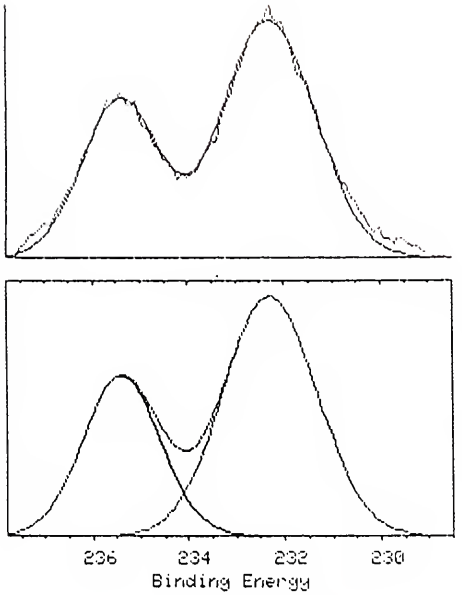

Line	Elmt.	Energy	Int.	FWHM	Area
GAUSS	MO3D	232.2	93.7	2.3	62.8
GAUSS	MO3D	235.4	62.5	1.9	34.5

Figure 4-24. XPS of the Mo 3d orbitals of MoO_3/AX21 pre-catalyst.

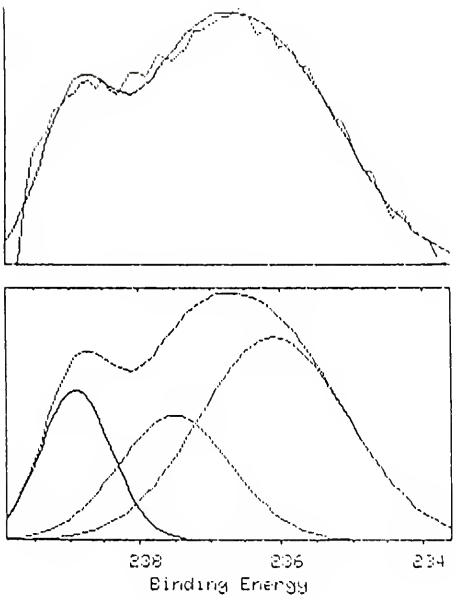

Line	Elmt.	Energy	Int.	FWHM	Area
GAUSS	M03D	236.0	80.0	2.5	55.1
GAUSS	M03D	238.9	59.4	1.2	19.4
GAUSS	M03D	237.5	49.4	1.9	26.0

Figure 4-25. XPS of the Mo 3d orbitals of MoO_3/SiO_2 pre-catalyst.

system due to the non-conducting nature of this material. The broad envelope of peaks show that this species is more involved than just Mo(VI) oxide. The presence of shoulders in the lower binding energy regions illustrates that reduced species exist. This observation suggests that species similar to the molybdeno-silicate compound discussed above are present. The Si 2s spectral region for this sample is shown in Figure 4-26. It is evident that there are several different silicon species present. This is further evidence of an inter-metallic composite since uncomplexed SiO_2 should display just one peak.

The XPS spectrum for the Mo 3d region of the MoO_3/AX21 post catalyst is shown in Figure 4-27. Virtually no change is observed in the AX21 based system before and after catalysis. The spectrum is very typical of a supported Mo(VI) oxide compound. This is the result originally anticipated. Since the reaction is run in an air atmosphere and the catalyst is not observed to be deactivated, the fully oxidized molybdenum moiety is expected. The fact that this does not coincide with the XRD results is most likely due to the inherent differences in these techniques. XRD, as previously mentioned, is a bulk method; whereas, XPS is only surface sensitive.

The Mo 3d region of the MoO_3/SiO_2 post catalyst is shown in Figure 4-28. Like its AX21 counterpart there are not major differences before and after catalysis. There does appear to be an increase in the peaks most likely associated with Mo(VI) oxide. The C 1s spectrum of this material is shown in Figure 4-29. It is evident that there is a number of different types of species present on the surface of this catalyst.

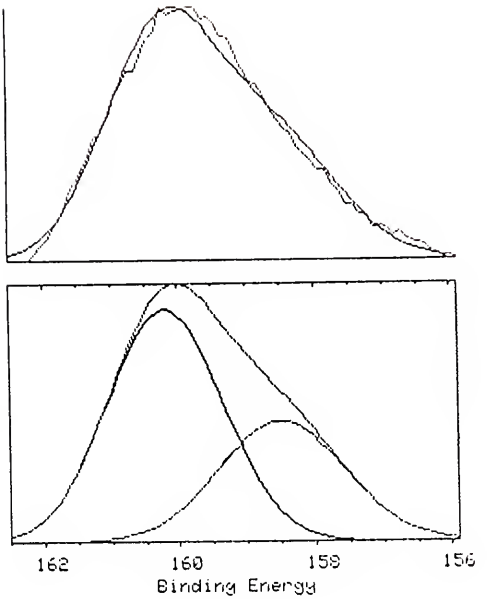

Line	Elmt.	Energy	Int.	FWHM	Area
GAUSS	Si2S	158.5	46.3	2.3	36.4
GAUSS	Si2S	160.2	90.0	2.0	64.3

Figure 4-26. XPS of the Si 2s orbital of MoO_3/SiO_2 pre-catalyst.

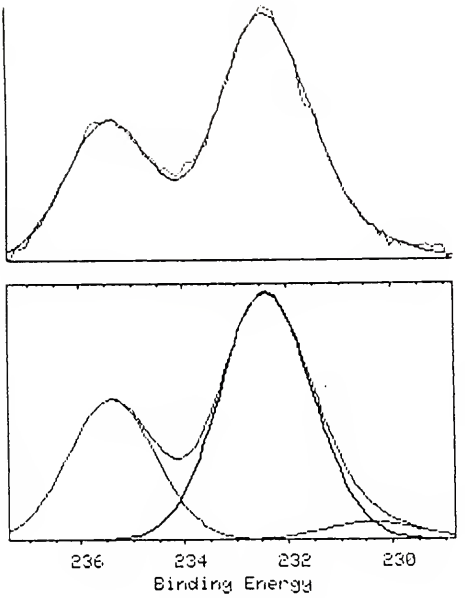

Line	Elmt.	Energy	Int.	FWHM	Area
GAUSS	MO3D	230.3	6.9	2.1	4.3
GAUSS	MO3D	232.4	96.3	2.1	61.9
GAUSS	MO3D	235.4	55.0	2.0	33.4

Figure 4-27. XPS of the Mo 3d orbitals of MoO_3/AX21 post-catalyst.

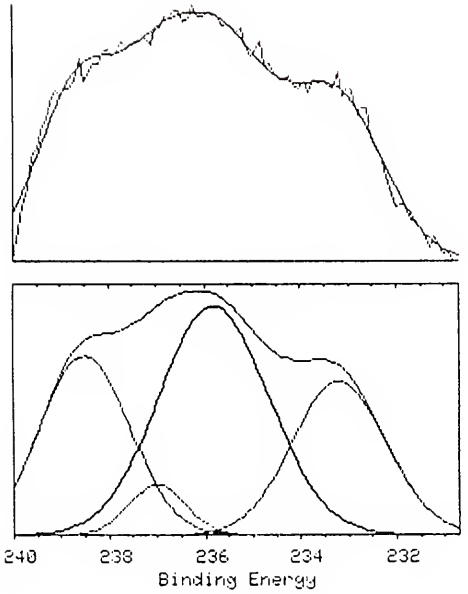

Line	Elmt.	Energy	Int.	FWHM	Area
GAUSS	MO3D	238.5	71.3	2.2	26.7
GAUSS	MO3D	235.8	91.3	2.8	44.1
GAUSS	MO3D	233.1	60.6	2.3	24.8
GAUSS	MO3D	237.0	20.0	1.5	5.0

Figure 4-28. XPS of the Mo 3d orbitals of MoO_3/SiO_2 post-catalyst.

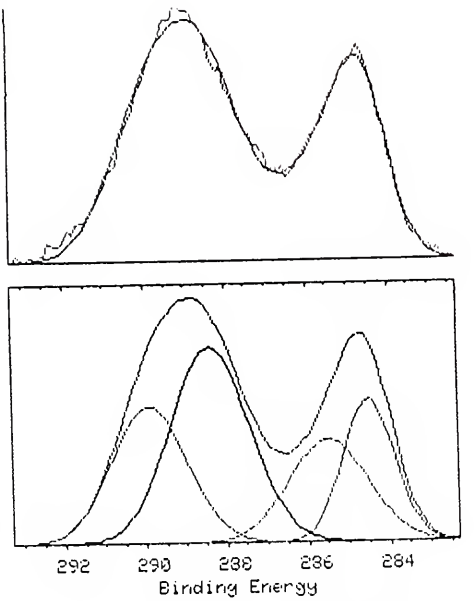

Line	Elmt.	Energy	Int.	FWHM	Area
GAUSS	C1S	284.5	54.4	1.5	17.6
GAUSS	C1S	288.3	75.0	2.3	37.2
GAUSS	C1S	289.9	52.5	2.2	24.9
GAUSS	C1S	285.5	39.4	2.3	19.5

Figure 4-29. XPS of the C 1s orbital of MoO_3/SiO_2 post-catalyst.

The various analytical techniques discussed here--SEM, XRD, and XPS--underscore the difficulty in characterizing heterogenous catalytic materials in general and carbonaceous based systems in particular. As is evident from the above discussion, there are several instances where the information obtained from these studies is conflicting. The experimental data clearly shows that there is a synergistic relationship between the MoO_3 dopant and the AX21 support. The SEM results suggest that the AX21 support inhibits sintering of the metal. The XRD studies show that if this sintering inhibition is apparent, it cannot be occurring to any great extent. These studies further complicate matters by suggesting that the post catalyst has been reduced. The XPS work reveals that at least at the surface the catalyst is still in its fully oxidized state. Nevertheless these studies do yield insight regarding the fundamental nature of these novel catalytic materials. It is apparent that the physical properties of the AX21 material, i.e. surface area and adsorption capability, may be the most significant contributors to the synergistic interaction.

Deep Oxidation of Chlorinated Hydrocarbons

The success of the MoO_3/AX21 catalyst for methanol oxidation led to its use in the deep oxidation of CH_2Cl_2 reaction scheme. As described in the experimental section, the reactivity of the system is followed during the experiment by the presence of CO_2 in the post gas stream and the overall conversion is based on a titration of the HCl formed at the end of the experiment. Initial studies are done analogously to the other oxidation systems. In particular, the flow

rate first employed is 5 ml/min. Under these conditions the system is not very active. Only 3.46×10^{-3} moles of HCl are formed. Since two moles of HCl are formed per mole of CH_2Cl_2 reacted (equation 4-?), only 1.73×10^{-3} moles of CH_2Cl_2 were converted via the deep oxidation process. This calculates to an overall conversion of 2.2%.

Nevertheless, there are some encouraging aspects of the above results. No other products, for example, phosgene ($COCl_2$), are observed. This is very important because in incineration disposal methods, hazardous products such as $COCl_2$ are often generated. Furthermore, the experimental conditions for the above reaction are clearly not optimized. Unlike other catalytic processes where it is desirable to have high space velocities in order to control selectivity and maximize efficiency, an application such as this does not require a fast throughput. The whole goal is to completely degrade the substrate. In light of this, subsequent studies are done with a considerably slower carrier flow rate. At 1.0 ml/min, the conversion is raised by nearly an order of magnitude--2.91×10^{-2} moles of HCl are detected which corresponds to an 18.5% conversion.

Several observations are made during the above experiment. As mentioned previously, the dynamic reactivity of the system can be followed by the presence of CO_2 in the post reactor stream. Through the first five hours of this experiment, large amounts of CO_2 are detected. Over the remainder of the study, however, these levels diminish appreciably. When the system is disassembled, a ring of light yellow crystals is observed at the bottom of the reactor. As the tube is allowed to sit in the fume hood, the crystals appear to become hydrated

and a bluish liquid forms. The yellow crystals are most likely MoO_2Cl_2 formed by a reaction between the MoO_3 dopant and HCl it generated from the CH_2Cl_2 reactant. The MoO_2Cl_2 then sublimed off the surface and condensed in the cool zone of the reactor. The bluish liquid is most likely one or more of the so-called "molybdenum blue" complexes. The general formula for these is $Mo_2O_5 \cdot xH_2O$, but they may have variations in the molybdenum and oxygen content. These complexes can readily form when MoO_2Cl_2 is exposed to warm moist air such as that present in the laboratory.

The formation of the oxychloride complex explains why the levels of CO_2 diminished. This suggests that the initial conversion of CH_2Cl_2 was quite high, but it fell off as the catalyst deactivated. As mentioned above, the MoO_2Cl_2 is produced from MoO_3 and CH_2Cl_2. The unbalanced reaction below is probably involved in this process.

$$MoO_3 + CH_2Cl_2 \text{ ------> } MoO_2Cl_2 + HCl + CO_2 \qquad (4\text{-}8)$$

Since this reaction scheme also produces HCl and CO_2, one has to be sure that the activity observed is truly catalytic and not just a stoichiometric process. The amount of MoO_3 present in the catalyst sample is 5.79×10^{-4} moles. As mentioned above, 2.91×10^{-2} moles of HCl are formed. Thus there are 50 times more HCl produced than MoO_3 present. This clearly shows that the system is catalytic initially, but that it eventually loses activity due to the breakdown of the catalyst.

In order to remedy this problem, several tungsten complexes are studied. The Lewis acid, WO_3, should have comparable catalytic activity

to MoO_3 and it does not form volatile oxychlorides. Table 4-5 shows the results of all the Mo and W systems that have been studied for the deep oxidation of CH_2Cl_2. As is shown, the WO_3 and $(NH_4)_2WO_4$ catalysts are active while the Na_2WO_4 system is not. These results concur with the previous work in methanol oxidation systems--Lewis acid nature is essential for activity. The conversions for the WO_3/AX21 and $(NH_4)_2WO_4$/AX21 systems are not as high as those for MoO_3/AX21 (10.56% and 15.27% respectively), however, this is most likely due to the lower H_2O solubility of these dopants. WO_3, which is not soluble at all, did not get supported well on the AX21 material. After the reflux step of the preparation, there was a distinct segregation of the dopant and support phases. Thus this system did not benefit from the high surface area and adsorption capability of the support. The $(NH_4)_2WO_4$ compound was more soluble, but there was still a noticeable heterogeneity of the catalyst constituents. The use of the tungsten species is successful, though, because no loss in CO_2 production or oxychloride formation is observed throughout the reaction.

Clearly, the goal of a deep oxidation scheme such as this is to design a system that will exhibit 100% conversion. Nevertheless, these preliminary results are encouraging. The experimental conditions for these systems, in terms of metal loading, carrier gas flow rate, and the reaction temperature, have not been optimized. Furthermore, the conversion data based on HCl formation are probably significantly underestimated. It is known that a considerable amount of HCl does not get quenched in the H_2O trap and simply leaves the system. Blue litmus paper placed at the exit port of the trap turns red during the course of

Table 4-5 Deep Oxidation of CH_2Cl_2 Over Doped AX21 Catalysts

CATALYST[a]	%CONVERSION[b]
	MoO_3/CMS20.2
Na_2MoO_4	1.1
WO_3/CMS	15.6
$(NH_4)_2WO_4$/CMS	15.2
Na_2WO_4/CMS	2.0

a) 3.47×10^{-3} moles of each dopant is mixed with 2.5 g of AX21 to prepare these catalysts. This is a 10-15% by weight loading. 0.5 g of catalyst is used in each experiment.

b) Based on a titration of the HCl condensed in the post reactor trap.

the reaction to indicate that some HCl is escaping. Future work should be done with a known concentration of base in the trap which can then react with the acid and thus prevent it from exiting. Calculation of the conversion could be performed by back titration methods. Other improvements, such as better supported WO_3 species via increased solubility in the deposition step, may also greatly increase reactivity.

CHAPTER 5
CARBON MOLECULAR SIEVES IN ADVANCED MATERIALS APPLICATIONS

Introduction

This chapter focuses on the use of pyrolyzed poly (2,6 dimethlparaphenylene) oxide (PPPO) composites in advanced materials applications. Titanium doped PPPO systems have been investigated as electrocatalysts for the four electron reduction of O_2. Lithium chloride doped PPPO systems have been studied as ion selective electrodes. Lastly, PPPO has been studied as a resin matrix support material to enhance the structural stability of advance materials such as carbon fibers and high Tc superconductors. In each of these applications, the unique structure and characteristics of PPPO impart novel properties to the composite systems.

The structure of PPO and PPPO were shown in Figure 1-2. The various dopants become dispersed in the composite matrix when the material is pyrolyzed. Initial studies are done to see if the various chemical and physical properties of the dopant could be probed while it is encapsulated in the pyrolyzed polymer matrix. Fe(0) PPPO composites are prepared as describe in Chapter 2. It is found that at 30% by weight loading, the pyrolyzed composites exhibit the electrical and magnetic properties of metallic iron. Below this level of doping, the materials are not conductive and show no attraction to a magnet.

Unpyroloyzed samples, up to a loading of 50%, are equally unresponsive to a magnet or a volt meter (measuring conductivity). Thus during the pyrolysis process, the Fe particles are able to move through the matrix and interact with each other in such a way that there is appreciable metal/metal contact. A simple chemical experiment is done by placing the Fe/PPPO pellet in a 1 M solution of $AgNO_3$. An immediate reaction occurs. The solution becomes slightly brownish due to the liberation of Fe(III) (aq) and large platelets of Ag(0) deposit on the pellet. The pellet maintains its structural integrity, but now it is a Ag/PPPO composite as opposed to an Fe/PPPO system. These experiments, although relatively trivial from a research standpoint, do verify that the PPPO matrix can be employed as a medium for studying the chemical and physical properties of various dopant species.

As mentioned, one of the applications studies is the design of electrocatalysts for the full four electron reduction of O_2. The development of such an electrode material would constitute a major advance in fuel cell technology. Present (acid-electrolyte) oxygen cathodes employing platinum metal as the electrode catalyst are too expensive for widespread application and, moreover, produce useful current densities only at overpotentials of several hundred millivolts-far from the theoretical potential of 1.23 V vs. SHE.[191] A great deal of work has been done on macrocyclic transition metal complexes as O_2 reduction catalysts, but most function at negative potentials and only effect the two electron reduction of O_2 to H_2O_2.[192,193] Recently a lot of research effort has been focused on chemically modified electrodes which employ elegant ligand systems. A host of studies has been done on

the cobalt face-to-face porphyrin complexes which are capable of binding O_2 and fully reducing it to H_2O without going through a H_2O_2 intermediate.[191,194-197] Although these systems have been demonstrated to function efficiently, there are some problems associated with the exotic nature of their composition. The ligand materials are not trivial to synthesize even on a laboratory scale and they are not stable towards self-oxidation during repeated cycling.

In light of this, the criteria for designing a viable electrocatalyst for the four electron reduction of O_2 is straightforward: The electrode must be able to bind O_2 and stabilize the intermediates long enough so the full reduction can occur. Additionally, the system must be easily constructed of inexpensive materials which have long term stability. Ti/PPPO has the potential to meet these requirements. Graetzel and co-workers as well as other researchers have done a great deal of work with TiO_2 colloids in electrocatalysis systems.[198-200] Their studies show that TiO_x species are capable of binding and stabilizing peroxide moieties. Another recent study has shown that Ti(III) species are efficient electrocatalysts for O_2 and H_2O_2 reduction.[201] Clearly, the PPPO matrix is stable over long periods of time and Ti/PPPO electrodes should be very easy to construct. Cyclic Voltammetry (CV) experiments are conducted employing Ti/PPPO as the working electrode. Variations in purge gas environments (N_2 or O_2), pH of electrolyte, scan rate, and anodic voltages limits are studied.

Electrodes which can selectively respond to a particular ion in solution when in the presence of a mixture of ionic species have

widespread analytical uses. Ion selective electrodes are now commercially available for a variety of cations and anions. For the most part, these devices employ glass electrodes and the ion specificity is function of the affinity of the anionic surface sites of the membrane for a certain cation.[202-204] Although these systems have been demonstrated to work, there are some difficulties involved with their use. The electrode response is particularly sensitive to pH. The materials typically only function in a narrow pH range. Furthermore, these electrodes are usually sensitive to a number of similar ions rather than being selective for only one.

These realities led to the study of alkali metal salt doped PPPO composites as ion selective electrodes. Since the pyrolyzed polymer matrix forms around the dopant, the final material should be shape selective for the particular dopant employed. If the system can be charged up in a battery cell to cause the migration of the ionic species, there may be a dependency of the voltage measured on the ability of the ions to move in and out of the lattice. This mobility should be regulated by the size of the cavities of the particular electrode being used. Further detail on the actual cell design and the particular methods practices is described in the experimental section of this chapter.

The last section of this chapter briefly outlines some of the studies that have been attempted to utilize the structural strength of PPPO composites together with their demonstrated ability to encapsulate a variety of dopant species. There is widespread interest in the design of carbon fiber resin matrix composites for advanced materials

applications in the aerospace and construction industries.[205,206] These lightweight materials have extremely high stress/strain tolerances. In typical systems, the majority of the strength is provided by the carbon fibers. The role of the resin is to hold the system together and provide some interfacial stability. The weak link in there materials is the resin. Delamination--the separation of the resin from the fiber--occurs after just a few experimental stress cycles for most systems currently being studied. The reason for this is that there is no significant chemical attraction between the fiber and the resin at the interface.

Experiments have been performed using PPO as the resin and the pyrolyzing the composite. The goal is to encapsulate the fiber in the pyrolyzed matrix. Since as discussed in Chapter 2, the pyrolysis is a radical process, the possibility of some type of chemical bonding between the fiber and the resin exists. Further studies in chemically modifying the fibers to increase this interaction have also been conducted.

The last study in this chapter pertains to the encapsulation of the new high Tc superconductors in order to provide structural support and chemical sensitivity. In the aftermath of the initial excitement over the synthesis of these materials,[207,208] there has been a lot of interest in designing composites that can be formed into various shapes and can stabilize these materials for long periods of time.

Experimental

Reagents

The titanium metal sample (Cerac Chemicals Company, Milwaukee, Wisconsin) used in the electrocatalyst studies had a minimum purity of 99.5% and a mesh size of 325. The Kel-F wax (3M Company) material used to prepare all the electrodes was heated in a petri dish on a hot plate until it was a viscous liquid and then it was applied to the particular device with a wooden applicator stick (Fisher). The electrolyte employed for most of the Cyclic Voltammetric (CV) studies was 0.1M tetrabutylammonium perchlorate (TBAP--Aldrich) in acetonitrile (Eastman Kodak). For the lower pH studies, aqueous solutions of perchloric acid (Fisher) were employed.

The alkali metal salts used in the ion selective electrode studies--LiCl, KCl, and CsCl--were all purchased from Fisher. The carbon fiber samples (type AS-4) for the structural composite studies were provided by Professor Willard Bascom of the University of Utah. The pre-pregs of AS-4 and PPO were prepared by Dr. Norman Johnston of the National Aeronautics and Space Administration (NASA). The high Tc superconductivity oxide materials used for composite matrix studies were prepared according to the method of Chu[207] (this is the $YBa_2Cu_3O_x$ system). An additional sample (a $GdBa_2Cu_3O_x$ compound) was supplied by the Los Alamos National Laboratory. Verification of the superconducting properties was done by the observation of the Meissner effect at liquid nitrogen temperature.

Preparation of materials

The Ti/PPPO composite pellets are prepared as described in Chapter 2. Two different techniques are employed for the construction of the electrodes. The first method involved cementing a glass tube into the Ti/PPPO pellet (through an indentation that was made prior to pyroloysis which is retained in the final pyrolyzed pellet) with Kel-F wax. A drop of mercury is placed inside the tube and a platinum wire is lowered into the mercury. This technique has some advantages because the mercury provides excellent electrical contact and the tube prevents the platinum from coming in contact with the solution and thus complicating the results. The problem with this process, however, is that the wax does not hold firm to the tube--especially after sitting in the electrolyte solution for any length of time. The result of this is that mercury leaks out into the solution. To simplify matters, subsequent studies are done with an electrode made by merely cementing a piece of platinum wire onto the pellet. Care is taken to ensure that there is no bare platinum exposed to the solution.

All the CV data that is presented in this chapter is done with electrodes made by this latter technique. Clearly this method is not ideal because it was not possible to ensure that the same amount of electrode surface area was exposed from experiment to experiment. Additional difficulties were incurred because of the poor degree of electrical contact this process permits. These problems occasionally led to non-reproducible results. All the CV data reported in this chapter, however, were reproduced a minimum of three times.

Nevertheless, improvements in electrode design should be a focus of future work.

The CV experiments were run with a PAR model 175 Universal Programmer attached to a model 173 potentiostat/galvanostat. The reference electrode was Ag/AgCl. A gas line fitted with a Pasteur pipette is placed in contact with the solution in the electrochemical cell. This is used to cycle N_2 or O_2 into the system.

The LiCl/PPPO composites for ion selective electrode studies are prepared as described in Chapter 2. Two identical pellets are used as electrodes by cementing a piece of platinum wire on to them with Kel-F wax. The battery cell used for these experiments is composed of a three inch diameter glass jar which has a two hole rubber stopper attached to the top. The electrodes are lowered into the cell and placed into the electrolyte solution. A schematic drawing of the cell design is shown in Figure 5-1. The platinum leads of the electrodes are attached through a universal breadboard (Archer Electrical Supply Company) to a variable power source (Lambda Electronics Corporation). Typically the system is charged for six hours with an applied voltage of 3.0 V. After this time the power source is taken out of the circuit and the volt meter (Radio Shack model 705 multimeter) is wired in so that the open circuit voltage can be monitored. In order to discharge the system, a 10 kΩ resistor is placed into the circuit.

The carbon fiber/PPPO composites are prepared by stacking successive layers of PPO and AS-4 onto the press die. The pellet is then made and pyrolyzed as usual. Further attempts to probe the fiber/resin interface are done by pretreating the AS-4 fiber with Br_2

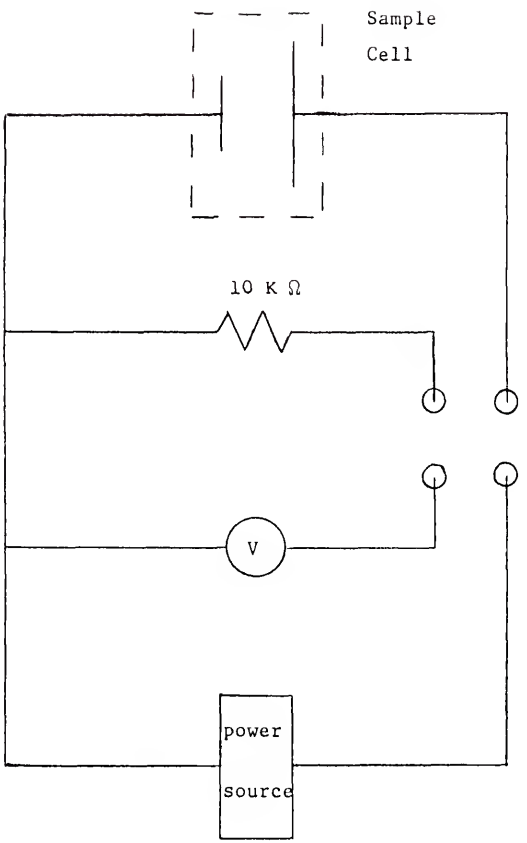

Figure 5-1. Schematic of cell design in ion selective electrode experiments.

vapors. This was done by putting 20 ml of bromine water--4% Br_2 (Fisher) in H_2O--into the bottom of a large desiccator. Strips of AS-4 are then placed on the ceramic stage plate and the lid is attached. The system is allowed to sit for 48 hours. The fibers are then removed and pellets are made and pyrolyzed as before.

The composites of the superconducting oxides are simply mixed in a mortar and pestle analogous to the Ti and Fe doped systems. Various weight compositions are investigated. Experiments to observe the Meissner effect are done by attaching a string to the pellet with Scotch tape and dipping the pellet into liquid nitrogen. The pellet is removed from the $N_2(l)$ and brought near a U-shaped magnet. A positive test is obtained when the pellet is repelled by the magnet.

Results and Discussion

Electrocatalysts for the Reduction of O_2

As mentioned in the introduction, the full four electron reduction of O_2 is the most desired, but the majority of systems stop halfway with the formation of H_2O_2. The overall reaction process for acid electrolytes shown in the equations below.

$$O_2 + 2H^+ + 2e^- \text{----> } H_2O_2 \quad 0.682\ V \qquad (5\text{-}1)$$

$$H_2O_2 + 2H^+ + 2e^- \text{----> } 2H_2O \quad 1.776\ V \qquad (5\text{-}2)$$

$$O_2 + 4H^+ + 4e^- \text{----> } 2H_2O \quad 1.229\ V \qquad (5\text{-}3)$$

Ti/PPPO electrodes are employed in these studies in the hope that the Ti species can stabilize any peroxo moieties formed and enable the system to react all the way to the formation of H_2O.

Figure 5-2 shows CV's of the Ti/PPPO system in a N_2 atmosphere and an O_2 atmosphere. It is evident that in the N_2 case, not much electrochemistry is occurring other than some general charging. In the presence of O_2, however, several distinct peaks are observed: two reduction peaks, one at 0.0V and the other centered at about -0.8V, and one oxidation wave at about +0.65. The shape of these reduction peaks is very similar to those observed in chemically modified electrode systems for O_2 reduction.[197,209] The fact that these peaks are only prominent in the presence of O_2 is strong evidence that some type of electroreduction of this species is occurring. The observation of two reduction peaks suggests that perhaps both two electron steps are taking place.

Since the reactions shown in equations 5-1 through 5-3 require protons, studies are done on varying the pH of the electrolyte. Figure 5-3 displays the CV's of an air saturated system at pH's of 8.0, 3.3 and 2.3 respectively. Several prominent changes are observed as the concentration of H^+ increases: The size of the reduction peaks increases significantly; the peak locations shift towards more positive values; and the reduction peaks at 0.0 V grows steadily from not being present at pH 8.0 to being the same size as the -0.55 V peak at pH 2.3. In interpreting these results, it should be kept in mind that not all of the observed changes are due to electrochemical phenomena associated with the Ti/PPPO. The lowering of the pH greatly changes the nature of

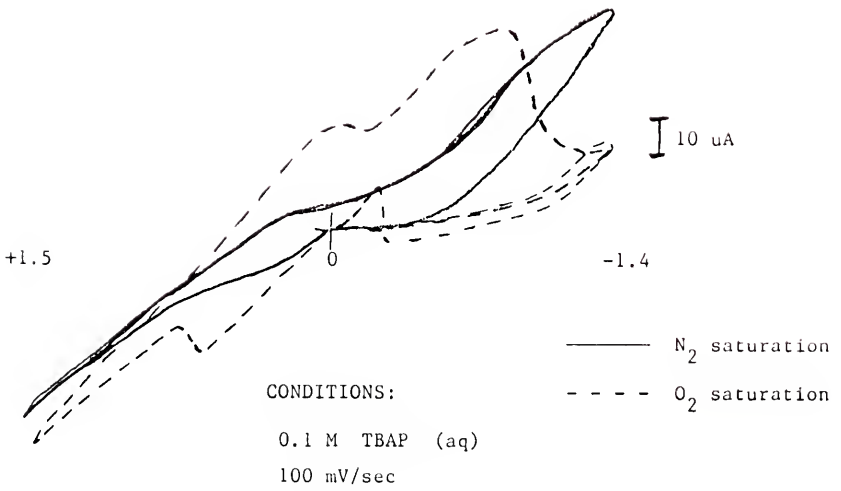

Figure 5-2. Cyclic voltammogram of Ti/PPPO system in N_2 and O_2.

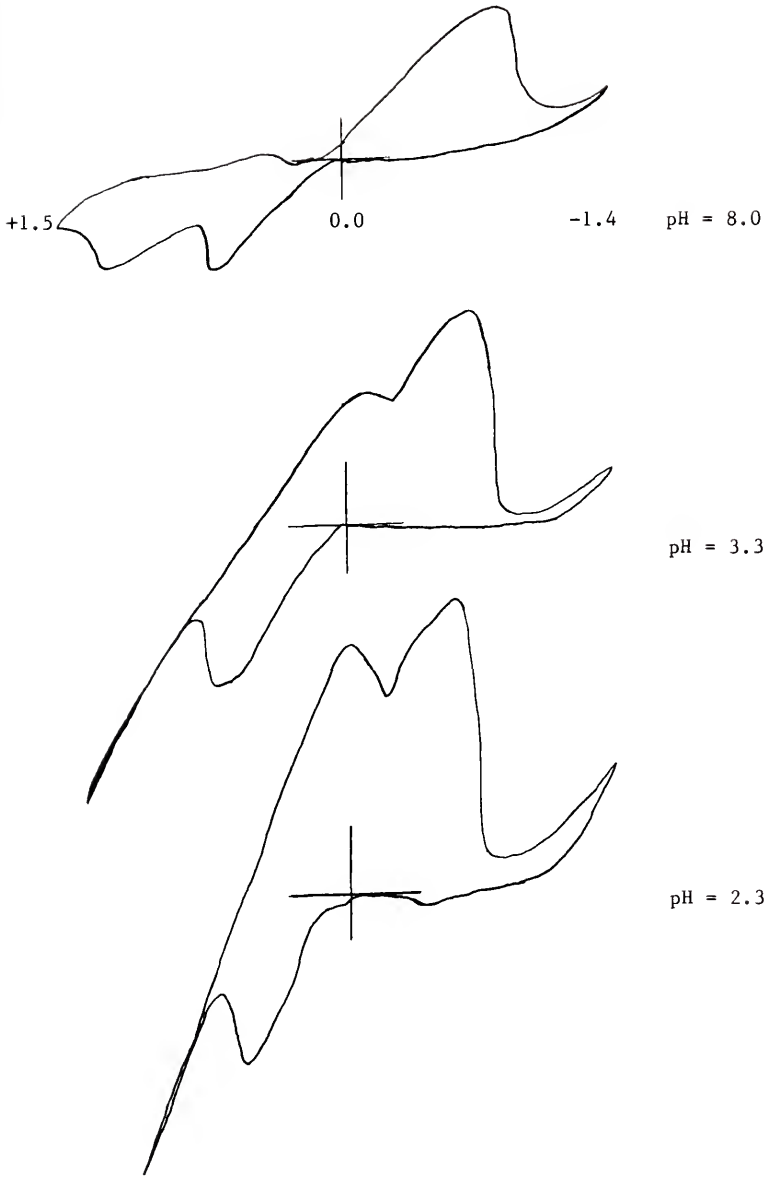

Figure 5-3. Effect of pH on Ti/PPPO O_2 reduction system.

the electrolyte media and some of the experimental results are merely due to this. Nevertheless the increase in the size of the cathodic peaks is encouraging because lower pH's should favor the reaction.

In order to further investigate the reactivity of this system, a series of studies is conducted involving the variation of both the anodic and cathodic potential extremes. Figure 5-4 shows the results of this investigation. For the sake of clarity, only one trace is shown for each CV, however, successive scans up to a total of four are run for each system. Very little change is observed in any of the subsequent scans. In Figure 5-4a, the typical CV for Ti/PPPO at 2.3 pH with a voltage range of +1.5 to -1.4V is seen. Figure 5-4b is the same system on the same current scale when the voltage range is decreased to +0.6 to -0.6. It is clear that the size of the reduction waves has diminished, while the oxidation wave has not changed. Figure 5-4c is the same system again at the full +1.5 to -1.4 range. The magnitude and shape of the cathodic peaks are completely restored. Lastly figure 5-4d shows the CV of this system when the potential is only scanned from +1.5 to -0.6. The reduction waves appear just as large and in the same location as those of the full range systems. Not shown in the figure, but also investigated are the CV's when the system in 5-4d was redone at full range and when this latter system was scanned from +0.6 - 1.4V. These results look very similar to 5-4c and 5-4b respectively.

This analysis shows that the ability of this system to reduce O_2 is greatly dependent on the anodic extreme applied. There are a couple of possible explanations for this. The first one focuses on the possibility that at the anodic extreme of +1.5V, H_2O from the

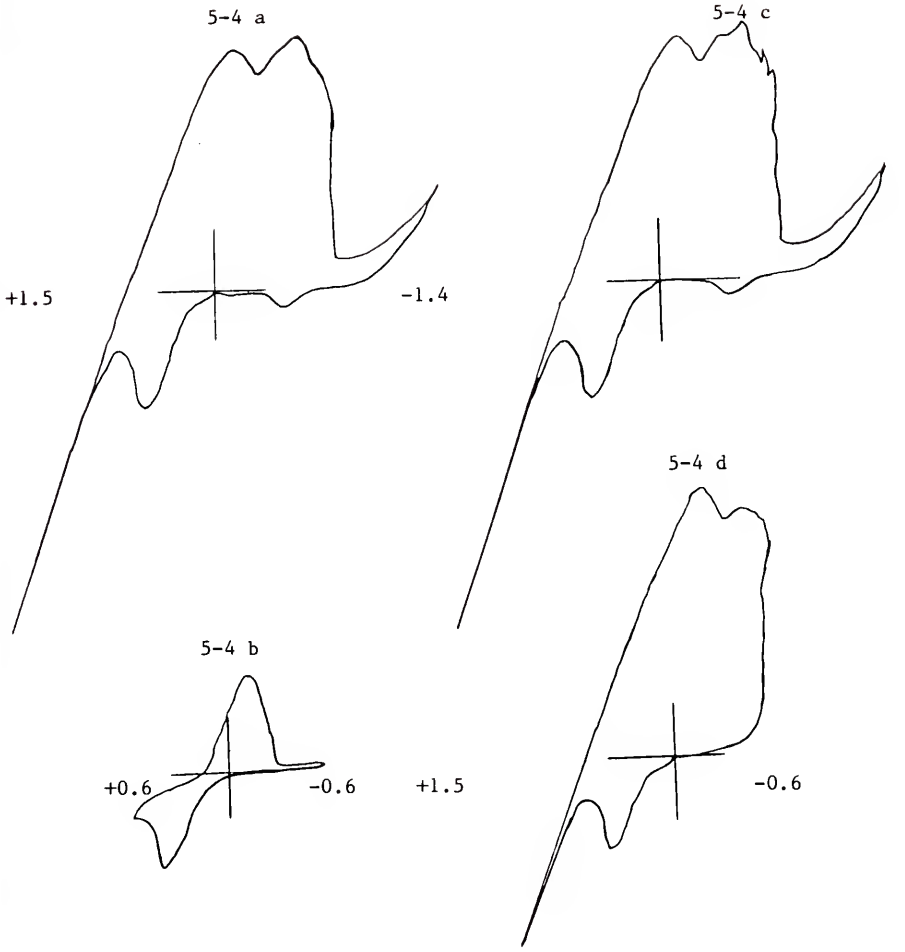

Figure 5-4. Effect of cathodic and anodic extreme potential variation on Ti/PPPO O_2 reduction system.

electrolyte can be oxidized to yield freshly generated O_2 right at the surface of the electrode. As the system is scanned back in the cathodic direction, it is this O_2 and not O_2 dissolved in the bulk which is reduced. The fact that these electrodes are not very porous and thus may only work when O_2 is actually generated at the electrode surface is one of the reasons for suggesting this mechanism. This explanation is not very exciting from a research standpoint because it suggests a physical rather than chemical solution to the phenomenon observed in Figure 5-4.

An alternative explanation which is potentially much more interesting is also possible. The Lattimer diagram for Ti species vs. the NHE is shown below.

$$TiO^{2+} \xrightarrow{.10} Ti^{3+} \xrightarrow{-.37} Ti^{2+} \xrightarrow{-1.63} Ti \qquad (5\text{-}4)$$

The studies in this work use a Ag/AgCl reference. The anodic extreme would be +1.697 if the NHE was employed. Thus it is feasible that the dependence on the anodic limit is due to the necessity of generating a cationic Ti species, e.g. Ti^{3+}, which is the active component for binding and reducing O_2. A recent study revealed that Ti^{3+} moieties are capable of undergoing such reactivity.[201] Obviously, the Ti/PPPO composite even before any CV studies are done is a mixture of oxide species. When it is originally prepared, zero valent Ti is used, but no particular precautions are taken to prevent oxidation. The surface of the pyrolyzed pellet clearly has a significant quantity of TiO_x species on it. Nonetheless, there must still be a large amount of

Ti(0) present because the pellet is highly conductive. This mechanism proposes that the high anodic extreme produces an active oxide moiety from all the various other Ti species that are present prior to the experiment. A recent study on a cobalt doped carbon electrode for O_2 reduction also reports that active species are generated by applying very negative potentials to the system.[210]

The last study on this system involves varying the scan rate of the CV experiment. The results of this analysis are shown in Figure 5-5. It is clear that scan rate has a direct effect on the number of peaks present and their relative intensities. At the slowest rate shown, 10mV/sec (5-5a), there is just one reduction peak at 0.0V. At 100 mV/sec (5-5b), there are two peaks which, upon subsequent scans, coalesce into one. The first is again at 0.0V and the second is at about -0.4V. When the scan rate is further increased to 200mV/sec, the more negative peak begins to dominate the voltammogram. By 500 mV/sec, this peak is clearly the most prominent. Before drawing any conclusion from this study, the caveat mentioned previously must be considered. Such significant changes in scan rate effect the fundamental aspects of the experimental method to a great enough extent that the observed changes may not be related to any electrochemical property of the Ti/PPPO sample. Nevertheless, this study does infer that the reactions associated with the reduction of O_2 are dynamic properties which may be able to be monitored by other techniques.

The work described in this section supports the contention that the Ti/PPPO composite does function as an electrocatalyst for the reduction of O_2. The results can not conclusively show if the four

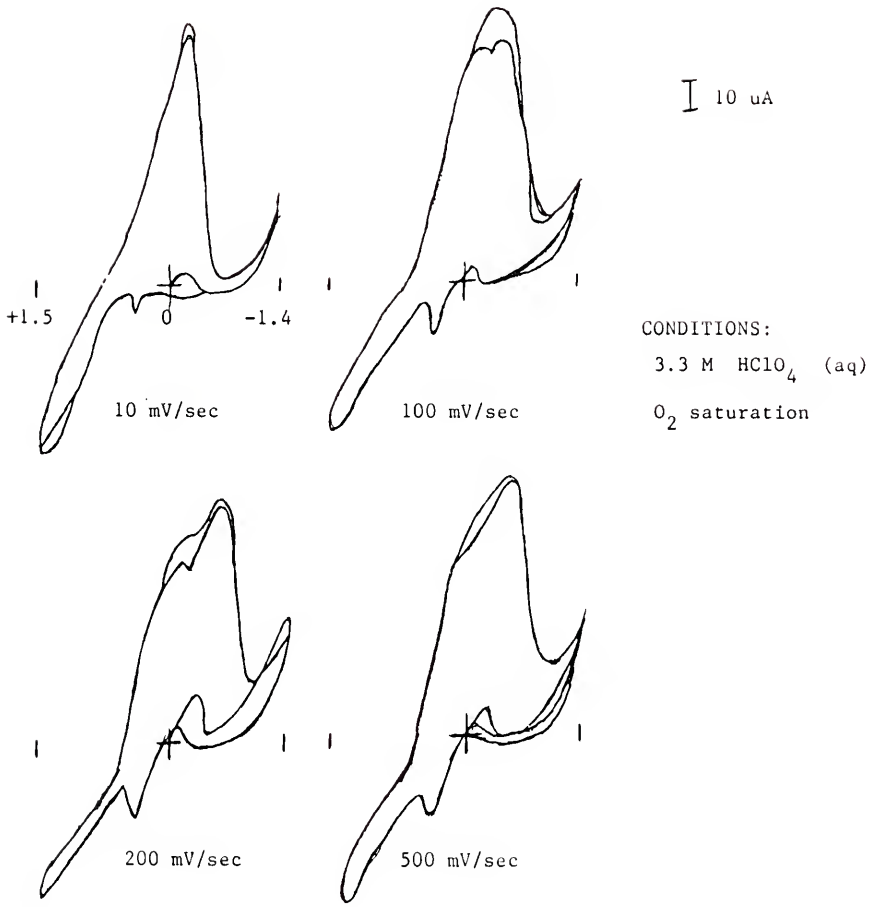

Figure 5-5. Effect of scan rate variation on Ti/PPPO O_2 reduction system.

electron reduction is occurring or if it is just the two electron step. The continued observation of two reduction peaks is some evidence that both steps are taking place, but a more detailed technique such as Rotating Ring Disk Electrochemistry is needed to definitively show this. The problem of overvoltage is still present with these systems. One of the reduction peaks is located at 0.0V and the other is in the negative region at about -0.5 V depending on the nature of the electrolyte. These values are far below the theoretical potentials of either the two or four electron steps. Nevertheless there results are quite encouraging and should provide a foundation for future studies which will employ more exotic techniques and experimental designs.

Ion Selective Electrodes

The theory behind employing LiCl/PPPO composites as ion selective electrodes is that as the cell is energized by the applied power source, there will be a migration of ionic species to balance the charges produced. Initially before any applied potential, the two electrodes are identical, so there is no open circuit voltage measured. During the charging cycle, one electrode is reduced and the other is oxidized. Now when the open circuit voltage is monitored a potential is observed. The redox chemistry is occurring in the polymer; the role of the LiCl dopant is merely to move in and out of the lattice to prevent the build up of charges. The necessity of the dopant is shown in blank studies where undoped PPPO pellets are employed. No open circuit voltage is observed in these blank systems no matter how long potential is applied.

Since the PPPO matrix is somewhat analogous to a solid crown ether, it is believed that the majority of the dopant/matrix charge interaction is done by the cation. Thus in the anode where the pyrolyzed polymer is being oxidized, there is a net flow of cations out of the matrix. Conversely in the cathode, cations move in to balance the charge. The ion "sink" where these species move into and come from is the electrolyte solution. Due to the shape selectivity of the PPPO composite, the most efficient system for this ion mobility (and hence the one which will exhibit the highest open circuit voltage) is the one where the electrolyte contains the same ions as those used in the preparation of the electrode.

The results for a typical experimental cycle are shown in Table 5-1. The experiment starts with two identical LiCl/PPPO pellets which are charged for 6 hours with an applied voltage of 3.0 V in a 1M LiCl electrolyte solution. After charging, the open circuit voltage is 2.01 V. This value gradually decreases with time. The discharge is hastened by attaching the 10 KΩ resistor to the circuit. In about three hours, the system is completely discharged (no measurable open circuit voltage). At this point, the system is disassembled and the electrodes are washed with deionized H_2O. The cell is cleaned and the electrolyte is changed to 1 M KCl. The charging cycle is then repeated. When the open circuit voltage is monitored for this system it is only 1.24 V. The system is discharged, cleaned and set up again with 1M LiCl. As in the first cycle, the open circuit voltage after charging is over 2 V. A repeat of the KCl system again shows about 1.2 V and when 1M CsCl is studied, the potential is less than 200 millivolts.

Table 5-1 Results of LiCl/PPPO Ion Selective Electrode Experiments

ELECTROLYTE	OPEN CIRCUIT VOLTAGE (V)
1 M LiCl	2.01
1 M KCl	1.24
1 M LiCl	2.06
1 M KCl	1.26
1 M CsCl	< 0.20

This data shows, as anticipated, that the best system is the one in which the dopant and the electrolyte are the same. The ions are the same size so that mobility in and out of the lattice is the least impeded. Since K^+ is larger than Li^+, it can not migrate in and out as well and hence the system does not achieve as high a potential. The very large Cs^+ has even more difficulty traversing the matrix and the potential is very low. The ability to cycle different ions and then return to a previous one and observe the same value shows that the size and nature of the cavities remains relatively constant.

These results are very encouraging, but like the Ti/PPPO electrocatalysts described in the previous section, the complicated chemical nature of this system sometimes makes reproducibility a problem. The data shown in Table 5-1 have been repeated in several different experiments. It needs to be pointed out though that some system studied showed the same open circuit voltage values for all electrolytes. Since the preparative method employed does not allow much control over the formation of the product, one can not ensure the exact same material is being made every time. If the ionic dopants do not become intimately mixed with the polymer matrix before pyrolysis, the necessary shape selectivity will not be achieved. This problem arose in trying to prepare KCl/PPPO electrodes. The solubility of KCl in the several azeotropic solvent systems attempted was too low. Thus the salt became located mainly on the surface and the resulting system was a very poor electrode. These problems can be alleviated in future work. The method of ion selectivity in these systems is very novel, and in light of this, is worth further investigation.

Structural Materials Applications

Attempts to achieve a strong chemical attraction between the carbon fiber materials and the PPPO matrix are largely unsuccessful. Three different types of experiments are attempted. Initially just the untreated fiber is mixed with the polymer powder. After pyrolysis the pellets are very fragile. The presence of the fibers actually weakens the usually very hard PPPO structure. Slightly better results are obtained with the pre-pregged fiber that was supplied by NASA. The pre-preg process involves towing the fiber through a bath of a particular polymer solution. This procedure puts a thin film of the polymer on the fiber. Pellets layered with this material stay intact, however, it is easy to visually observe that the fiber is not becoming strongly bound to the matrix. The best results are obtained with the brominated fibers. The idea behind these experiments is to try to take advantage of the fact that the pyrolysis produces a large quantity of organic radicals. By coating the fibers with bromine atoms, the possibility of having a chemical reaction to evolve HBr and produce carbon-carbon bonds exists. The pellets made from these samples appear visually to be well mixed, but they break apart when any appreciable stress is applied. Apparently rather than forming C-C bonds, the Br species merely attach the polymer and brominate it. Brominated PPO is actually prepared in this way.[211]

The experiments with the superconducting oxides in PPPO composites are equally unproductive. The pellets do possess a high degree of structural strength, however, the materials are no longer

superconducting--at least not at liquid nitrogen temperatures. There are a number of possibilities why the superconducting nature is lost. Although there is not a consensus yet on exactly how these materials work, most researchers agree the stacked layers of Cu-O sheets are the key features. If during the process of making the composite, this microstructure is disturbed, the materials would lose their ability to be superconductive. Another possible reason is that the paramagnetic nature of the pyrolyzed polymer may interact with the $Cu^{2+/3+}$ redox pair which some studies have invoked to be essential for these materials to function properly.

Although both of these particular structural composites did not prove to be tremendously successful, this type of application is an area where CMS materials can have a significant impact. A great deal of work is being done in materials science fields with carbon based systems. More study on the chemistry of these composites--specifically at the interface between the dopant and the matrix--is clearly warranted.

CHAPTER 6
CONCLUSIONS

The studies focusing on CMS systems as catalysts have shown that the PPAN and AX21 materials are active for variety of catalytic transformations. Dehydrogenation reactivity has been demonstrated for both ethyl benzene to styrene and butene to butadiene conversions. These systems are particularly active towards the former substrate. Mechanistically the two catalysts both function via hydrogen abstraction, but in a slightly different manner. The PPAN material forms an acridan type moiety when hydrogenated; the AX21 system employs its surface oxygen functionalities to abstract the hydrogen. The AX21 catalyst is extraordinarily active for the ethyl benzene substrate and may have commercial viability if the oxidative dehydrogenation process is ever pursued by industry.

Oxygenated substrates are also shown to be reactive over the AX21 catalyst. Substrate variation studies show that this material can function by either hydride or hydrogen atom abstraction mechanisms depending on the specific chemical nature of the reactant.

The studies focusing on CMS systems as catalyst supports have shown that PPAN and AX21 materials can function as synergistic supports which not only disperse and stabilize metal dopant species, but also can impart their own catalytic ability and other advantageous properties to

the heterogeneous catalytic system. Novel Fischer-Tropsch catalysts have been developed which utilize the unique structural characteristics of the CMS supports to give rise to narrow product distributions with high selectivity for small molecular weight hydrocarbons. Mechanistic studies employing an acetaldehyde co-feed have provided new insight into the fundamental reaction sequences of this long-studied process.

MoO_3 doped AX21 catalysts have been shown to be extremely active and selective for the conversion of methanol to methyl formate. By varying the nature of the Mo dopant, it is shown that Lewis acidity is necessary for this reactivity. Through various catalyst preparations, some in which the constituents are intimately mixed and others in which they are not, conclusions regarding the nature of the synergistic interaction can be made. The highly reactive surface structure of the AX21 material, together with its ultra high surface area and exceptional adsorption capabilities, are the key features which make this compound such a unique support.

Molybdenum and tungsten doped AX21 systems have been shown to be active for the deep oxidation of CH_2Cl_2 to CO_2 and HCl. These systems combine the catalytically active metal species with the adsorption capabilities of the support to produce a system which is more advantageous than currently employed methods which only utilize one or the other of these components. In light of the growing waste disposal crisis, these catalysts should invite a great deal of industrial interest.

Novel metal doped/PPPO composites have been studied in advanced materials applications as electrocatalysts for O_2 reduction, ion

selective electrodes and in structural support applications. Ti/PPPO systems are shown to be active for O_2 reduction in cyclic voltammetric studies. The mechanism most likely involves the in-situ generation of an cationic Ti species which is able to bind and stabilize O_2 moieties. This system has some advantages over the widely studied chemically modified electrode materials because it is significantly more stable. LiCl/PPPO materials have been shown to function as very novel ion selective electrodes. This type of selectivity, which is based on the cavity structure of the composite that is formed around the dopant, constitutes an entirely new method of producing such electrodes. Structural composites of PPPO with carbon fibers and high Tc superconductors are not found to be very successful. This type of application, however, is shown to have some promise if the proper materials can be chosen so that the chemistry of the dopant/matrix interface can be probed and influenced.

In summary, this work shows that CMS materials have a great deal of promise for a vast number of applications. It is probably accurate to compare the present state of CMS research to that of zeolite research thirty years ago. Future work will show if these CMS systems can match the development of their alumino-silicate counterparts.

REFERENCES

1. Sinfelt, J. H. Ind. Eng. Chem. Fundam., 1986, 25, 2-9

2. Pines, H. The Chemistry of Catalytic Hydrogen Conversion, Academic Press, Inc. New York, 1981.

3. Corma, A; Wojciechowski, B. W. Catal. Rev., 1985, 27, 29.

4. Breck, D. W. Zeolite Molecular Sieves, Wiley: New York, 1974.

5. Ruthven, D. M.; Raghavan, N. S.; Hassan, M. M. Chem. Eng. Sci., 1986, 41, 1325.

6. Koresh, J. E.; Sofer, A. Sep. Sci. Tech., 1983, 18, 723.

7. Schumacher, H.; Juentgen, H.; Preuss, E.; Zuendorf, D.; Hodek, W.; Romey, I. U.S. Patent No. US 4,261,832, 1981.

8. Hassan, M. M.; Raghavan, N. S.; Ruthven, D. M. Chem. Eng. Sci., 1987, 42, 2037.

9. Dessau, R. M. U.S. Patent No. US 4,413,154, 1983.

10. Connolly, J. F.; Wennerberg, A. N.; Waters, R. F. U.S. Patent No. US 4,478,954, 1984.

11. Foley, H. C., "Novel Carbon Molecular Sieve Catalysts For Wax Suppression in the Fischer - Tropsch Reaction;" DOE Contract No. DE-AC22-84 PC 70031, Final Report, 1987.

12. Kashiwase, M. Jap. Patent No. JP 61/191510, 1986.

13. Ida, S.; Matsuoka, M.; Matsufuji, Y. Jap. Patent No. JP 61/68312, 1986.

14. Wennerberg, A. N. Eur. Pat. Appl. EP 120,604.

15. Connor, H. Ger. Patent No. DE 3006105, 1980.

16. Song, G.; Jiang, Z. Sepu, 1987, 5, 58.

17. Surinova, S. I.; Kostomarova, M. A.; Petukhov, S. S. Zh. Prikl. Khim., 1987, 60, 640.

18. Brunauer, S.; Emmett, P.; Teller, E. J. Am. Chem. Soc., 1938, 60, 309.

19. Emmett, P. Chem. Rev., 1948, 43, 69.

20. Franklin, R. E. Trans. Farad. Soc., 1949, 45, 274.

21. Anderson, R. B.; Hall, W. K.; Lecky, T. A.; Stein, K. S. J. Phys. Chem., 1956, 60, 1548.

22. Lamond, T. G.; Metcalfe, J. E.; Walker, P. L. Carbon, 1965, 3, 59.

23. Trimm, D. L.; Cooper, B. J. J. Chem. Soc. D, 1970, 8, 477.

24. Trimm, D. L.; Cooper, B. J. Chem. Comm., 1970, 477.

25. Schmitt, J. L.; Walker, P. L. Carbon, 1971, 10, 791.

26. Koresh, J. E.; Soffer, A. J. Chem. Soc. Farad. Trans. 1, 1981, 77, 3005.

27. Konnert, J.; D'Antonio, P. Carbon, 1983, 21, 193.

28. Wennerberg, A.; O'Grady, T. U.S. Patent No. US 4,082,694, 1978.

29. Burlant, W. J.; Parsons, J. L. J. Polym. Sci., 1956, 12, 249.

30. Conley, R. T.; Bieron, J. F. J. Appl. Polym. Sci., 1963, 7, 1757.

31. Manassen, J.; Wallach, J. J. Am. Chem. Soc., 1965, 87, 2671.

32. Grassie, N.; M^{C}Guchan, R. Europ. Polym. J., 1970, 6, 1277.

33. Grassie, N.; M^{C}Guchan, R. Europ. Polym. J., 1971, 7, 1091.

34. Grassie, N.; M^{C}Guchan, R. Europ. Polym. J., 1971, 7, 1357.

35. Coleman, M. M.; Petcavich, R. J. J. Polym. Sci. Polym. Phy. Ed., 1978, 16, 821.

36. Rafalko, J. J. J. Polym. Sci. Polym. Phy. Ed., 1984, 22, 1211.

37. Chung, T. C.; Schlesinger, Y.; Etemad, S.; Macdiarmid, A. G.; Heeger, A. J. J. Polym. Sci. Polym. Phy. Ed., 1984, 22, 1239.

38. Teoh, H.; Metz, P. D.; Wilhelm, W. G. Mol. Cryst. Liq. Cryst., 1982, 83, 297.

39. Gallard, J.; Nechtschein, M.; Soutif, M.; Traynard, P. Bull. Soc. Chim. Fr., 1963, 10, 2204.

40. Ohigashi, H. Rep. Prog. Polym. Phy., Japan, 1963, 6, 245.

41. Manassen, J.; Khalif, S. J. Am. Chem. Soc., 1966, 88, 1943.

42. Ademodi. B.; Macaulay, S.; Cattaneo, M. J. Chem. Tech. Biotechnol., 1987, 40, 11.

43. Degannes, P.; Ruthven, D. Canad. J. Chem. Eng., 1979, 57, 627.

44. Tighe, B. US Patent No. 4,197,272, 1980.

45. Holler, H. V. US Patent No. 3,892,679, 1975.

46. Bai, R.; Zong, H.; He, J.; Jiang, Y. Makromol. Chem., Rapid Commun., 1984, 5, 501.

47. Neely, J. W.; Isacoff, E. G. Carbonaceous Adsorbents for the Treatment of Ground and Surface Waters, Marcel Dekker: New York, 1982.

48. D. Chung, J. Murphy, and T. Taylor, Clin. Toxicol., 1982, 19, 219.

49. D. O. Cooney, Clin. Toxicol., 1980, 16, 123.

50. D. O. Cooney, Clin. Toxicol., 1979, 15, 287.

51. Mahoney, C. L.; Barnum, E. R. Synthetic Lubricants, Gunderson and Hart, Eds., Reinhold, New York, 1962.

52. Archer, W. L.; Bozer, K. B. Ind. Eng. Chem. Prod. Res. Develop., 1966, 5, 145.

53. Factor, A. J. Polym. Sci. A., 1969, 7, 363.

54. Jachowicz, J.; Kryszewski, M.; Mucha, M. Macromolecules, 1984, 17, 1315.

55. Thomas, W. M. Advances in Polymer Science, Vol. 2, Ferry, J. D., Ed., Springer-Verlag, Berlin, 1960.

56. Krigbaum, W. R.; Tokita, N. J. Polym. Sci., 1960, 43, 467.

57. Lecayon, G.; Bouizem, Y.; Le Gressus, C.; Reynaud, C.; Boiziau, C.; Juret, C. Chem. Phys. Lett., 1982, 91, 506.

58. Le Roy, S.; Boiziau, C.; Perreau, J.; Reynaud, C.; Zalcaer, G.; Lecayon, G.; Le Gressus, C. J. Mol. Struct., 1985, 128, 269.

59. Clark, J. L., Ph.D., Dissertation, University of Florida, Gainesville, Fl., 1987.

60. O'Grady, T. M.; Wennerberg, A. N. "High-Surface-Area Active Carbon," Petroleum-Derived Carbons, ACS Symp. Ser., 1986, 303, 302.

61. Marsh, H.; Crawford, J.; O'Grady, T. M.; Wennerberg, A. Carbon, 1982, 20, 419.

62. Yehaskel, A. Activated Carbon, Noyes Data Corporation, Park Ridge, N. J., 1978.

63. Demorquay, J.; Frissard, J. Chem. Phys. Lett. 1987, 136, 314.

64. Derouane, E. G.; Nagy, J. B. Chem. Phys. Lett. 1987, 137, 341.

65. Ito, T.; Fraissard, J. J. Chem. Phys. 1982, 76, 5225.

66. de Madrual, L. C.; Ito, T.; Fraissard, J. J. Chem. Soc., Faraday Trans. 1982, 1,78, 403.

67. Ito, T.; Bohordet, J. L.; Fraissard, J.; Nagy, J. B.; Andre, C.; Gabelica, Z.; Derouane, E. G. Applied Catalysis, 1988, 43, L5.

68. Lim, Y. Y.; Drago, R. S.; Babich, M. W.; Wong, N.; Doan, P. E. J. Am. Chem. Soc. 1987, 109, 169.

69. Chem. Eng. News, 12 Dec., 1988, 30.

70. Rylander, P. N. Catalysis Science and Technology, Anderson and Boudart, Eds., Springer-Verlag Chemie, Berlin, 1983.

71. Pines, H. The Chemistry of Catalytic Hydrocarbon Conversion, Academic Press, New York, 1981.

72. Lee, E. H. Catal. Rev., 1973, 8, 285.

73. Kaeding, W. W. Catal. Rev., 1973, 8, 307.

74. Vrieland, G. E. J. Catal., 1988, 111, 1.

75. Bautista, F. M.; Campelo, J. M.; Garcia, A.; Luna, D.; Marinas, J. M. J. Catal., 1989, 116, 338.

76. Hattori, T.; Niwa, H.; Satsuma, A.; Kito, S.; Murakami, Y. Appl. Catal., 1989, 50, L11.

77. US Pat. 3,502,737 to J. R. Ghublikian (1970).

78. Y. Murakami, K. Iwayama, H. Uchida, T. Hattori, and T. Tagawa, J. Catal., 71 (1981) 257.

79. T. Tagawa, T. Hattori, and Y. Murakami, J. Catal., 75 (1982) 56.

80. T. Tagawa, K. Iwayama, Y. Ishida, T. Hattori and Y. Murakami, J. Catal., 79 (1983) 47.

81. G. E. Vrieland, J. Catal., 111 (1988) 14.

82. L. E. Cadus, L. A. Arrua, O.F. Gorriz, and J. B. Rivarola, Ind. Eng. Chem. Res., 27 (1988) 2241.

83. Emig, G.; Hofmann, H. J. Catal., 1983, 84, 15.

84. US Pat. 3,487,564 to R. H. Allen, T. Alfrey, and L.D. Yats 1970.

85. Y. Iwasawa, H. Nobe, and S. Ogasawara, J. Catal., 1973, 31, 444.

86. Matsuura, I.; Schut, R.; Hirakawa, K. J. Catal., 1980, 63, 152.

87. Lambert, J. C.; Germain, J. E. Bull. Soc. Chim. Fr., 1982, 33.

88. Herniman, H. J.; Pyke, D. R.; Reid, R. J. Catal., 1979, 58, 68.

89. Keulks, G. W. J. Catal., 1970, 19, 232.

90. Matsuura, I.; Schut, G. C. J. Catal., 1971, 20, 19.

91. Skarchenko, U. K. Int. Chem. Eng., 1969, 9, 1.

92. Ademodi, B.; Macaulay, S. ; Cattaneo, M. V. J. Chem. Tech. Biotechnol., 1987, 40, 11.

93. Davis, B. H. J. Catal., 1983, 79, 58.

94. Ai, M. J. Catal., 1975, 40, 327.

95. Ghublikian, J. R. U.S. Pat. No. US 3,502,737, 1970.

96. Iwasawa, Y.; Gates, B. C. Chemtech, 1989, 173.

97. Cutlip, M. B.; Peters, M. S. Chem. Eng. Prog. Symp. Ser., 1968, 89, 1.

98. Moser, W. R.; Chiang, C. C.; Thompson, R. W. J. Catal., 1989, 115, 532.

99. Fischer, F.; Tropsch, H. Brennst. Chem., 1926, 7, 97.

100. Henrici-Olive, G.; Olive, S. Angew. Chem. Intl. Ed. Engl., 1976, 15, 136.

101. Zwart, J.; Snel, R. J. Molec. Catal., 1985, 30, 305.

102. Giannelis, E. P.; Rightor, E. G.; Pinnavaia, T. J. J. Am. Chem. Soc., 1988, 110, 3880.

103. Madon, R. J. J. Catal., 1979, 57, 183.

104. Anderson, P. B. In Catalysis; Emmet, P. H., Ed.; Reinhold; New York, 1956; pp. 345-367.

105. Masters, C. Advances in Organometallic Chemistry, Stone, F. G. A.; West, R. Eds. Academic Press, New York, 1979.

106. Wender, I. Catal. Rev., 1976, 14, 97.

107. Bell, A. Catal. Rev., 1981, 23, 203.

108. Commereuc, D.; Chauvin, Y.; Hugues. F.; Basset, J. M.; Olivier, D. J. Chem. Soc. Chem. Commun., 1980, 154.

109. Hugues, F.; Besson, B.; Bussiere, P.; Dalmon, J. A.; Leconte, M.; Basset, J. M.; Chauvin, Y.; Commereuc, D. ACS Symp. Ser., 1982, 192, 255.

110. Hugues, F.; Besson, B.; Basset, J. M. J. Chem. Soc. Chem. Commun., 1980, 719.

111. Bein, T.; Jacobs, P. A. J. Chem. Soc. Faraday Tran. 1, 1983, 79, 1819.

112. Ballivet-Tkatchenko D.; Coudurier, G. Inorg. Chem., 1979, 18, 558.

113. Nagy, J. B.; van Eenoo, M.; Derouane, E. G. J. Catal., 1979, 58, 230.

114. Scheider, R. L.; Howe, R. F.; Watters, K. L. J. Catal., 1983, 79, 298.

115. Chung, J. S.; Miranda, R.; Bennett, C. O. J. Catal., 1988, 114, 398.

116. Ai, M. J. Catal., 1982, 77, 279.

117. Busca, G.; Tittarelli, P.; Tronconi, E.; Forzatti, P. J. Solid State Chem., 1987, 67, 91.

118. Forzatti, P.; Tronconi, E.; Busca, G.; Tittarelli, P. Catal. Today, 1987, 1, 209.

119. Schreck, D. J.; Busby, D. C.; Wegman, R. W. J. Mol. Cat., 1988, 47, 117.

120. Pruett, R. L.; Kacmarcik, R. T. Organomet., 1982, 1, 1693.

121. Wakamatus, H.; Sato, J.; Hamaoka, T. U.S. Pat. 3,798,267, 1974.

122. Otsuka, K.; Yamanaka, I.; Suga, K. Chem. Lett., 1987, 1087.

123. Hiratani, T.; Noziri, S. Chem. Economy Eng. Rev., 1985, 17, 21.

124. The Gainesville Sun, June 20, 1989, p.1.

125. Sokolovskii, V. D. React. Kinet. Catal. Lett., 1981, 17, 379.

126. Chem. Eng. News, 12 June 1989, 27.

127. Okahara, T.; Kimura, T.; Kobayashi, K.; Misono, M.; Yoneda, Y. Bull. Chem. Soc. Jpn., 1984, 57, 938.

128. Hugues, F.; Basset, J. M.; Taarit, Y. B.; Choplin, A.; Primet, M.; Rojas, D.; Smith, A. K. J. Am. Chem. Soc., 1982, 104, 7020.

129. M^{c}Vicker, G. B.; Vannice, M. A. J. Catal., 1980, 63, 25.

130. Budge, J. R.; Scott, J. P.; Gates, B. C. J. Chem. Soc. Chem. Commun., 1983, 342.

131. Ogata, A.; Kazusaka, A.; Yamazaki, A. ; Enyo, M. Chem. Lett., 1989, 15.

132. Ogata, A.; Kazusaka, A.; Enyo, M.; Toyoshima, I. Chem. Phys. Lett., 1986, 127, 283.

133. Louis, C.; Tatibouet, J. M.; Che, M. J. Catal., 1988, 109, 354.

134. Goldstein-Getty, C., Ph.D., Dissertation, University of Florida, Gainesville, Fl., 1988.

135. Weiss, K. D.; Ph.D., Dissertation, University of Florida, Gainesville, Fl., 1986.

136. Walker, J. F. Formaldehyde, Reinhold, New York, 1964.

137. Doi, Y.; Miyake, H.; Yokota, A.; Soga, K. J. Catal., 1985, 95, 293.

138. Morris, S. R.; Moyes, R. B.; Wells, P. B.; Whyman, R. J. Catal., 1985, 96, 23.

139. Okuhara, T.; Enomoto, T.; Tamura, H.; Misono, M. Chem. Lett., 1984, 1491.

140. Winslow, P.; Bell, A. T. J. Catal., 1985, 91, 142.

141. Okada, O.; Ipponmatsu, M.; Kawai, M.; Aika, K.; Onishi, T. Chem. Lett., 1984, 1041.

142. Chen, Y. W.; Wang, H. T.; Goodwin, J. G. J. Catal., 1984, 85, 499.

143. Yang, C. H.; Goodwin, J. G. J. Catal., 1982, 78, 182.

144. Baker, J. A.; Bell, A. T. J. Catal., 1982, 78, 165.

145. Kellner, C. S.; Bell, A. T. J. Catal., 1981, 71, 288.

146. King, D. L. J. Catal., 1978, 51, 386.

147. Darensbourg, D. J.; Bauch, C. G.; Ovalles, C. Rev. Inorg. Chem., 1985, 7, 315.

148. Ferkul, H. E.; Berlie J. M.; Stanton, D. J.; M^{C}Gowan, J. D.; Baird, M. C. Can. J. Chem., 1983, 61, 1306.

149. Ferkul, H. E.; Stanton, D. J.; M^{C}Gowan, J. D.; Baird, M. C. J. Chem. Soc. Chem. Comm., 1982, 955.

150. Solymosi, F.; Erdohelyi, A.; Kocsis, M. J. Chem. Soc. Faraday Trans. I, 1981, 77, 1003.

151. Beck, A.; Dobos, S.; Guczi, L. Inorg. Chem., 1988, 27, 3220.

152. Chojnacki, T. P.; Schmidt, L. D. J. Catal., 1989, 115, 473.

153. Kiwi, J.; Italiano, P. J. Molec. Catal., 1989, 50, 131.

154. Audier, M.; Klinowski, J.; Benfield, R. J. Chem. Soc. Chem. Commun., 1984, 626.

155. Lamb, H. H.; Gates, B. C. J. Am. Chem. Soc., 1986, 108, 81.

156. Tatsumi, T.; Muramatsu, A.; Yokota, K.; Tominaga, H. J. Mol. Catal., 1987, 41, 385.

157. Smith, D. F.; Hawk, C. O.; Golden, P. L. J. Am. Chem. Soc., 1930, 52, 3221.

158 Edius, Y. T. Russ. Chem. Rev., 1967, 36, 338.

159. Golovina, O. A.; Sakharov, M. M.; Roginskii, S. Z.; Dokukina, E. S. Russ. J. Phys. Chem., 1959, 33, 471.

160. Brady, R. C.; Pettit, R. J. Am. Chem. Soc., 1980, 102, 6182.

161. Buschmann, H. W.; Ritschel, M.; Vielstich, W. J. Catal., 1987, 106, 337.

162. Roder, K.; Werner, H. Angew. Chem. Int. Ed. Engl., 1987, 26, 686.

163. Van Barneveld, W. A. A.; Ponec, V. J. Catal., 1984, 88, 382.

164. Krebs, H. J.; Bonzel, H. P.; Gafner, G. Surf. Sci., 1979, 88, 269.

165. Kobori, Y.; Yamasaki, H.; Naito, S.; Onishi, T.; Tamaru, K. J. Chem. Soc. Faraday Trans. I, 1982, 78, 1473.

166. Araki, M.; Ponec, V. J. Catal., 1976, 44, 439.

167. Biloen, P.; Helle, J. N.; Sachtler, W. M. H. J. Catal., 1979, 58, 95.

168. Henrici-Olive, G.; Olive, S. Angew. Chem. Int. Ed. Engl., 1976, 15, 136.

169. Kummer, J. T.; Dewitt, T. W.; Emmet, P. H. J. Am. Chem. Soc. 1948, 70, 3632.

170. Blyholder, G.; Neff, L. D. J. Phys. Chem., 1962, 66, 1664.

171. Agarwal, A. K.; Wainwright, M. S.; Trimm, D. L.; Cant, N. W. J. Mol. Catal., 1988, 45, 247.

172. Henderson, M.A.; Zhou, Y.; White, J. M. J. Amer. Chem. Soc., 1989, 111, 1185.

173. Tseng, S. C.; Jackson, N. B.; Ekerdt, J. G. J. Catal., 1988, 109, 284. Mazenec, T. J. J. Catal., 1986, 98, 115.

174. Busca, G.; Elmi, A. S.; Forzatti, P. J. Phys. Chem., 1987, 91, 5263.

175. Farneth, W. E.; Ohuchi, F.; Staley, R. H.; Chowdhry, U.; Sleight, A. W. J. Phys. Chem., 1985, 89, 2493.

176. Carbucicchio, M.; Trifiro, F.; Vaccari, A. J. Catal., 1982, 75, 207.

177. Machiels, C. J.; Sleight, A. W. J. Catal., 1982, 76, 238.

178. Elmi, A. S.; Tronconi, E.; Cristiani, C.; Gomez-Martin, J. P.; Forzatti, P.; Busca, G. Ind. Eng. Chem. Res., 1989, 28, 387.

179. Tronconi, E.; Elmi, A. S.; Ferlazzo, N.; Forzattti, P.; Busca, G.; Tittarelli, P. Ind. Eng. Chem. Res., 1987, 26, 1269.

180. Tatibouet, J. M. Bull. Soc. Chim. Fr., 1986, 18.

181. Cullity, B. D. Elements of X-Ray Diffraction, Addison-Wesley Inc., Reading, Massachusetts, 1978.

182. Nat. Bur. Stand. (U.S.), Monogr. 25, Sect. 18, 1981.

183. Zhou, B.; Ceckiewicz, S.; Delmon, B. J. Phys. Chem., 1987, 91, 5061.

184. Petterson, T. A.; Carver, J. C.; Leyden, D. E.; Hercules, D. M. J. Phys. Chem., 1976, 80, 1700.

185. Berry, F. J.; Hallett, C.; Marbrow, R. Inorg. Chim. Acta., 1987, 133, 57.

186. Furukawa, H.; Kanzaki, T.; Katasura, T. J. Elec. Spec. Rel. Phen., 1985, 36, 1.

187. De Vries, J. E.; Yao, H. C.; Baird, R. J.; Gandhi, H. S. J. Catal., 1983, 84, 8.

188. Okamoto, Y.; Morikawa, F.; Degawa, J.; Imanaka, T.; Teranishi, S. Chem. Lett., 1983, 1853.

189. Okamoto, Y.; Morikawa, F.; Oh-Hiradi, K.; Imanaka, T.; Teranishi, S. J. Chem. Soc. Chem. Commun., 1981, 1018.

190. Okamoto, Y.; Imanaka, T.; Teranishi, S. J. Catal., 1980, 65, 448.

191. Collman, J. P.; Denisevich, P.; Konai, Y.; Marrocco, M.; Koval, C.; Anson, F. C. J. Am. Chem. Soc., 1980, 102, 6027.

192. Zagal, J. H.; Sen, R. K.; Yeager, E. J. Electroanal. Chem., 1977, 83, 207.

193. Jahnke, H.; Schonborn, M.; Zimmerman, G. Top. Curr. Chem., 1976, 61, 133.

194. Collman, J. P.; Anson, F. C.; Barnes, C.; Bencosme, C. S.; Geiger, T.; Evitt, E.; Kreh, R.; Meier, K.; Pettman, R. J. Am. Chem. Soc., 1983, 105, 2694.

195. Collman, J. P.; Bencosme, C. S.; Durand, R.; Kreh, R.; Anson, F. C. J. Am. Chem. Soc., 1983, 105, 2699.

196. Collman, J. P.; Bencosme, C. S.; Barnes, C.; Miller, B. J. Am. Chem. Soc., 1983, 105, 2704.

197. Durand, R.; Bencosme, C. S.; Collman, J. P.; Anson, F. C. J. Am. Chem. Soc., 1983, 105, 2710.

198. M^{c}Evoy, A. J.; Graetzel, M. J. Electroanal, Chem. Interfacial Electrochem., 1986, 209, 391.

199. Kiwi, J.; Graetzel, M. J. Phys. Chem., 1984, 88, 1302.

200. Sprunken, H. R.; Schumacher, R.; Schindler, R. N. Faraday Discuss. Chem. Soc., 1980, 70, 55.

201. Johnson, C. R.; Myser, T. K.; Shepherd, R. E. Inorg. Chem., 1988, 27, 1089.

202. Skoog, D. A.; West, D. M. Principles of Instrumental Analysis, Saunders, Philadelphia, 1980.

203. Vesely, J.; Weis, D.; Stulik, K. Analysis With Ion Selective Electrodes, Wiley, New York, 1979.

204. Freiser, H. Ion Selective Electrodes in Analytical Chemistry, Plenum Press, New York, 1978.

205. Derra, S. Res. And Devel., 1988, 54.

206. Chem. Eng. News, 22 February, 1988, 17.

207. Wu, M. K.; Ashburn, J. R.; Torng, C. J.; Hor, P. H.; Meng, R. L.; Gao, L.; Huang, Z. J.; Wang, Y. Q.; Chu, C. W. Phys. Rev. Lett., 1987, 58, 908.

208. Engler, E. M.; Lee, V. Y.; Nazzal, A. I.; Beyers, R. B.; Lim, G.; Grant, P. M.; Parkin, S. S. P.; Ramirez, M. L.; Vazquez, J. E.; Savoy, R. J. J. Am. Chem. Soc., 1987, 109, 2848.

209. Durand, R.; Anson, F. C. J. Electroanal. Chem., 1982, 134, 273.

210. Gupta, S.; Tryk, D.; Bae, I.; Aldred, W.; Yeager, E. J. Appl. Electrochem., 1989, 19, 19.

211. Chern, R. T.; Sheu, F. R.; Jia, L.; Stannett, V. T.; Hopfenberg, H. B. J. Mebr. Sci., 1987, 35, 103.

BIOGRAPHICAL SKETCH

Gerald Charles Grunewald was born in Philadelphia, Pennsylvania on February 11, 1963. He attended Father Judge High School where he was active in football and a variety of extracurricular activities before graduating in June 1981. The following fall, he enrolled at La Salle University on a Christian Brothers Scholarship. While at La Salle, he was active in Speech and Debate, the Honors Board, and the Chymian Society, holding offices in each of these organizations. He performed undergraduate research at La Salle under Professor George Shaloub in inorganic photochemistry. He also spent a summer at the University of Utah on an ACS Summer Research Fellowship working on field flow fractionation with Professor J. Calvin Giddings. He graduated magna cum laude in May 1985.

In August 1985, he continued his chemistry education at the University of Florida under the direction of Professor Russell S. Drago. While at Florida, he presented papers at the Florida Catalysis Conference, the Florida Advanced Materials Conference, and several regional and national ACS conferences.

The author has published two papers and is currently working on several others. Upon receiving the degree of Doctor of Philosophy, he will begin his career with the Du Pont Chemical Company in Orange, Texas.

I certify that I have read this study and that in my opinion it conforms to acceptable standards of scholarly presentation and is fully adequate, in scope and quality, as a dissertation for the degree of Doctor of Philosophy.

Russell S. Drago
Graduate Research Professor
of Chemistry

I certify that I have read this study and that in my opinion it conforms to acceptable standards of scholarly presentation and is fully adequate, in scope and quality, as a dissertation for the degree of Doctor of Philosophy.

George E. Ryschkewitsch
Professor of Chemistry

I certify that I have read this study and that in my opinion it conforms to acceptable standards of scholarly presentation and is fully adequate, in scope and quality, as a dissertation for the degree of Doctor of Philosophy.

Gus J. Palenik
Professor of Chemistry

I certify that I have read this study and that in my opinion it conforms to acceptable standards of scholarly presentation and is fully adequate, in scope and quality, as a dissertation for the degree of Doctor of Philosophy.

Kenneth B. Wagener
Associate Professor of Chemistry

I certify that I have read this study and that in my opinion it conforms to acceptable standards of scholarly presentation and is fully adequate, in scope and quality, as a dissertation for the degree of Doctor of Philosophy.

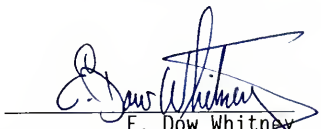

E. Dow Whitney
Professor of Materials Science
and Engineering

This dissertation was submitted to the Graduate Faculty of the Department of Chemistry in the College of Liberal Arts and Sciences and to the Graduate School and was accepted as partial fulfillment of the requirements for the degree of Doctor of Philosophy.

December 1989

Dean, Graduate School

UNIVERSITY OF FLORIDA
3 1262 08553 6687